Solvated electron precursors: a computational approach to the development of novel catalysts from gas-phase to condensed-phase

by

Benjamin A. Jackson

A dissertation submitted to the Graduate Faculty of
Auburn University
in partial fulfillment of the
requirements for the Degree of
Doctor of Philosophy

Auburn, Alabama
May 6, 2023

Keywords: Catalysis, solvated electrons, electronic structure theory, quantum theory, materials design

Approved by

Evangelos Miliordos, Chair, James E Land Assistant Professor, Department of Chemistry and Biochemistry

Konrad Patkowski, S. D. and Karen H. Worley Associate Professor, Department of Chemistry and Biochemistry

J. Vincent Ortiz, Ruth W. Molette Professor, Department of Chemistry and Biochemistry

David M. Stanbury, Professor Emeritus, Department of Chemistry and Biochemistry

Jordan Harshman, Assistant Professor, Department of Chemistry and Biochemistry

ABSTRACT

The solvated electron precursor (SEP) is a complex consisting of a positively charged metal core, $M^{n+,}$ surrounded by sufficient ligands, L, whose coordination leads to n number of valence electrons being displaced from the metal to periphery of the complex as $M^{n+}L_x@ne^-$. These solvated electrons occupy hydrogenic type orbitals which surround the periphery of the SEP complex. Here, multi-reference wavefunction and density functional theory calculations are employed to demonstrate the systematic development of SEPs as novel catalytic material. The first detailed mechanistic study for the use of SEPs as a catalyst for CO_2 functionalization is presented. The reaction pathways for conversion of CO_2 to formic acid/methyldiol and to δ-lactone are studied computationally. The use of aliphatic chains and diamine chains is introduced as a means for bridging two SEPs together and are denoted as linked-SEPs. The isoelectronic systems of $(NH_3)_3Be(CH_2)_nBe(NH_3)_3$ and $(NH_3)_3LiNH_2(CH_2)_nH_2NLi(NH_3)_3$ are studied, with each SEP terminus bearing 1 diffuse electron in a s-type orbital. The coupling of these electrons is investigated as a function of chain length. The system of $(NH_3)_3B(CH_2)_nB(NH_3)_3$ is studied as well, with each SEP terminus bearing two diffuse electrons. Finally, observations from the Li-diamine linked-SEP system inspired the proposal of a novel material consisting of a grid of Li^+ linked by diamine chains. The proposed material is diamond-like in structure, where carbon atoms have been replaced with Li^+ and C−C bonds with diamines. Each lithium tetra-amine center is surrounded by a diffuse orbital occupied by one solvated electron. The electronic band structure and magnetic properties are investigated as a function of diamine chain length illustrating the ability to produce materials of metallic or semiconductor character by tuning the chain length. We propose the SEP materials as a highly tunable redox active catalyst

where reactivity may be controlled by varying pore size and functionalization of carbon chains. Critically, presented gas-phase calculations accurately predict material behaviors, offering an avenue for further development of SEP materials and testing of their tunability. This work in total presents a systematic approach for the design of novel catalytic materials, beginning with high level gas-phase calculations which inform the development of the condensed phase.

ACKNOWLEDGEMENTS

I would like to first express my sincere gratitude and appreciation to my advisor Evangelos Miliordos. I knew nothing about computational chemistry before starting work with you, but you invested the countless hours in training and teaching that got me here. I could not have asked for a better mentor, working with you has been the highlight of my entire graduate program. I look forward to us working together again.

To my committee members Jordan Harshman, Konrad Patkowski, Vincent Ortiz, and David Stanbury, thank you for the many contributions you've made and all of your feedback throughout my doctoral program. To all of the countless teachers, instructors, and professors who have helped and guided me on this academic journey, thank you. Your contributions to my education and growth could not be overstated.

To Andresa, you've been one of my closest friends throughout this program. Knowing I could always count on you has made this an easier journey. Your company has made my time in Auburn a happier one.

To Ron, Abi, Ryan, Larry, John, Taylor, and Garrett, thank you for all of the games, jokes, and laughter. Your friendship has kept me sane throughout this long and arduous process.

Finally, I'd like to acknowledge my mother, Tracie Wilhelm. From childhood you humored and fostered my joy in learning. Your strength in raising three kids on your own will always inspire me. I'm lucky to have had a mother as supporting as you.

TABLE OF CONTENTS

LIST OF TABLES

LIST OF FIGURES

CHAPTER 1. Introduction

The work of this dissertation is purely computational in nature. Computational chemistry is a general term encompassing all methods employing computing resources to investigate chemical systems. As a field, its origins date back to the early 20th century. In 1926, the Schrödinger equation, the basis for most quantum chemical methods, was derived. Soon thereafter was the development of the Hartree Fock equations allowing some of the earliest quantum chemical calculations. By the 1950s the field saw significant development resulting from new quantitative methods and the advent of digital computers. Today, the ever-growing computational power has enabled the application of highly accurate methodologies and the study of increasingly more complex and larger systems such biological macromolecules and bulk materials.

The following chapter will provide a very brief overview of the computational methods which are applied in the present work. This overview should not be considered a complete description of these methods and will serve only as an outline for their fundamentals. For a more detailed account, the reader is referred to outside works such as that of *Modern Quantum Chemistry: Introduction to Advanced Electron Structure Theory* by Szabo and Ostland, *Density Functional Theory: A Practical Introduction* by Scholl and Steckel, and *Introduction to Computational Chemistry* by Jensen. These texts were instrumental in the writing of the present chapter.

1.1 Fundamentals of Electronic Structure Theory

1.1.1 The Schrödinger Equation

In quantum mechanics, it is postulated that for a given system there exists a function Ψ, known as the wavefunction, which contains within it all possible information about the system. One method for obtaining this wavefunction is given by the time-independent Schrödinger equation:

$$\hat{\mathrm{H}}\Psi = E\Psi \qquad 1\text{-}1$$

Here, $\hat{\mathrm{H}}$ is the Hamiltonian operator and E the energy of the system. For a molecular system, the Hamiltonian is given by Equation 1-2 and each term is correspondingly expanded in Equation 1-3.

$$\hat{\mathrm{H}} = \hat{T}_{e,el} + \hat{T}_{e,nuc} + \hat{V}_{e,N} + \hat{V}_{e,e} + \hat{V}_{N,N} \qquad 1\text{-}2$$

$$\hat{\mathrm{H}} = -\sum_{i}^{n}\frac{1}{2}\nabla_i^2 - \sum_{A}^{N}\frac{1}{2M_A}\nabla_A^2 - \sum_{i}^{n}\sum_{A}^{N}\frac{Z_A}{\vec{r}_{iA}} + \sum_{i}^{n}\sum_{j>i}^{n}\frac{1}{\vec{r}_{ij}} + \sum_{A}^{N}\sum_{B>A}^{N}\frac{Z_A Z_B}{\vec{R}_{AB}} \qquad 1\text{-}3$$

The terms $\hat{T}_{e,el}$ and $\hat{T}_{e,nuc}$ denote the kinetic energy of the electrons and the nuclei, respectively. While $\hat{V}_{e,N}$, $\hat{V}_{e,e}$, and $\hat{V}_{N,N}$ denote the electron-nuclei attraction, electron-electron repulsion, and nuclei-nuclei repulsion, respectively. Equation 1-3 is written in atomic units whereby e, the electric charge of an electron, ħ, the reduced Planck constant, and m_e, the mass of an electron, are all set equal to 1. The terms $\vec{r}_{ij}$, $\vec{R}_{AB}$, and $\vec{r}_{iA}$ denote

relative electron or nuclei interparticle distances, see Figure 1-1. M_A and Z_A denote the nuclear mass and the nuclear charge, respectively.

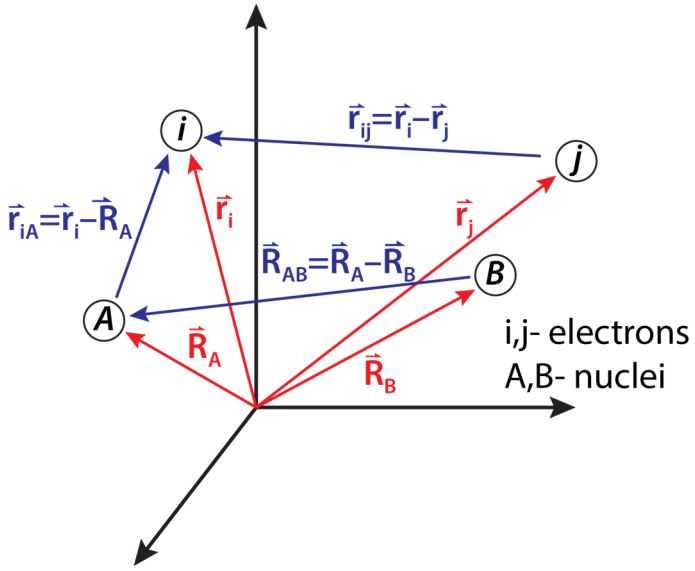

Figure 1-1. The molecular coordinate system.

1.1.2 Born-Oppenheimer Approximation

We may simplify the Hamiltonian by decoupling the motion of the electrons and the nuclei to give a separate electronic $\hat{\mathrm{H}}_{elec}$ and nuclear $\hat{H}_{nuc}$ Hamiltonian. A post-hoc explanation for the ability to decouple these two motions notes that the nuclei are much heavier than the electrons, $m_{electron} \div m_{neutron/proton} \approx 1/1838$, and will move significantly slower. From this we may approximate a molecule as having a number of electrons which move in a field of fixed nuclei. As a result, we may neglect $\hat{T}_{e,nuc}$ and consider $\hat{V}_{N,N}$ to be constant. The remaining terms of the Hamiltonian gives us $\hat{\mathrm{H}}_{elec}$:

$$\hat{\mathrm{H}}_{elec} = -\sum_{i}^{n}\frac{1}{2}\nabla_i^2 - \sum_{i}^{n}\sum_{A}^{N}\frac{Z_A}{\vec{r}_{iA}} + \sum_{i}^{n}\sum_{j>i}^{n}\frac{1}{\vec{r}_{ij}} \qquad 1\text{-}4$$

The Schrödinger equation then gives:

$$\hat{\mathrm{H}}_{elec}\varphi_{elec} = E_{elec}\varphi_{elec} \qquad \textit{1-5}$$

To obtain the total energy of the system the nuclear-nuclear repulsion of the fixed nuclei must be included to give:

$$\mathrm{E}_{total} = E_{elec} + \sum_{A}^{N}\sum_{B>A}^{N}\frac{Z_A Z_B}{\vec{R}_{AB}} \qquad \textit{1-6}$$

By that same reasoning, we may approximate a nuclear Hamiltonian $\hat{H}_{nuc}$ wherein the nuclei move within a potential produced from the average field of the electrons to give:

$$\begin{aligned}\hat{H}_{nuc} &= -\sum_{A}^{N}\frac{1}{2M_A}\nabla_A^2 + E_{elec} + \sum_{A}^{N}\sum_{B>A}^{N}\frac{Z_A Z_B}{\vec{R}_{AB}} \\ \hat{\mathrm{H}}_{nuc} &= -\sum_{A}^{N}\frac{1}{2M_A}\nabla_A^2 + E_{total}\end{aligned} \qquad \textit{1-7}$$

In this way, the nuclei under the Born-Oppenheimer approximation move along a potential energy surface resulting from the solution to the electronic Hamiltonian, see Figure 1-2. Here, $\{\vec{R}_A\}$ denotes the collection of all nuclear positions.

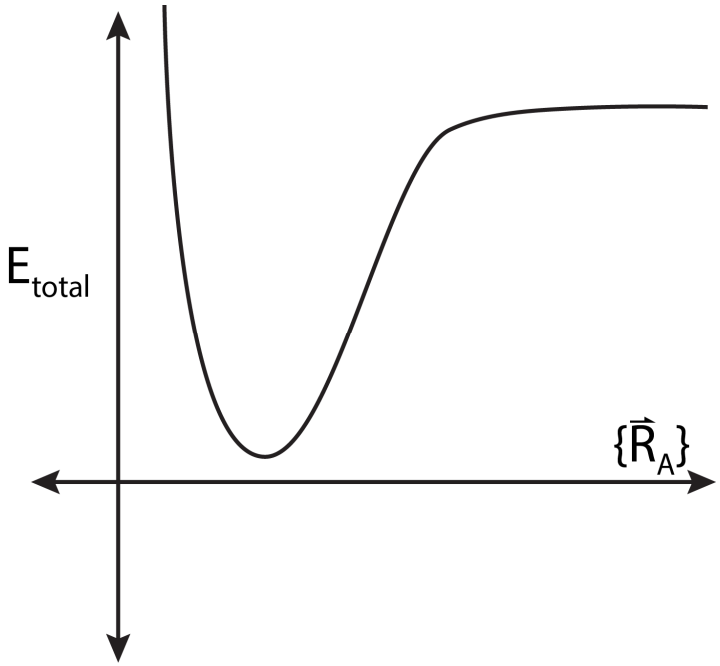

Figure 1-2. Potential energy surface for nuclear motion under the Born-Oppenheimer approximation.

1.1.3 Spin-orbitals and the Pauli Exclusion Principle

To completely describe an electron, its spin variable s_i must be specified in addition to its spatial coordinates. Here, the spin functions $\alpha(s_i)$ and $\beta(s_i)$ are introduced corresponding to the spin up and spin down, respectively. The combination of the spatial orbital $\varphi(\vec{r}_i)$ and the spin $\alpha(s_i)$ gives a spin-orbital $\chi(\vec{x}_i)$ where $\vec{x}_i$ denotes both the spatial and spin coordinates.

$$\chi(\vec{r}_i, s_i) = \begin{cases} \varphi(\vec{r}_i)\alpha(s_i) \\ \varphi(\vec{r}_i)\beta(s_i) \end{cases} \qquad 1\text{-}8$$

As a result of the fermionic nature of the electrons, a many electron wavefunction must be antisymmetric with respect to the interchange of any two electrons. A method for

incorporating this requirement is through the construction of wavefunctions in the form of a Slater determinant:

$$\Psi(\vec{\mathrm{x}}_1, \vec{\mathrm{x}}_2, \ldots \vec{\mathrm{x}}_n) = \frac{1}{\sqrt{n!}} \begin{vmatrix} \chi_1(\vec{\mathrm{x}}_1) & \chi_1(\vec{\mathrm{x}}_2) & \cdots & \chi_1(\vec{\mathrm{x}}_n) \\ \vdots & \vdots & & \vdots \\ \chi_n(\vec{\mathrm{x}}_1) & \chi_n(\vec{\mathrm{x}}_2) & \cdots & \chi_n(\vec{\mathrm{x}}_n) \end{vmatrix} \qquad \textit{1-9}$$

The factor of $(n!)^{-\frac{1}{2}}$ here serves as a normalization constant. We may simplify Equations 1-8 and 1-9 further by replacing $\vec{r}_i$ and s_i or $\vec{x}_i$ with the corresponding index *i*. For example, the slater determinant for a three-electron system occupying two spatial orbitals with the configuration $\varphi_1^2\varphi_2^1$ could be expressed as:

$$\Psi(\vec{\mathrm{x}}_1, \vec{\mathrm{x}}_2, \vec{\mathrm{x}}_3) = \frac{1}{\sqrt{3!}} \begin{vmatrix} \varphi_1(1)\alpha(1) & \varphi_1(1)\beta(1) & \varphi_2(1)\alpha(1) \\ \varphi_1(2)\alpha(2) & \varphi_1(2)\beta(2) & \varphi_2(2)\alpha(2) \\ \varphi_1(3)\alpha(3) & \varphi_1(3)\beta(3) & \varphi_2(3)\alpha(3) \end{vmatrix} \qquad \textit{1-10}$$

1.2 Hartree-Fock Theory

Generally, the exact form of the functions which describe spatial orbitals is unknown. A method for obtaining them is to express each as a linear combination of known functions, referred to as a basis set.

$$\varphi_i(r) = \sum_{\mu}^{K} c_{\mu i} g_\mu(r) \qquad \textit{1-11}$$

Where K is the number of basis functions, $c_{\mu i}$ the coefficients, and g_i the basis functions. Under the variational principle, the best wavefunction is the one which gives the lowest energy possible. As such, we may obtain the coefficients by minimizing the energy with

respect to variations in $c_{\mu i}$. The best wavefunction is obtained by Equation 1-12 where E_0 is the minimum energy (for a given methodology and basis set combination, provided Ψ_0 is normalized).

$$E_0 = \langle \Psi_0 | \hat{H} | \Psi_0 \rangle \qquad \textit{1-12}$$

A method for finding the approximate solution to Equation 1-12 and therefore the $c_{\mu i}$ is given by the Hartree-Fock (HF) methodology, which serves as the starting point for most other methods. Under HF, we obtain the Fock equation:

$$\hat{F}\varphi_i(r) = E_i\varphi_i(r) \qquad \textit{1-13}$$

$$\left(h_1(1) + \sum_{b \neq a} J_b(1) - \sum_{b \neq a} K_b(1)\right)\chi_a(1) = E_a\chi_a(1) \qquad \textit{1-14}$$

Where $\hat{F}$ is the Fock operator, $\varphi_i(r)$ the i$^{\text{th}}$ orbital, and E_i its energy. $h_1(1)$ is the energy of one electron in absence of any additional electrons and given by:

$$h_1(i) = -\frac{1}{2}\nabla_i^2 - \sum_A \frac{Z_A}{r_{iA}} \qquad \textit{1-15}$$

The coulomb operator J_b is defined as:

$$J_b(1) = \int \mathrm{d}\chi_2 \frac{|\chi_b(2)|^2}{r_{12}} \qquad \textit{1-16}$$

While the exchange operator K_b is given by:

$$K_b(1)\chi_a(1) = \left[\int \mathrm{d}\chi_2\, \chi_b^*(2)\frac{1}{r_{12}}\chi_a(2)\right]\chi_b(1) \qquad \textit{1-17}$$

A critical result of the Hartree-Fock method is seen in the coulomb term. Here, electron 1 experiences the mean-field of electron 2 from $\mathrm{d}\chi_2|\chi_b(2)|^2$ rather than its instantaneous position. This approximation replaces the complex many-electron problem with a one-electron problem in which electron-electron repulsion is treated in an average way.

1.2.1 Basis Sets

The choice to express the molecular orbitals of system in the form of linear combination of basis functions aids in reducing the complexity of the problem.

$$\varphi_i(r) = \sum_{\mu}^{K} c_{\mu i} g_\mu(r) \qquad \textit{1-18}$$

Increasing the number of basis functions increases the variational freedom and lowers the energy E_0. However, obtaining the *exact* molecular orbitals for a system would require an infinite number of basis functions. This is not feasible. Instead, it is common to select a basis set containing a finite series of functions which aim to mimic the structure of atomic orbitals. This method is commonly known as MO-LCAO, or molecular orbitals from linear combination of atomic orbitals. The introduction of basis sets mathematically results in the production of more orbitals than are occupied by the electrons in a system. These unoccupied orbitals are known as virtual orbitals. Larger basis sets lead to more virtual orbitals.

Two main types of basis sets exist: the Slater type orbitals (STOs) and the gaussian type orbitals (GTOs). STOs have functions of the form:

$$\chi_{\zeta,\mathrm{n,l,m}}(r,\theta,\varphi) = NY_{l,m}(\theta,\varphi)r^{n-1}e^{-\zeta \mathrm{r}} \qquad \textit{1-19}$$

Where N is a normalization constant and $Y_{l,m}$ are spherical harmonic functions. The exponential dependence on distance offers an advantage as it mirrors the exact orbitals for hydrogen-like atoms. The evaluation of STO type functions though poses significant computational challenge. More commonly used are the GTO type functions which have the form:

$$\chi_{\zeta,\mathrm{l}_x,\mathrm{l}_y,\mathrm{l}_z}(x,y,z) = Nx^{l_x}y^{l_y}z^{l_z}e^{-\zeta \mathrm{r}^2} \qquad \textit{1-20}$$

The r^2 exponential dependence of individual gaussian functions have the disadvantage of poorly describing the regions very close to the nucleus and GTOs fall off too rapidly at distances far from the nucleus. This requires a linear combination with a greater number of GTOs, compared to STOs, to obtain an accurate orbital representation. This disadvantage is more than made up by the ease of evaluating GTO integrals leading to improved computational efficiency.

Unless otherwise specified, the basis functions used in this work will be the GTO type, correlation consistent family developed by Dunning et al. Denoted generally as cc-pV*n*Z or correlation consistent polarized valence *n* zeta (e.g., cc-pVDZ, cc-pVTZ, etc.).

These functions may be further augmented with diffuse functions to give the aug-cc-pV*n*Z, d-aug-cc-pV*n*Z, etc.

Previous work with solvated electron precursors has shown the cc-pVTZ family, with aug-cc-pVTZ for H atoms, to be sufficient for geometries. The augmentation of the H atom basis set is necessary to accurately describe the diffuse orbitals which surround the periphery of solvated electron precursor (SEP) complexes. For the study of excited states, the use of doubly augmented d-aug-cc-pVTZ basis set for H atoms is sufficient with CASPT2 excitation energies with respect to the complete basis set limit to within 0.01 eV.[1]

1.3 Improving the Wavefunction

The mean field approximation of the Hartree-Fock method, for a sufficiently large basis set is often able to account for ~99% of the total energy. However, the remaining ~1% is often very important for accurately describing chemical properties and processes. The difference in energy between the exact energy E_{exact} the HF energy E_{HF} is known as the correlation energy E_{corr}:

$$E_{corr} = E_{exact} - E_{HF} \qquad 1\text{-}21$$

Physically, this is a result of the motion of the electrons being correlated and as a result are on average further apart than described by the HF wavefunction, which describes interactions on a mean-field basis. The correlation energy may be broken into two categories: dynamic and static. Separating and defining these two terms is a matter of dispute, but generally static correlation is defined as the energy difference resulting from multiconfigurational methods

and dynamic correlation is defined as the energy difference from configuration interaction (or similar methods). These are explained in more detail below.

1.3.1 "Excited" Determinants

The HF method obtains the minimal energy, best one-determinant trial wavefunction (within a given basis set). In recovering the missing correlation energy, it is necessary to include more than just one Slater determinant in the wavefunction. As HF obtains ~99% of the total energy, it serves as a good starting point for constructing additional determinants to include. A generic multideterminant wavefunction may be written as:

$$\Psi = c_0\varphi_{HF} + \sum_{i=1} c_i\varphi_i \qquad \textit{1-22}$$

These new determinants may be constructed from singly, doubly, triply, etc. "excited" configurations or rearrangements relative to the HF determinant up to N_{elec}. Here, 1, 2, 3 etc. electrons from the HF wavefunction are "excited" or moved to the virtual orbitals. The number of determinants is limited by the size of the basis set as this determines the number of virtual orbitals. For an infinite basis and all possible "excitations" the Schrödinger equation is solved exactly.

1.3.2 Configuration Interaction

The method of *configuration interaction* (CI) is an extension of this process where the wavefunction is written as linear combination of determinants and the expansion coefficients are determined by minimizing the total energy. MO orbitals used in the expansion are obtained from the Hartree-Fock wavefunction. The CI wavefunction is written as:

$$\Psi_{CI} = c_0\varphi_{HF} + \sum_S c_S\varphi_S + \sum_D c_D\varphi_D + \sum_T c_T\varphi_T + \sum_Q c_Q\varphi_Q + \cdots \qquad 1\text{-}23$$

The subscripts S, D, T, Q,… represent single, double, triple, quadruple,… "excited" determinants relative to the HF configuration.

To ensure the tractability of calculations, the full CI expansion may be truncated. Truncation at the first excitations gives CIS which is equivalent to HF. The inclusion of the double and single excitations gives CISD which may recover 80-90% of the missing correlation energy.

1.3.3 Multiconfigurational Self-Consistent Field

The *multiconfigurational self-consistent field* (MCSCF) method is an extension of the CI method in which both the configurational expansion coefficients and the MOs used in constructing the determinants are optimized. While the HF wavefunction generally provides a sufficient orbital description, there are many cases in which the HF wavefunction and orbitals provide an inadequate representation for "excited" determinants. For these cases we may include additional determinants constructed with orbitals optimized for that configuration. However, including all possible configurations for a given system will be

prohibitively expensive. As with CI, we can truncate the expansion, but this introduces a question of how to decide which configurations will be included. One procedure for making this decision is offered by the *complete active space self-consistent field* (CASSCF) method.

CASSCF partitions the orbital space into a set of active and inactive orbitals (see Figure 1-3). The inactive orbitals may consist of either doubly occupied, denoted as closed, or unoccupied orbitals. The active orbitals may consist of both occupied orbitals and orbitals which are virtual at the HF level. The multiconfigurational wavefunction is then constructed as a linear combination of all possible electron rearrangements within the active space.

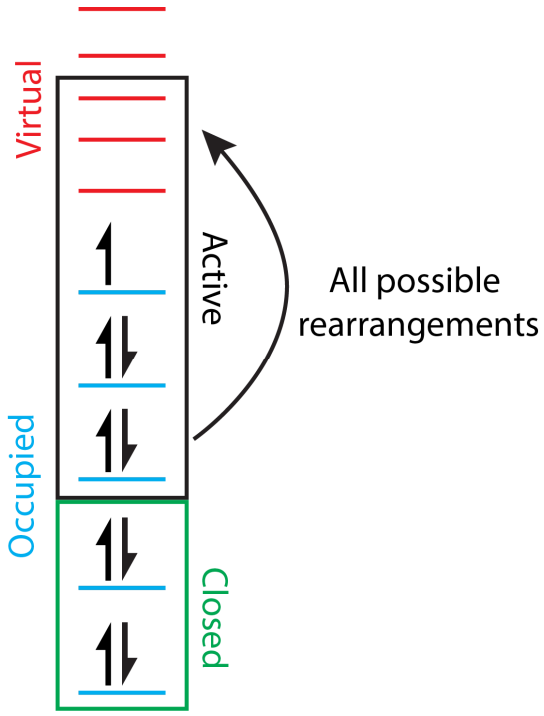

Figure 1-3. Schematic of CASSCF methodology.

1.3.4 Perturbation Theory

Another method for recovering correlation energy is offered through *many-body perturbation theory* (MBPT). Under perturbation methods it is assumed that the present problem differs only slight from another problem of known solution, therefore the solution of the unknown problem may be obtained through applying a small perturbation to the known system. This is done mathematically by defining a Hamiltonian operator which consists of two parts, the perturbation $\widehat{H}'$ and the reference $\widehat{H}_0$. With λ being the perturbation strength this gives:

$$\widehat{H} = \widehat{H}_0 + \lambda\widehat{H}' \qquad \textit{1-24}$$

The wavefunction and the energy may be expressed as expansions in powers of the perturbation parameter λ.

$$\widehat{H} = \lambda^0\widehat{H}_0 + \lambda^1\widehat{H}^{(1)} + \lambda^2\widehat{H}^{(2)} + \lambda^3\widehat{H}^{(3)} + \cdots$$
$$\Psi = \lambda^0\Psi_0 + \lambda^1\Psi^{(1)} + \lambda^2\Psi^{(2)} + \lambda^3\Psi^{(3)} + \cdots \qquad \textit{1-25}$$

The $\Psi^{(1)}$, $\Psi^{(2)}$, … and $\widehat{H}^{(1)}$, $\widehat{H}^{(2)}$, … are the first-order, second-order, etc. corrections. The *n*-th order energy or wavefunction then becomes a sum of all terms up to order *n*.

So far, this method is a general application of perturbation theory. The selection of the unperturbed Hamiltonian to be a sum over Fock operators results in the *Møller-Plesset* (MP) *perturbation theory*, a very common methodology. The notation MP*n* is used to denote correction up to order *n*, e.g. MP2 includes the first and second order corrections. Another common implementation of perturbation theory is through *complete active space*

perturbation theory CASPT*n* where *n* again denotes order of correction, e.g. CASPT2 is the second order.[2,3] Under CASPT*n,* the CASSCF wavefunction is used as the reference wavefunction.

1.4 Density Functional Theory

Density Functional Theory is an alternative approach to solving the Schrödinger equation than the previously discussed wavefunction methods. It is based on the following postulates:

1. The ground-state energy E of a system is a unique functional of the electron density ρ:

$$E[\rho] = E \qquad \textit{1-26}$$

2. The electron density which minimizes the energy of the overall functional is the true electron density, corresponding to the full solution of the Schrödinger equation.

In this way, density functional theory converts the problem from the 3N variables of the wavefunction (the 3 variables x, y, z for N electrons) to a problem of finding the electron density which depends only on 3 spatial variables. To find this electron density the Kohn-Sham equation (Equation 1-27) is employed. Further, under the Kohn-Sham equations it is assumed that the density may be expressed as the square of a Slater determinant.

$$\left[-\frac{1}{2}\nabla^2 + V(\vec{r}) + V_H(\vec{r}) + V_{xc}(\vec{r})\right]\Psi_i(\vec{r}) = E_i\Psi_i(\vec{r}) \qquad \textit{1-27}$$

The left-hand terms include the kinetic energy of an electron, the Coulomb potential between an electron and the atomic nuclei $V(\vec{r})$, the Hartree potential $V_H(\vec{r})$ defined in Equation 1-28 and $V_{xc}(\vec{r})$ the exchange and correlation contributions (Equation 1-29). The Hartree potential describes the Coulomb interaction between an electron and the total electron density for all electrons.

$$V_H(\vec{r}) = \int \frac{\rho(\vec{r}')}{\vec{r} - \vec{r}'} d^3r' \qquad 1\text{-}28$$

The potential of the exchange and correlation contributions $V_{xc}(\vec{r})$ is formally defined as a functional derivative of the exchange correlation energy:

$$V_{xc}(\vec{r}) = \frac{\delta E_{xc}(\vec{r})}{\delta \rho(\vec{r})} \qquad 1\text{-}29$$

An exact expression for $V_{xc}(\vec{r})$ is not known, instead various approximations of it have been proposed. These give the various "flavors" of DFT including local density approximation (LDA), generalized gradient approximation (GGA), meta-GGA, and the hybrid functionals.

1.4.1 V_{xc} and the DFT Functionals

Under the local density approximation, the exchange-correlation energy functional is assumed to depend only on the local electronic density at each point, giving:

$$E_{xc}^{LDA}[\rho] = \int \rho(\vec{r}) E_{xc}[\rho(\vec{r})] d\vec{r} \qquad 1\text{-}30$$

The exchange-correlation energy is decomposed into separate exchange E_x and correlation E_c terms for which expressions of these are sought. These are typically derived from a homogeneous electron gas model.

$$E_{xc} = E_x + E_c \qquad 1\text{-}31$$

The construction of LDA functionals is often used as the basis for construction of more sophisticated approximations of GGA and the hybrid functionals. Under GGA, the E_{xc} is assumed to be a functional of both the electron density and the gradient of the electron density:

$$E_{xc}^{GGA}[\rho] = \int \rho(\vec{r})\{E_x^{GGA}[\rho(\vec{r}), |\nabla\rho(\vec{r})|] + E_c^{GGA}[\rho(\vec{r}), |\nabla\rho(\vec{r})|]\}d\vec{r} \qquad 1\text{-}32$$

The various GGA functionals differ in the construction of the E_x^{GGA} and E_c^{GGA} terms. An example is that of the PBE[4] functional, one of the most commonly used functionals for condensed-phase periodic calculations.

One of the errors introduced by the DFT theory is that of the self-interaction energy or delocalization error. As $\hat{V}_H$ is expressed as the potential produced from the interaction of an electron with the total density of all electrons, this includes an interaction with its own density. One solution to this is provided by the use of hybrid functionals which are typically constructed as linear combination of the Hartree-Fock exchange energy E_x^{HF}, which explicitly lacks a self-interaction, and some number of DFT exchange and correlation functionals. For example, the PBE0[5,6] functional is:

$$E_{xc}^{PBE0} = \frac{1}{4}E_x^{HF} + \frac{3}{4}E_x^{PBE} + E_c^{PBE} \qquad 1\text{-}33$$

For the present work, unless otherwise specified, all DFT calculations will use the CAM-B3LYP[7] functional. CAM-B3LYP is a hybrid GGA functional which includes the hybrid functional B3LYP along with a series of long-range corrections. Previous work with SEPs has demonstrated CAM-B3LYP to provide ground state geometries comparable to higher-level MP2 and CCSD(T) optimizations.[8–10]

1.5 Periodic Methods

When studying large systems such as solid-phase materials, the number of atoms needed to describe the material is immense. For example, studying the electronic structure of a bar of iron metal. To make such a problem more manageable, the system may be divided into a smaller subunit (denoted the unit cell) which can be repeated infinitely to produce the bulk material, see Figure 1-4.

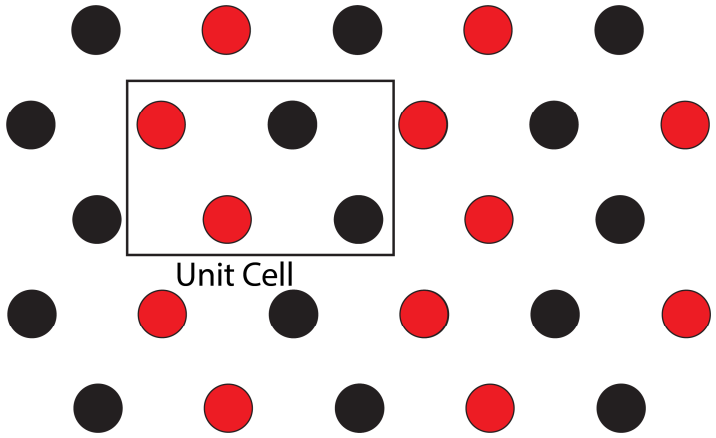

Figure 1-4. Unit cell schematic for periodic methods.

To describe the periodicity of such a system, the system's wavefunction must obey Bloch's theorem, where $\vec{R}$ is a cell lattice parameter:

$$\Psi_k(\vec{r} + \vec{R}) = e^{i\vec{k}\cdot\vec{R}}\Psi_k(\vec{r}) \qquad 1\text{-}34$$

Commonly, the wavefunction is expanded as a set of basis functions consisting of plane waves, as these will obey the boundary conditions. Here, $\vec{G}$ is a reciprocal lattice vector.

$$\Psi_k(\vec{r}) = e^{i\vec{k}\cdot\vec{r}} \sum_{\vec{G}} c_{\vec{G}} e^{i\vec{G}\cdot\vec{r}} \qquad 1\text{-}35$$

From here, we may apply the same methods described in the previous sections to solve the Schrödinger equation for a system of periodic boundary conditions.

CHAPTER 2. Solvated Electron Precursors and $Li(NH_3)_4$

2.1 Historical Background

Research into metal-ammonia interactions date back to the work of Sir Humphry Davy with the newly discovered sodium and potassium in 1807 where he observed their characteristic "fine blue colour".[11] In 1907, C.A. Kraus would be the first to identify metal-ammonia solutions resulting in "freed" electrons and attributing the blue color to this.[12] This would be later confirmed by G.E. Gibson and W.L. Argo in 1918, first coining the term solvated electron.[13] Significant research has gone into studying the wide variations in physical properties that metal-ammonia solutions have at different concentrations.[14–20] In 1897, H. P. Cady measured the molecular conductivity of sodium ammonia solutions increasing with concentration and made the first observation of a transition to metallic state (TMS) for such solutions.[19,20] In 1938, E. Huster was the first to measure the magnetic susceptibility of metal-ammonia solutions as a function of concentration.[14] Despite extensive theoretical and experimental investigations of alkali and alkaline earth metal-ammonia solutions and complexes, a detailed microscopic understanding over the full composition range remains lacking.[11]

2.2 Properties of Ammonia-Metal Solutions and the SEP

The addition of small amounts of alkali or alkaline earth metals to a solution of ammonia results in the production of solvated electrons through a $M \rightarrow M_s^+ + e_s^-$ dissolution process.[11] Here, M_s^+ denotes the solvated metal cation and e_s^- the solvated electron. Focusing on the case of lithium, the first solvation shell of the solvated Li_s^+ consists of $Li(NH_3)_4^+$. For the

solvated electron, the exact number of ammonia ligands constituting its first coordination sphere remains unclear, experimental and theoretical results predict it as 5-8 ligands.[11,21,22]

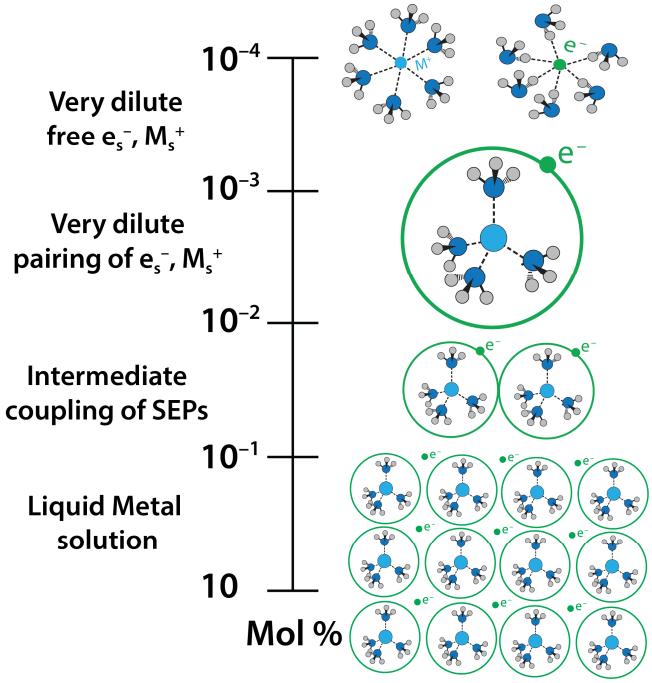

Figure 2-1. Formation of $Li(NH_3)_4$ solutions. Adapted from ref[11].

Increasing the metal concentration leads (see Figure 2-1) to the association of the solvated electron e_s^- with the $Li(NH_3)_4^+$ to form a neutral $Li(NH_3)_4$ complex with the solvated electron surrounding the periphery of the lithium-ammonia complex. To emphasize this aspect, the notation $Li(NH_3)_4^+@1e^-$ has been used previously.[11] Here, the asperand "@" is used to denote an electron which is delocalized over a group of molecules, compared to the dot "•" denoting an electron localized to a specific region/atom, e.g., the radical $•CH_3$. The formation of the $Li(NH_3)_4$ complex occurs within the concentration range of 10^{-3} to 1 mol % metal (MPM).[11]

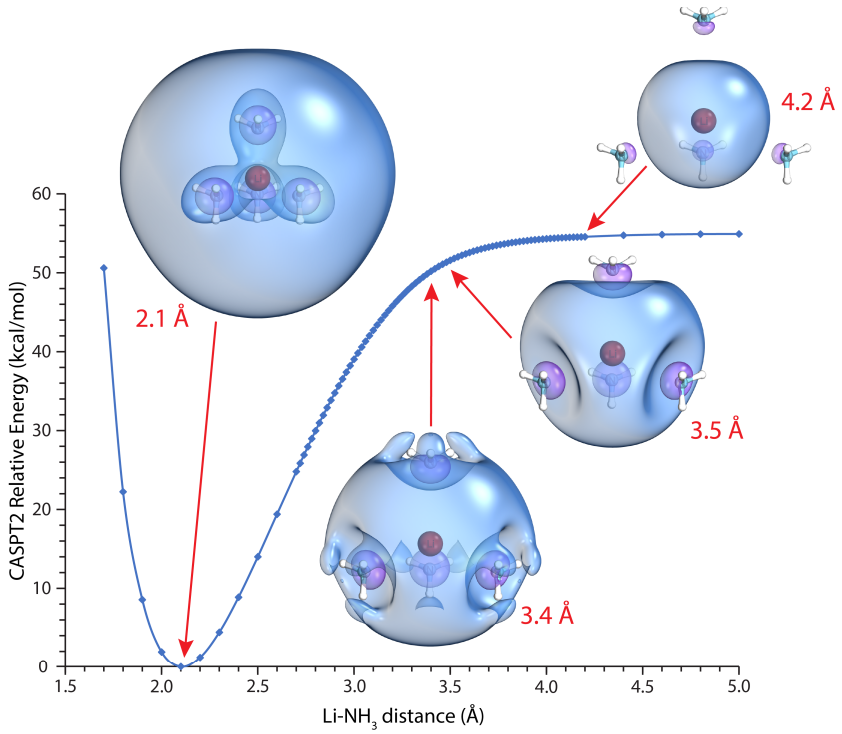

Figure 2-2. CASPT2 Potential Energy Curve for the formation of $Li(NH_3)_4$.

Shown in Figure 2-2 is the potential energy curve for the formation of the $Li(NH_3)_4$ complex as calculated at CASPT2 with the basis sets cc-pVDZ (Li, N) and d-aug-cc-pVDZ (H). Beginning at large separation, four ammonia ligands approach the Li atom. As the ligands near, the valence 2s electron of Li is displaced from the metal until it is removed to the periphery of the complex where it occupies a pseudospherical orbital analogous to the hydrogenic s-type. This provides a definition of the solvated electron precursor:

Solvated Electron Precursor (SEP)- *a complex consisting of a positively charged metal core, M^{n+}, surrounded by sufficient ligands, L, whose coordination leads to n number of valence electrons being displaced from the metal to periphery of the complex as $M^{n+}L_x@n(e^-)$.*

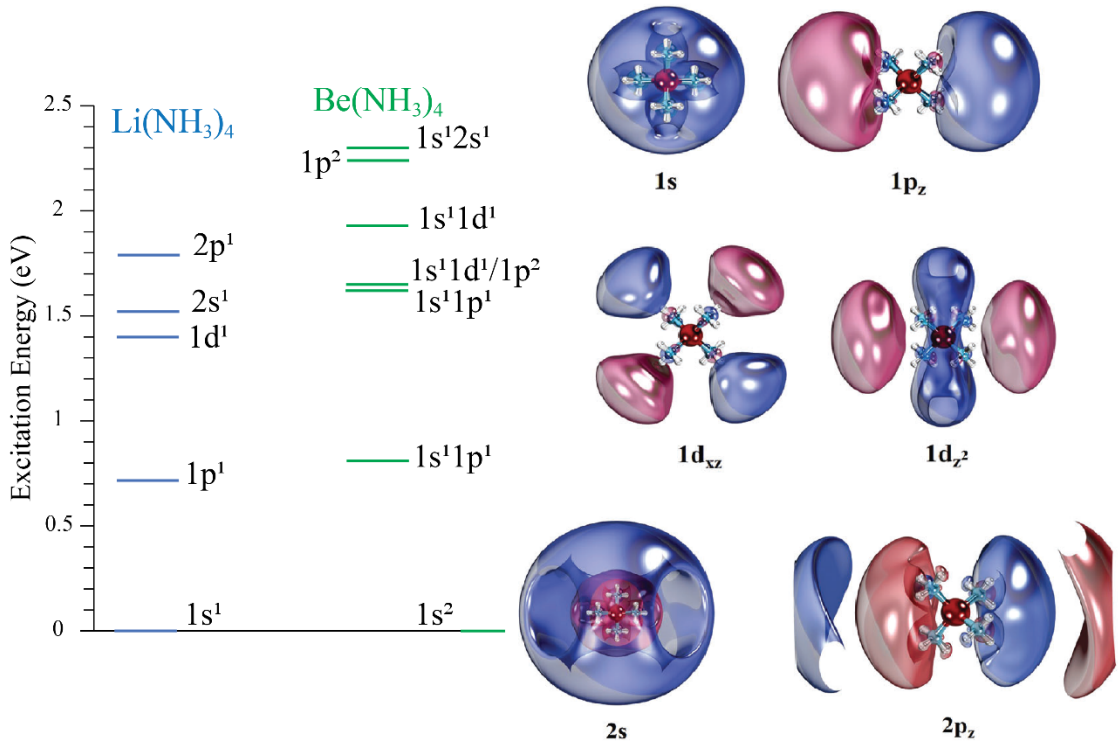

Figure 2-3. Excited states and orbitals of $Li(NH_3)_4$ and $Be(NH_3)_4$. Reproduced from ref [10].

Quantum chemical calculations of excited states for $Li(NH_3)_4$ and $Be(NH_3)_4$ illustrate how these solvated electrons may be further excited to orbitals of s-, p-, d-, and f-type character (see Figure 2-3). SEPs follow a *1s, 1p, 1d, 2s, 2p, 1f, 2d, 3s, 1g…* Aufbau Principle which is distinct from the atomic Aufbau Principle and independent of the metal identity.[1,8–10,23–29] Here, the notation of 1s, 1p, etc. no longer denotes discrete quantum number, but rather an energy ordering with subsequent orbitals of each character (e.g., 1s, 2s, 3s) introducing additional radial nodes. It can be concluded that SEPs display an electronic structure which is superatomic in character with systems like $Li(NH_3)_4$ and $Na(NH_3)_4$ as analogs to the hydrogen atom while systems like $Be(NH_3)_4$, with its two diffuse electrons, as an analog to the helium atom.

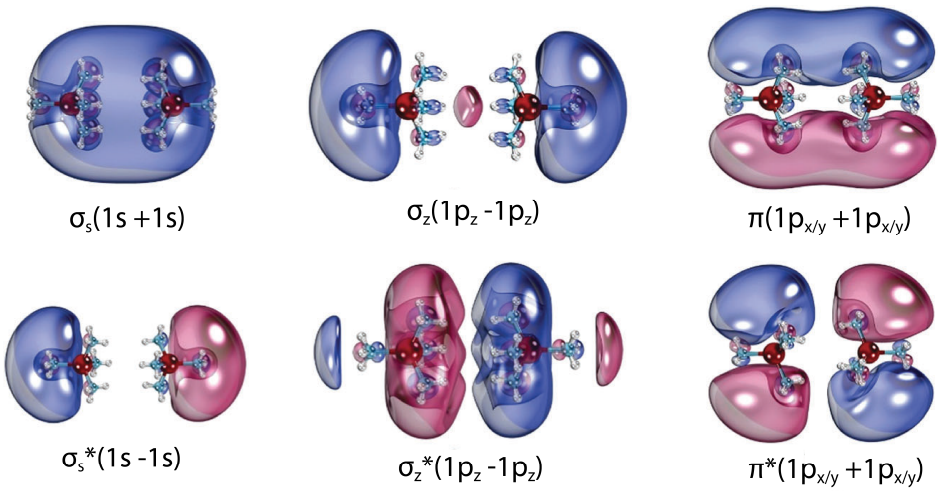

Figure 2-4. The $Li(NH_3)_4$ dimer. Shown are the superatomic orbitals of the dimeric $Li(NH_3)_4$ illustrating bonding and antibonding orbitals of σ and π character.

Just as two hydrogen atoms may couple their atomic $1s^1$ electrons in sigma bond to form the dimer H_2, two $Li(NH_3)_4$ complexes couple to form a dimeric $Li(NH_3)_4$–$Li(NH_3)_4$ with their "superatomic" $1s^1$ electrons coupling in a σ-type bond (see Figure 2-4) with a calculated binding energy of 14.7 kcal/mol,[10] Compare this to H_2 with a binding energy of 104.15 kcal/mol[30] or the average Li-NH_3 binding energy in $Li(NH_3)_4$ which is 10.54 kcal/mol, calculated here at CAM-B3LYP. The dimer's optimal structure has the hydrogen atoms of the ammonia ligands aligning in an "eclipsed" fashion. Based on sterics this initially seems counter-intuitive but results from the hydrogens in the polar N-H bonds solvating or attracting the negatively charged electrons. Arranged this way electron density is concentrated between the two complexes, binding them together. Excited states of the dimer populate orbitals of σ*, π, and π* character (Figure 2-4).

The existence of SEP dimers serves as an explanation for the interesting magnetic properties of lithium-ammonia solutions. At low metal concentrations these solutions are paramagnetic due to the existence of the solution as independent M_s^+ and e_s^- ions and later

as the SEP $Li(NH_3)_4$.[11] Increasing the metal concentration further up to ~1 MPM the magnetic susceptibility drops, which can be explained by dimeric coupling of the SEPs as above. Finally, as concentrations increase to saturation, the solutions take on a metallic character as the many SEP complexes coalesce to form a grid of positively charged $Li(NH_3)_4^+$ centers surrounded by a free flowing "sea" of electrons producing a material known as an expanded metal or liquid metal (see Figure 2-1).

2.3 Transition metal SEPs (TM-SEPs)

Transition metal SEPs (TM-SEPs) is a topic which has seen very little exploration as compared to the alkali and alkaline earth metal SEPs. Currently, detailed characterization of these systems is available for only $Sc(NH_3)_n$, $Y(NH_3)_n$, and $V(NH_3)_n$.[8,23,25] Together these three exhibit a range of structural and electronic properties.

Vanadium can accommodate up to 6 ammonias in its first solvation shell, where it forms an approximately octahedral $V(NH_3)_6^{2+}$ core with the vanadium $4s^2$ electrons displaced to the peripheral superatomic 1s orbital. The vanadium atomic d orbitals are retained and, in the octahedral ligand field, split into 3 t_{2g} and 2 e_g orbitals (see Figure 2-5). These inner d orbital electrons are well separated from the outer shell with no transitions between 3d to the outer orbitals occurring within 2.0 eV (Figure 2-6).[25] Transitions within the inner d space are similarly unfavored requiring approximately 1.7 eV[25] for the two complexes, as expected by the antibonding character of the e_g orbitals. The TM-SEPs follow the same *1s, 1p, 1d, 2s, 2p…* Aufbau Principle observed for the alkali and alkaline earth metal SEPs (Figure 2-6).

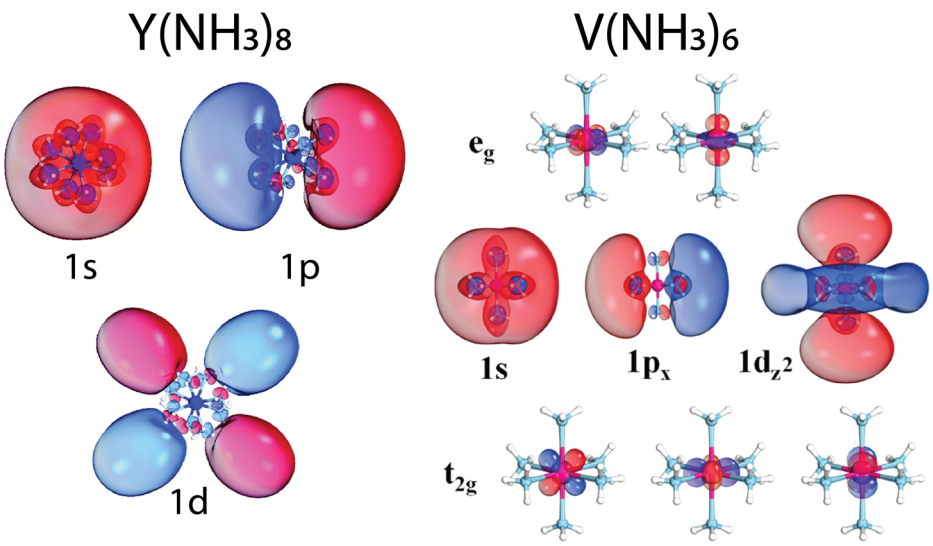

Figure 2-5. Orbitals of $V(NH_3)_6$ and $Y(NH_3)_8$. Adapted from refs [23,25].

The ground state of the lone yttrium atom is ^2D ($4d^15s^2$) followed by a ^2P ($5s^25p^1$) 10,765 cm^{-1} (M_j averaged).[31] Upon coordination by 8 ammonia ligands a pseudo D_{4d} complex is formed, and all three valence electrons of yttrium are displaced to the periphery to form the $Y(NH_3)_8^{3+}$ core whose ground state is $^2B_2$ ($1s^21p^1$). The inner d-shell is not available to the metal valence electrons and instead the 4d orbitals facilitate the dative $H_3N \rightarrow Y$ bonds- its transition metal character is quenched.

Scandium, which lies between the two in ionization energy and atomic size, demonstrates a transition between the TM character of V and the quenched character of Y.[8] The $Sc(NH_3)_{6/8}$ and $Sc(NH_3)_{6/8}^{2+}$ prefer a $Sc^{2+}(3d^1)$ oxidation state with zero or two ($1s^2$) outer electrons. Conversely, $Sc(NH_3)_{6/8}^{+}$ structures with either $Sc^{2+}(3d^1)$ and Sc^{3+} are nearly isoenergetic.

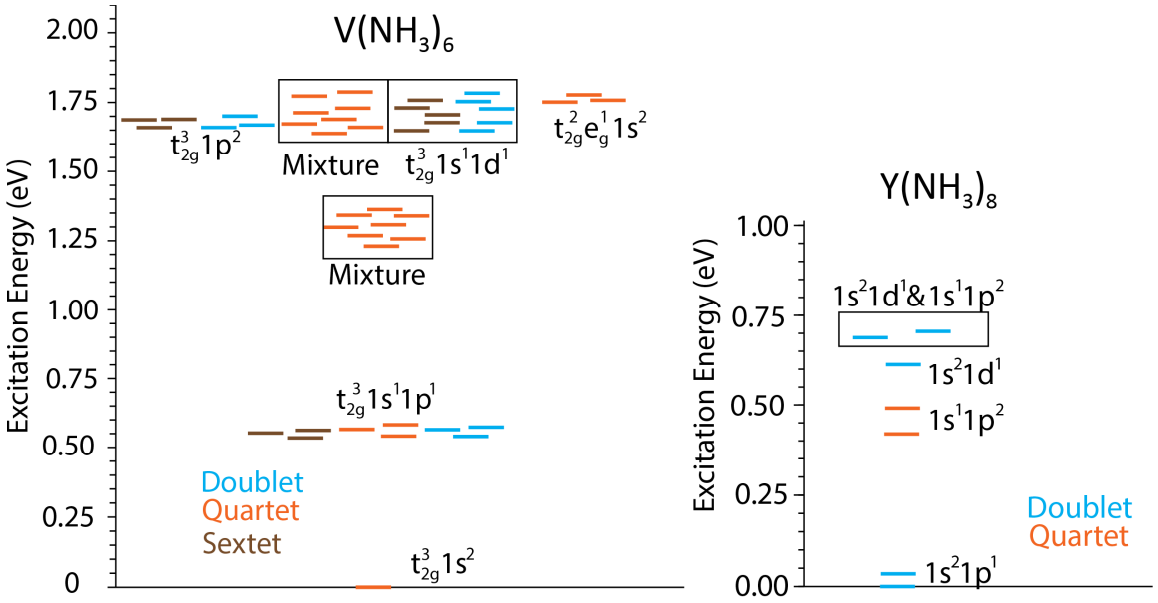

Figure 2-6. Excited states of $V(NH_3)_6$ and $Y(NH_3)_8$. Adapted from refs [23,25].

2.4 SEP Ligands

While the following text focuses primarily on ammonia/amine complexes, SEPs can be produced using a wide variety of ligands. These have included dimethyl ether,[32,33] crown ethers,[34–36] methanol,[37,38] cyclams,[36] cryptands,[36] methylated ammonia,[39–46] and diamines[47]. SEPs produced from metal hydrates have similarly seen abundant work.[48–54]

Focusing on the hydrates, these have an inherent disadvantage to them. Depicted in Figure 2-7 is the reaction mechanism for the release of H_2 from the $Be(H_2O)_4$ and $Be(NH_3)_4$. Both complexes have a ground state electronic configuration where two electrons occupy the outer 1s orbital. In both cases, the reaction begins with the dissociation of an H^+ to produce an NH_2^- or OH^- bound to the metal. This free H^+ attracts the two diffuse electrons to produce H^- which then may abstract another H^+ and form H_2. For the hydrate, this is a concerted mechanism. The remaining complexes of $Be(NH_3)_2(NH_2)_2$ and $Be(H_2O)_2(OH)_2$ are no longer SEPs, having lost their outer electrons to H_2. In the case of $Be(H_2O)_4$, this barrier for H_2

release is 8.0 kcal/mol, nearly a third the barrier for $Be(NH_3)_4$. Further, the final product of $Be(H_2O)_2(OH)_2$ is significantly stabilized over $Be(H_2O)_4$ by 94.7 kcal/mol, more than twice that of the amine complex.

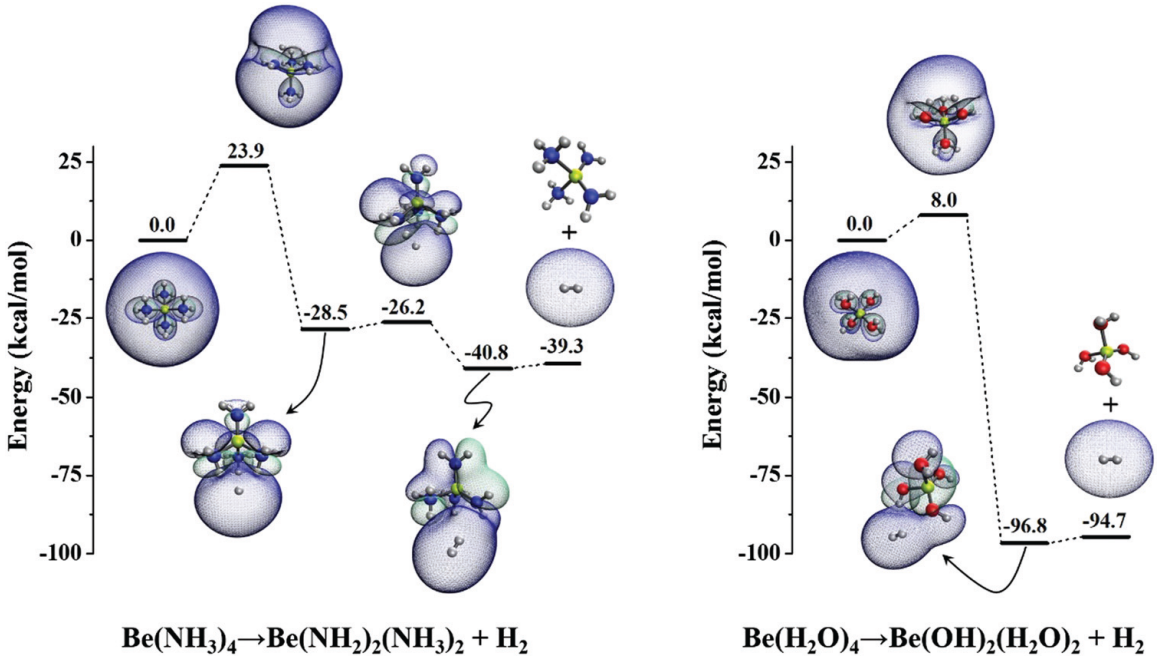

Figure 2-7. Mechanism for H_2 release in $Be(H_2O)_4$ and $Be(NH_3)_4$. Image obtained from ref [24].

In systems like $Li(NH_3)_4$ and $Li(H_2O)_4$ where only one outer electron is present, a similar mechanism is expected but requiring the presence of a second SEP to provide the two electrons required for the H_2. For the case of $Cr(NH_3)_6$ and $Mo(NH_3)_6$, discussed in more detail later, we demonstrated that the barrier for H_2 release is independent of the metal's identity, agreeing within 5 kcal/mol.[9] As such, the use of amine ligands to produce SEPs offers significantly higher stability over water.

2.5 Application of SEPs in Catalysis

In this section the findings reported in ref [55] are summarized. For computational details and more information see the provided copy in APPENDIX A: Supporting Material for Chapter 2.

*B. Jackson and E. Miliordos, "Simultaneous CO_2 capture and functionalization: solvated electron precursors as novel catalysts", Chemical Communications **58**, 1310 (2022),*

2.5.1 Introduction

Solvated electrons in solutions of ammonia or otherwise are known to be powerful reducing agents. A classic example of this is offered by the Birch reduction which uses solvated electrons to enable the conversion of benzene to a cyclohexadiene.[56] It follows that the diffuse electrons of SEPs should be similarly reactive. If so, SEPs would offer a promising candidate for the development of novel redox catalysts with tunable reactivity through the functionalization of their ligands. There exist multiple experimental studies demonstrating previously the ability of metal SEP hydrates to reduce O_2, CO_2, CH_3CN, and NO.[57–60] However, the mechanism of this reduction remains poorly understood. The present work aimed to provide the first mechanistic study employing an SEP as a redox catalyst. To this end, two reactions were explored: 1. the reaction of CO_2 and H_2 to produce formic acid or methanediol and 2. the reaction of CO_2 and C_2H_4 to produce δ-lactone. These reactions were chosen as their simplicity offers a good entry point for exploring fundamental SEP reactivity and because the functionalization of CO_2 is one of environmental and industrial importance due to its role as a greenhouse gas and potential as a chemical platform.

2.5.2 *The Mechanism of SEP Catalysis*

Shown in Figure 2-8 is the observed reaction pathway for CO_2 and H_2. Beginning with the coordination of CO_2 to the SEP (-1.7 kcal/mol), this is followed by an electron transfer from the SEP to CO_2 forming a radical $\bullet CO_2^-$. The activation barrier E_a for this (eTS1) is only 2.6 kcal/mol and the resulting $\bullet CO_2^-$ is bound to $Li(NH_3)_4^+$ (CO_2p). Following, the unpaired electron of carbon may abstract a hydrogen from H_2 with a barrier of 14.8 kcal/mol (CHTS1) and form a C-H bond (CHp1).

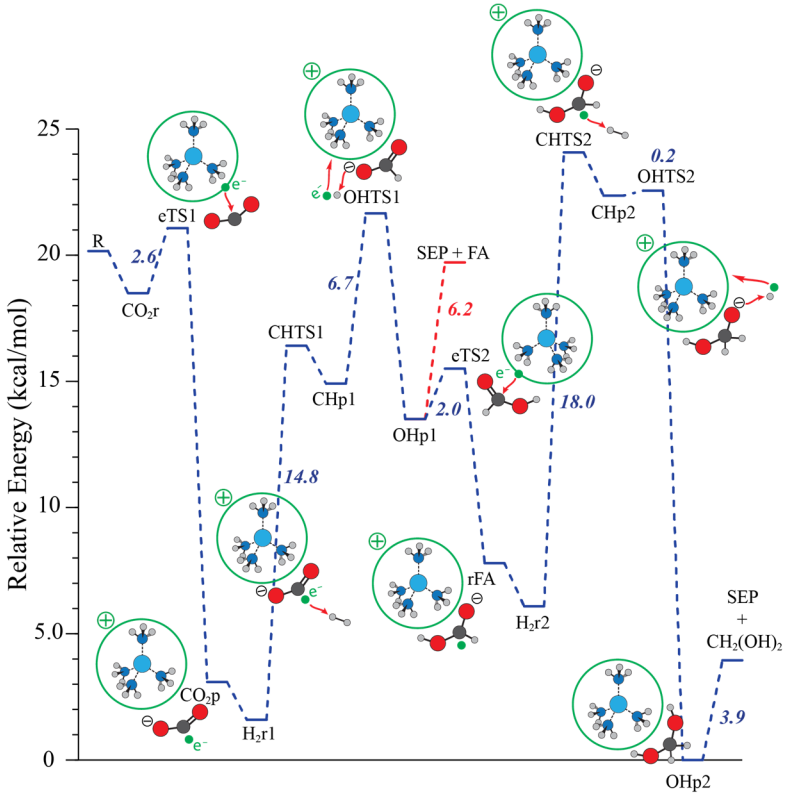

Figure 2-8. Reaction pathway of CO_2 + $2H_2$⟶ $CH_2(OH)_2$ as catalyzed by $Li(NH_3)_4$.

The transition state OHTS1 (E_a = 6.7 kcal/mol) then involves the formation of an O-H bond producing formic acid (FA) and the H electron transfers to $Li(NH_3)_4^+$ to complete the cycle. The formic acid can be released from the SEP with a barrier of 6.2 kcal/mol or undergo a

second oxidation to produce a radical $\bullet CH_2O_2^-$ (rFA) at a barrier of 2.0 kcal/mol. Following this, a second H_2 may be added through an identical process to produce finally $CH_2(OH)_2$. The barrier for the second C-H bond increases to 18.0 kcal/mol (CHTS2) while the barrier of the second O-H bond drops to only 0.2 kcal/mol (OHTS2).

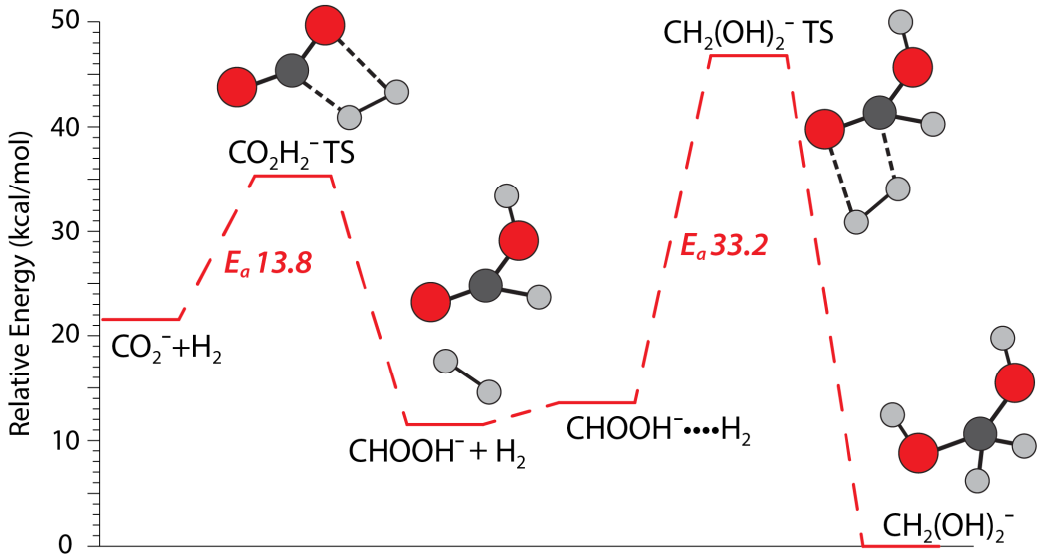

Figure 2-9. Reaction pathway of CO_2 + $2H_2$⟶ $CH_2(OH)_2$ without $Li(NH_3)_4$.

The reaction in absence of the SEP varies slightly; each H_2 addition occurs in a concerted step with a barrier of 13.8 kcal/mol and 33.2 kcal/mol for the first and second, respectively (see Figure 2-9). This first addition has a lower E_a than the combined two steps of the SEP mechanism (13.8 vs. 14.8 + 6.7); however, this is off set by the SEP's lower E_a for the second H_2 (33.2 vs 18.0 + 0.2). More importantly, $\bullet CO_2^-$ is inherently unstable with the calculated electron affinity (EA) of CO_2 as -20.1 kcal/mol, offering an additional barrier to functionalizing CO_2 in this manner. However, when coordinated to $Li(NH_3)_4^+$ the $\bullet CO_2^-$

is stabilized by 15.4 and 17.1 kcal/mol relative to $Li(NH_3)_4$•CO_2 (CO_2r) and free CO_2 (R), respectively.

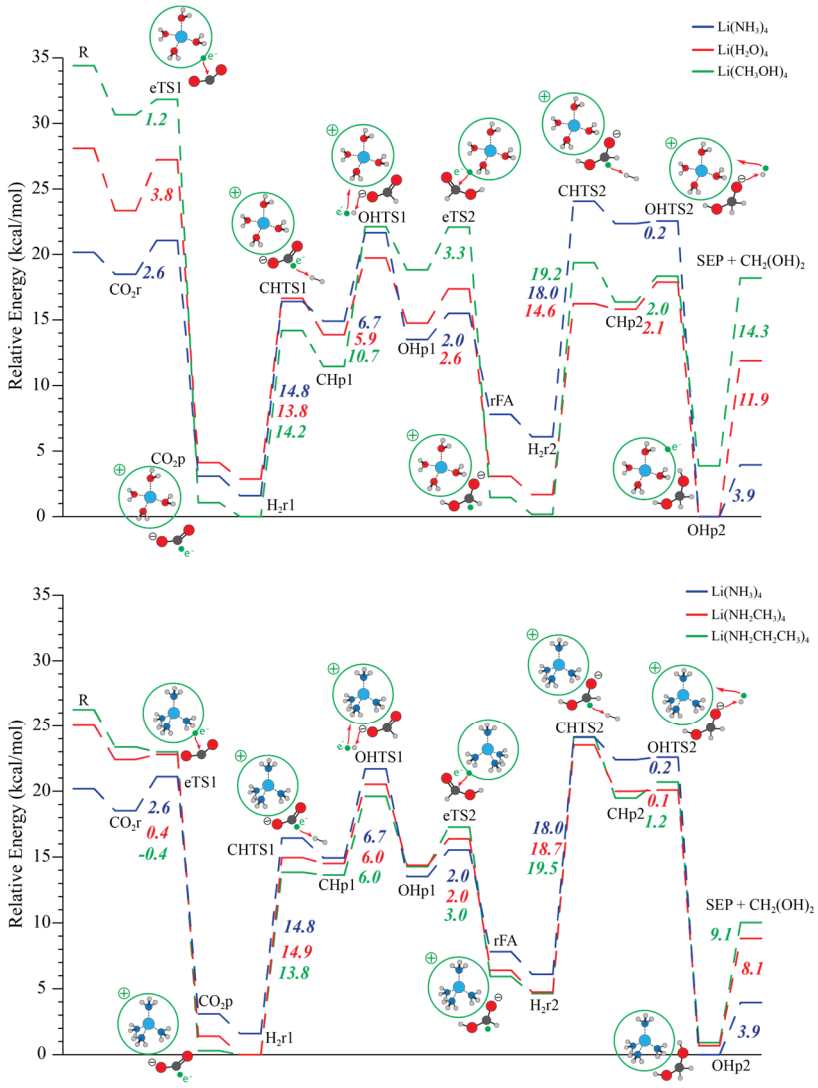

Figure 2-10. Comparison of SEP ligand effects on $CO_2 + 2H_2 \rightarrow CH_2(OH)_2$.

2.5.3 Effect of SEP Ligands on the Reaction

To examine the effect of the ligand identity on the reaction mechanism, various SEP ligands were examined; the pathways produced are shown in Figure 2-10. These ligands

may be broken into two categories: the hydroxy ligands (H_2O, CH_3OH) and the amine ligands (NH_3, NH_2CH_3, $NH_2CH_2CH_3$). From Figure 2-10, we can see the different ligands have no effect on the reaction mechanism and minimal effects on the energetics (E_a ±3 kcal/mol). One notable point of difference exists for the electron transfer step eTS1. The largest barrier occurs for $Li(H_2O)_4$ which has the most strongly bound SEP electron with an ionization energy of 3.7 eV. The IE drops to 3.4 eV with the addition of a methyl group (CH_3OH), reducing the eTS1 E_a by 2.6 kcal/mol. For the amines we see a similar trend NH_3: E_a 2.6 kcal/mol & IE 3.02 eV then NH_2CH_3: Ea 0.4 kcal/mol & IE 2.76 eV, and $NH_2CH_2CH_3$: E_a N/A & IE 2.59 eV, where ethylamine lacks a barrier for eTS1. The increasing carbon chain length results in a more diffuse SEP electron which is more weakly bound to the complex, increasing the reactivity.

2.5.4 Improving the Reaction Energetics

The energy landscapes of Figure 2-8 and Figure 2-10 plot only the relative electronic energy; in this way, they initially appear energetically favorable, but considering enthalpic and entropic effects this is no longer the case. At 298 K the methanediol reaction is endothermic and endergonic by 3.5 and 12.5 kcal/mol, respectively (see ref [55] for more details). For the SEP catalyzed reaction of CO_2 and C_2H_4, we demonstrate how reduction by the SEP leads to a radical $\bullet CO_2^-$ which may react with ethene to form a C-C bond with a radical terminal carbon which may continue reacting with ethenes in a polymerization reaction or complete the cycle to produce a lactone (see ref [55] for more details). Overall, the C_2H_4 reaction is exothermic by -22.3 kcal/mol at 298 K, but the entropy penalty of three molecules (CO_2 and 2 C_2H_4) to one (δ-lactone) results in it being endergonic by 0.94 kcal/mol. However, based on the ethene mechanism we have proposed several alternative

reactants (Figure 2-11) that we anticipate proceeding through the same mechanism and whose end products would be more energetically favorable by decreasing the number of reactants (reaction 2), increasing the number of σ-bonds formed (reaction 3), or producing aromatic products (reaction 4).

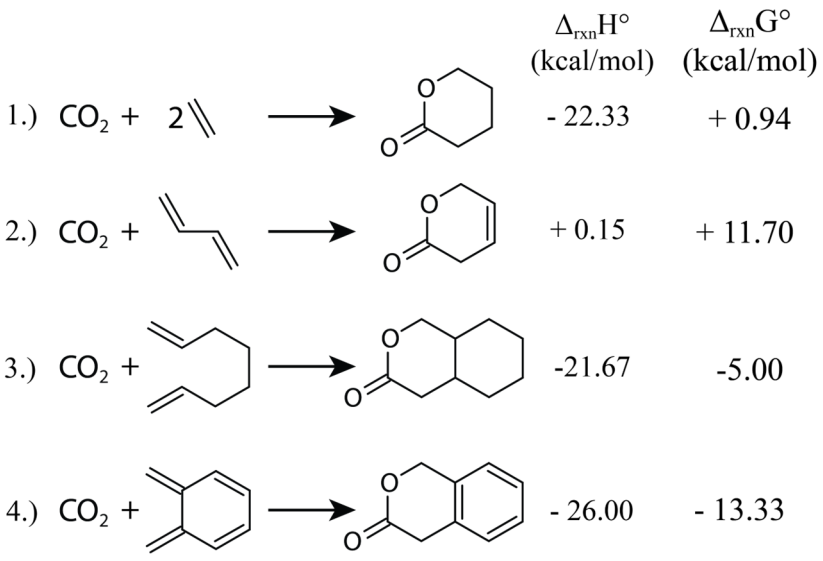

Figure 2-11. Alternative reactants for improving the SEP catalyzed reaction. Calculated at 298K.

2.5.5 Conclusions

Summarizing this work, we preformed the first mechanistic study examining the application of SEP as redox catalysts. Two trial reactions were chosen CO_2 + 2 H_2 → $CH_2(OH_2)$ and CO_2 + 2 C_2H_4 → δ-lactone. The observed energetics of these reactions were favorable at the electronic energy. For example, the methanediol pathway had low activation barriers but overall, the process was enthalpically and entropically unfavored. While not an ideal outcome, these reactions do demonstrate a major advantage offered by SEP catalysis: Currently, practical applications of carbon capture and conversion require two different molecular systems one to capture and one for the catalytic conversion of CO_2.[61] Here, the

SEP is capable of simultaneously capturing CO_2 ($\Delta H° = -0.8$ kcal/mol at 298 K) and converting it. We see that after the electron transfer, the SEP cation plays a critical role in stabilizing $\bullet CO_2^-$, which on its own is unstable with an EA of -20.1 kcal/mol. This critical first step is both enthalpically and entropically favored when the SEP is present. From there, the $\bullet CO_2^-$ may go on to react with other reagents for its conversion. Improving the overall energetics is then only a matter of selecting appropriate reactants for $\bullet CO_2^-$. Several alternatives are proposed for future study. Further, a variety of hydroxy and amine ligands were tested and shown to have negligible effect on the overall reaction pathway allowing future work to select ligands based on convenience. Notably, the ligands did affect the energetics for the reduction step with larger ligands resulting in a more diffuse SEP electron which is more reactive.

CHAPTER 3. Linked-SEPs

3.1 Aliphatic Linked-SEPs: Boron

In this section findings reported in ref [62] are briefly summarized. For computational details and more information see the provided copy in APPENDIX B: Supporting Material for Chapter 3.

Z. Jordan, S. N. Khan, B. A. Jackson, E. Miliordos, "Can boron form coordination complexes with diffuse electrons? Evidence for linked solvated electron precursors", Electronic Structure 4, 015001 (2022)

3.1.1 Introduction

In the following work we aimed to provide the first demonstration of the ability for a p-block metalloid element, boron, to form a stable solvated electron precursor where previous work existed only for s- and d- block metals. For these, it was previously shown that ligands like NH_3 may readily coordinate to valence configurations of s^1 and s^2, displacing them to the periphery to form the SEP. *Will the same be true for valence p configurations?*

3.1.2 The $(NH_3)_3BCH_3$ monomer

For boron, with a ^2P ($2s^22p^1$) ground state configuration, the occupied p orbital offers a challenge to SEP formation. Three NH_3 ligands may readily coordinate to form a stable $B(NH_3)_3$, but a fourth NH_3 ligand must approach along the axis of the occupied p orbital. From Figure 3-1 we see this approach involves a barrier of ~30 kcal/mol to form $B(NH_3)_4$ which is unstable by ~10 kcal/mol. Approaching boron instead with CH_3 is barrierless,

forming a B-CH_3 σ-bond with an energy of ~110 kcal/mol. The resulting $(H_3N)_3BCH_3$ is an SEP with an outer electron configuration of $1s^2$ and no unpaired electrons on boron.

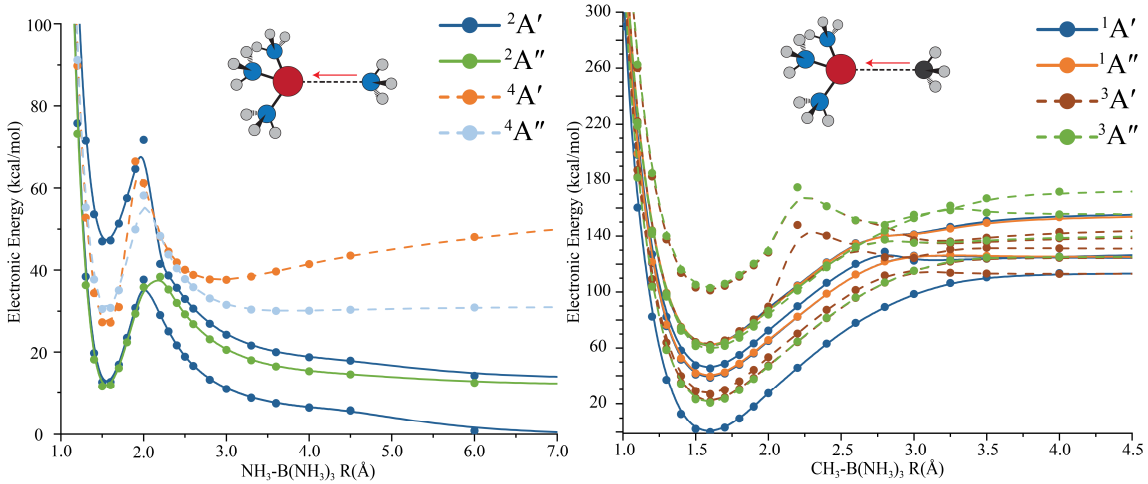

Figure 3-1. Potential energy curve for the approach of NH_3 to $B(NH_3)_3$.

The $(H_3N)_3BCH_3$ SEP is shown to follow the same *1s, 1p, 1d, 2s…* Aufbau Principle seen for the s- and d- block metal SEPs. In addition to CH_3, the systems of $(H_3N)_3BF$, $(H_3N)_3BCl$, and $(H_3N)_3BNH_2$ were studied. The identity of X in $(H_3N)_3BX$ was shown to have negligible effect on the excited states of the SEP electron. All closely agree in excitation energy with the results for $Be(NH_3)_4$ (for more details see ref [62]). Of the different $(H_3N)_3BX$ tested, $(H_3N)_3BCH_3$ was the most stable complex with an average binding NH_3 energy $D_{e,ave}$ of 14.0 kcal/mol, compared to 3.2, 8.2, and 6.6 kcal/mol for X=F, Cl, and NH_2, respectively. Compare this to $Li(NH_3)_4$ and $Be(NH_3)_4$ at 13.6[10] and 12.8[29] kcal/mol, respectively.

3.1.3 The Boron linked-SEP

Given the increased stability of $(H_3N)_3BCH_3$, this inspired us to wonder: *"What would happen if we were to connect two $(H_3N)_3BCH_3$ monomers through an aliphatic chain? In doing so, can we link two SEP centers together?"* To answer this, the stability, structure, and excited states of $(H_3N)_3B(CH_2)_{3\text{-}6}B(NH_3)_3$ were investigated. With each $(H_3N)_3BCH_2$– moiety possessing an outer electron configuration of $1s^2$, the system behaves as an analog to the He_2 molecule with fixed He-He bond length. As is the case for the $Li(NH_3)_4$ dimers, the *1s*, *1p*$_x$, *1p*$_y$, *1p*$_z$, etc. orbitals of each $(H_3N)_3BCH_2$– moiety mix to produce orbitals of σ, σ*, π, and π* character. Like He_2, the two outer electrons of each SEP couple to produce a ground state configuration of $\sigma_s^2\sigma_s^{*2}$. Where this results in an unstable molecule for He_2, the presence of the aliphatic chains keeps the two SEPs strongly bound. As the carbon chain length increases from 3 to 6 carbons, the bonding orbitals and their antibonding counterpart approach degeneracy.

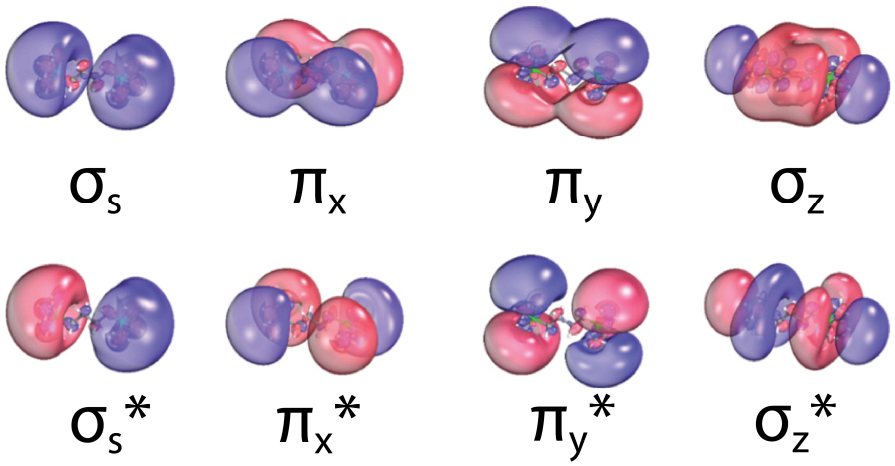

Figure 3-2. Orbitals of the linked-SEP $(H_3N)_3B(CH_2)_4B(NH_3)_3$.

The resulting work on $(H_3N)_3B(CH_2)_{3\text{-}6}B(NH_3)_3$ led to the proposal of class of compounds which we have dubbed the linked-SEP and define as:

Linked-Solvated Electron Precursor (linked-SEP)*- a complex consisting of two or more positively charged metal centers* M^{n+}*, bridged by a linker molecule(s), B, such as an alkyl chain. Each* M^{n+} *is surrounded by sufficient ligands, L, whose coordination leads to n number of valence electrons being displaced from the metal to periphery of the* L_xM^{n+} *complex. The case of a linked-SEP dimer would give:* L_xM^{n+}*–B–*$M^{n+}L_x$

3.1.4 Conclusions

In summary, this work demonstrated for the first time the ability to form solvated electron precursors using a p-block metalloid when proper ligands are chosen. We found $B(NH_3)_4$ to be unstable and ammonia alone cannot displace the three valence electrons of boron. Instead, by covalently bonding a ligand to boron the remaining two electrons can be displaced by NH_3 to form an SEP. The complexes $(H_3N)_3BX$ for X = F, Cl, NH_2, CH_3 were studied; each possessed a ground state configuration of an outer $1s^2$. While the X ligand introduced an anisotropy which destabilized the s-type and $1p_z$ orbitals; overall, the excited state energetics strongly agree with $Li(NH_3)_4$ and $Be(NH_3)_4$. The $X = CH_3$ complex exhibited the highest stability with NH_3 average dissociation energies comparable to that of $Li(NH_3)_4$ and $Be(NH_3)_4$. We demonstrated for the first time the ability to use an aliphatic chain to bind two SEPs together to produce a linked-SEP. Excited states of $(H_3N)_3B(CH_2)_{3\text{-}6}B(NH_3)_3$ were calculated and shown to have a structure comparable to the He_2 dimer, with the two terminal SEPs interacting to produce orbitals of σ, σ*, π, and π* character.

3.2 Aliphatic Linked-SEPs: Beryllium

In this section the most important findings reported in ref [29] are summarized. For computational details and more information see the provided copy in APPENDIX B: Supporting Material for Chapter 3.

B. Jackson and E. Miliordos, "The nature of supermolecular bonds: investigating hydrocarbon linked beryllium solvated electron precursors", Journal of Chemical Physics 156, 194302 (2022)

3.2.1 Introduction

The work with boron and the linked-SEP $(H_3N)_3B(CH_2)_{3\text{-}6}B(NH_3)_3$ inspired us to wonder what other kinds of linked-SEPs could be constructed. The alkaline earth metal SEPs have seen significant theoretical and experimental exploration. *Could we use the same aliphatic technique to bridge an s-block metal? How would the aliphatic chain alter the properties of the SEP, which are well described previously?*

3.2.2 The $(NH_3)_3BeCH_3$ monomer

Shown in Figure 3-3 are the MRCI curves for the formation of $BeCH_3$ and the resulting orbitals. In its ground state Be is a valence $2s^2$, approaching $\bullet CH_3$ the two form a strong covalent bond (D_e 57.8 kcal/mol at MP2) and Be retains one electron in a s-type orbital polarized away from CH_3. Three ammonia ligands may coordinate to Be with ZPE corrected MP2 binding energy D_0 of 18.6, 22.9, and 22.5 kcal/mol for the first, second, and third ammonia. The average binding energy $D_{0,ave}$ is 21.3 kcal/mol. Coordination of the three NH_3 displaces the polarized 2s electron of Be to an outer 1s-type orbital. Like all SEPs,

$(H_3N)_3BeCH_3$ exhibits the same outer electronic structure of 1s, 1p, 1d, etc.; however, the methyl group is unable to solvate electrons resulting in these outer orbitals being polarized away from the CH_3 and any orbitals with components along this bond axis (the z-direction) are destabilized (see Figure 3-4).

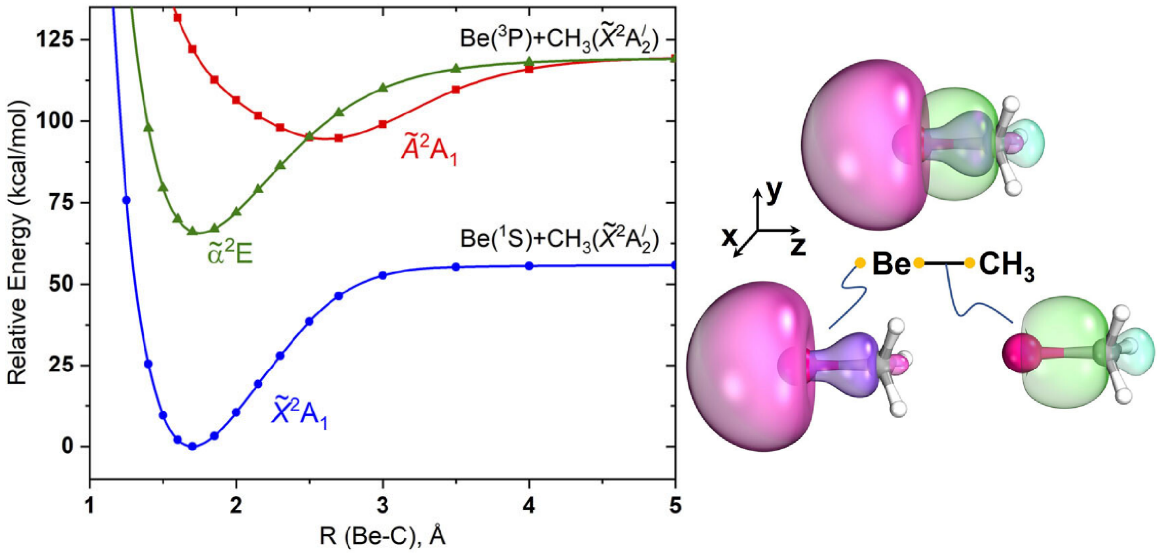

Figure 3-3. The formation of the Be-C bond in $BeCH_3$.

Now we compare the excitation energies for the isoelectronic, "one electron" systems of $Li(NH_3)_4$, $Be(NH_3)_4^+$, and $(H_3N)_3BeCH_3$. We would expect that the smaller nuclear charge of the Li^+ center in $Li(NH_3)_4$ would result in lower excitation energies than $Be(NH_3)_4^+$ with its Be^{2+} center. Comparing them, the excitations of $Li(NH_3)_4$ from 1s to 1p, 1d, and 2s occur at 0.72, 1.42, and 1.52 eV, for $Be(NH_3)_4^+$ these are 1.39, 2.37, and 3.34 eV, confirming this.[1,10] Turning to $(H_3N)_3BeCH_3$ we find average excitation energy for 1s to 1p, 1d, and 2s are 1.05, 1.90, and 1.81 eV. These lie between that of $Li(NH_3)_4$ and $Be(NH_3)_4^+$, demonstrating the Be in $(NH_3)_3BeCH_3$ has an effective charge intermediate between +1 and +2.

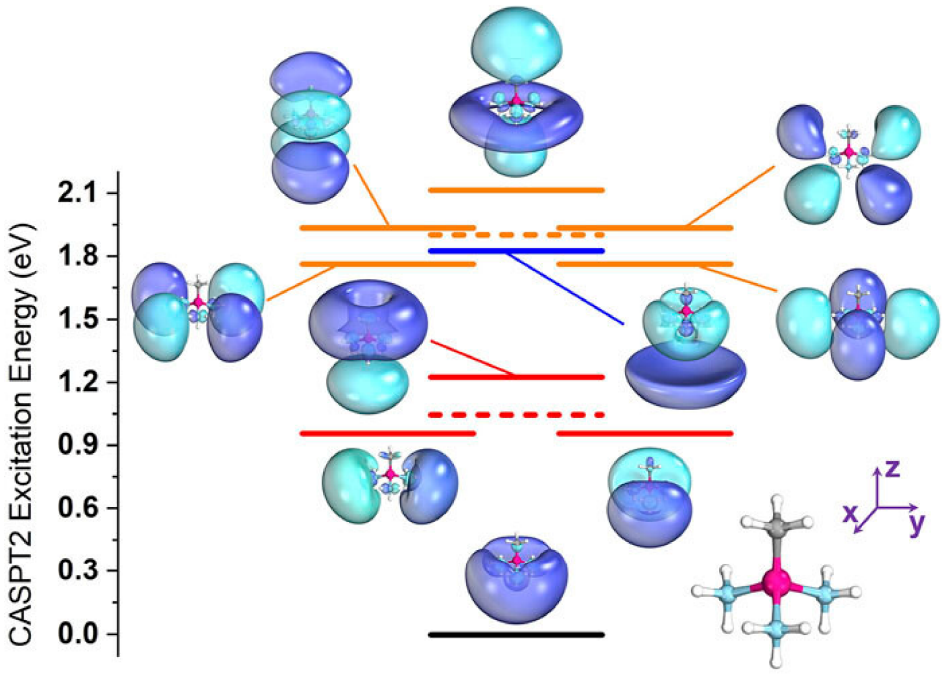

Figure 3-4. SEP orbitals of $(H_3N)_3BeCH_3$.

The use of $–CH_3$ permits two $(H_3N)_3BeCH_3$ monomers to be strongly linked through an aliphatic bridge to produce the linked-SEP dimer $(NH_3)_3Be(CH_2)_nBe(NH_3)_3$. Here, the structure and excited states of $(NH_3)_3Be(CH_2)_{1\text{-}6}Be(NH_3)_3$ were studied, examining the effect of the carbon chain length therein. Each $(NH_3)_3BeCH_2–$ moiety possesses one diffuse electron, as such they may couple as either a singlet or triplet. For SEPs previously, we've seen how sigma bonds can form between these diffuse orbitals. This begs the question: *As the carbon chain length grows, will it grow linearly (in a trans conformation) to reduce steric hinderance in the chain or will the chain favor a curved (or cis) structure to promote overlap between the SEP orbitals?*

3.2.3 "Linear" Be Linked-SEPs

Provided in Figure 3-5 are the optimal structures obtained for the 'linear' and 'curved' conformers of $(NH_3)_3Be(CH_2)_{1\text{-}6}Be(NH_3)_3$. Beginning with the linear system, the addition of each carbon grows the chain in a staggered orientation keeping the two Be units at 180° separation. Odd numbered chains are C_{2v} symmetry and the even are C_{2h}. Each carbon on average increases the Be-Be distance by 1.34 Å. The D_0 at MP2 for each ammonia ligand is 19.8 ± 6.4, 21.7 ± 7.6, 21.6 ± 3.6, 21.8 ± 2.0, 21.8 ± 2.6, and 21.8 ± 2.6 kcal/mol for n = 1−6, respectively. Comparing these to $(NH_3)_3BeCH_3$ (D_0 18.6-22.5 kcal/mol), we see the alkyl chain has a negligible effect on the ammonia binding energy. The same was seen for the boron linked-SEP (see Section 3.1 and ref [62]).

Shown in Figure 3-6 are the orbitals populated in the ground and lowest excited states. As with the boron linked-SEP (see Section 3.1) the two outer SEP 1s orbitals may combine in-phase and out-of-phase to give the σ_s and σ_s*. The $1p_x$ and $1p_y$ may combine similarly to give $\pi_{x,y}$ and $\pi_{x,y}$*. The $1p_z$ of each SEP may combine as σ_z^1 and σ_z* but are significantly destabilized due to their orientation along the carbon chain. As the carbon chain length increases, the overlap between the SEP 1s and 1p orbitals decreases leading to the bonding and antibonding orbitals approaching degeneracy. Table 3-1 lists excitation energies for the lowest lying excited states of linear $(NH_3)_3Be(CH_2)_nBe(NH_3)_3$ calculated at CASPT2.

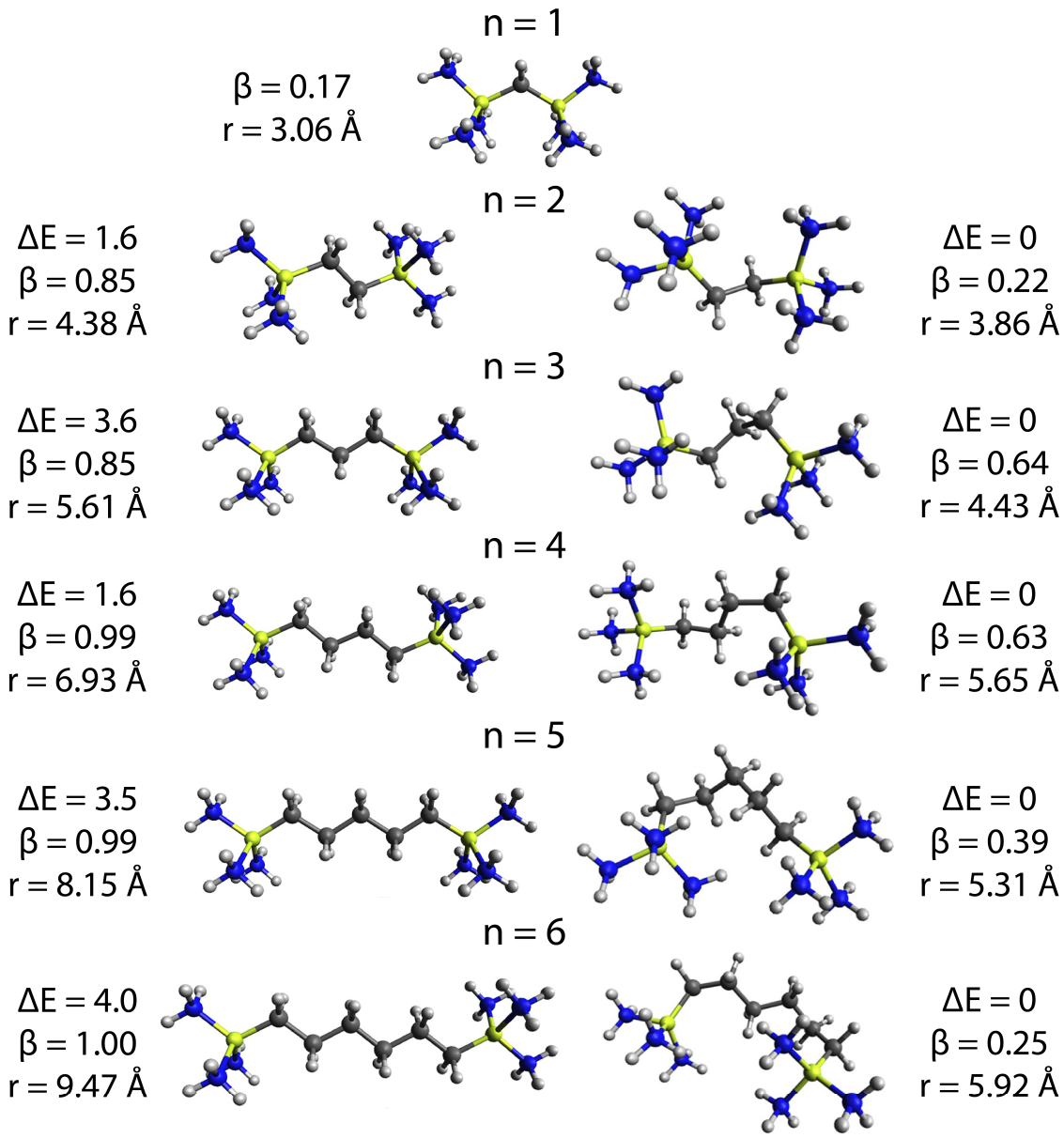

Figure 3-5. Optimized 'linear' and 'curved' structures of $(NH_3)_3Be(CH_2)_{1-6}Be(NH_3)_3$. Relative energy, ΔE, of the two conformers is calculated at CASTP2 (kcal/mol). The diradical character β (see Equation 3-1*) and r the Li-Li distance is also provided.*

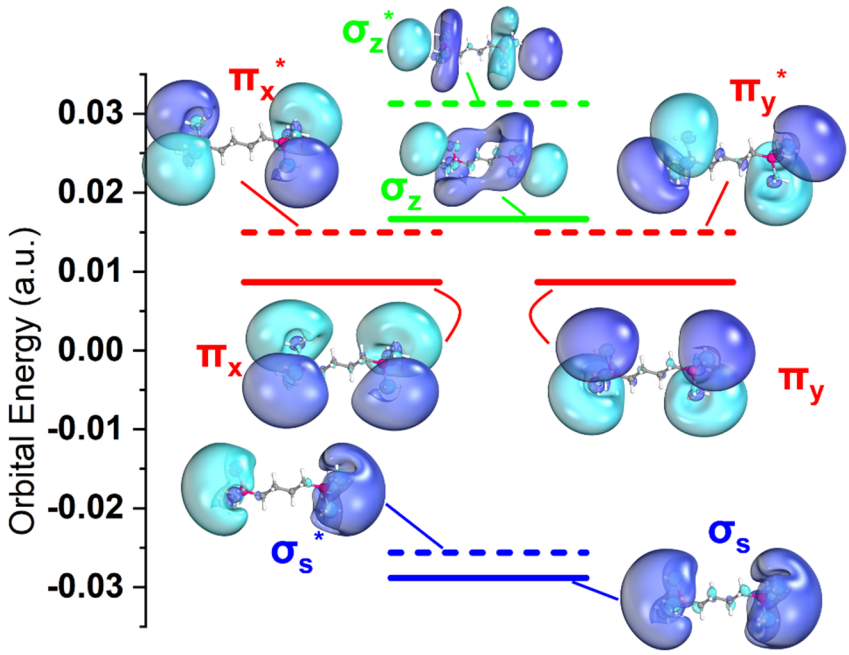

Figure 3-6. Orbitals of the "linear" $(NH_3)_3Be(CH_2)_nBe(NH_3)_3$.

The ground state of all chain lengths studied is a singlet involving two major components of σ_s^2 and σ_s^{*2} character. Following this, are excitations to a triplet $\sigma_s^1\sigma_s^{*1}$ state which for n = 1 is 0.33 eV. At n = 2, 3 this drops to 0.03 and 0.02 eV, respectively, before becoming degenerate with the singlet for n > 3. Following this are a set of several singlet and triplet states ranging from 0.5-1.0 eV involving various combinations $\sigma_s^1\pi^1$, $\sigma_s^{*1}\pi^1$, $\sigma_s^1\pi^{*1}$, and $\sigma_s^{*1}\pi^{*1}$. As the carbon length increases, these states become increasingly multireference due to the degeneracy of bonding and antibonding orbitals.

Table 3-1. Excited states of the "linear" $(NH_3)_3Be(CH_2)_nBe(NH_3)_3$.

State [a]	Config.	$n = 1$	$n = 2$	$n = 3$	$n = 4$	$n = 5$	$n = 6$
$^1A_1/^1A_g$	σ_s^2/σ_s^{*2}	0.00	0.00	0.00	0.00	0.00	0.00
$^3B_2/^3B_u$	$\sigma_s^1\ \sigma_s^{*1}$	0.33	0.03	0.02	0.00	0.00	0.00
$^3B_1/^3B_u$	$\sigma_s^1\ \pi^1/\sigma_s^{*1}\ \pi^{*1}$	0.57	0.76	0.78	0.90	0.89	0.93
$^3A_1/^3A_u$	$\sigma_s^1\ \pi^1/\sigma_s^{*1}\ \pi^{*1}$	0.70	0.70	0.76	0.87	0.89	0.91
$^1B_2/^1B_g$	$\sigma_s^{*1}\ \pi^1/\sigma_s^1\ \pi^{*1}$		0.81	0.75	0.88	0.89	0.91
$^1A_2/^1A_g$	$\sigma_s^{*1}\ \pi^1/\sigma_s^1\ \pi^{*1}$		0.85	0.86	0.90	0.89	0.93

The ground state for all chain lengths investigated is a multi-reference state characterized as $c_1\sigma_s^2 + c_2\sigma_s^{*2}$ with c_1 and c_2 varying by chain length, where $\sigma_s \approx 1s_L + 1s_R$ and $\sigma_s^* \approx 1s_L - 1s_R$ with $1s_L$ and $1s_R$ being the outer 1s orbitals of the left and right terminus. From this, the diradical character β may be calculated as:

$$\beta = \frac{2c_2^2}{c_1^2 + c_2^2}\ , |c_2| > |c_1| \qquad 3\text{-}1$$

Briefly, the diradical character describes the extent to which the two electrons are uncoupled, with β = 1.0 meaning fully separate and β = 0.0 meaning fully coupled. See Section 3.3 for more details. We would expect that as the carbon chain length grows and the SEPs are increasingly separated then the diradical character should correspondingly increase. Plotted in Figure 3-7 is the relationship between chain length and diradical character.

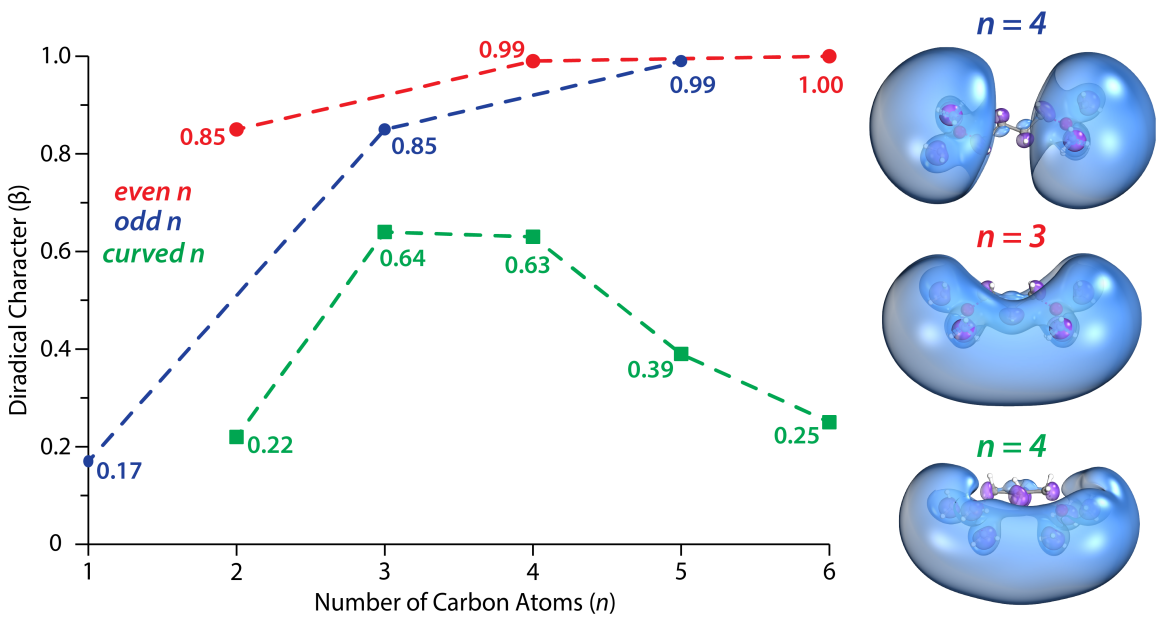

Figure 3-7. $(NH_3)_3Be(CH_2)_{1\text{-}6}Be(NH_3)_3$ and the effect of carbon chain length on diradical character.

For n = 1, β is 0.18 which indicates a system which is predominately a closed-shell σ_s^2. However, for n = 2 and 3 we get two nearly identical values of 0.78 and 0.81. This could be explained by the difference between the C_{2v} and C_{2h} structures where the former place four out of six ammonia ligands on the same side of the molecule and the latter have three on each side. For C_{2v}, this would promote solvation of the electrons on the side with four NH_3 and facilitate the overlap of the outer 1s orbitals. This is evidenced by the σ_s orbitals of n = 3 and 4 shown in Figure 3-7. Within the even and odd series, β smoothly converges to 1 with chain length.

3.2.4 The Curved Be Linked-SEPs

Moving on to the 'curved' systems, the carbon chain grows in a 'cis' or gauche configuration to promote interacting between the terminal SEPs. The optimized structures are shown in Figure 3-5. Two things determine the relative stability of the curved vs linear

isomers: the steric strain and gauche interaction introduced by rotation about the C-C bond and the stabilization resulting from the bonding occurring between the two SEPs. At MP2 the relative energies of the curved vs. linear are nearly degenerate with the linear favored by 1.8-3.4 kcal/mol. At CASPT2 though, the trend is flipped with the curved favored by 1.6-4.0 kcal/mol, illustrating the two isomers to be highly competitive.

Comparing the linear and curved structures, we see in Figure 3-7 that β of the $n = 2$ chain drops from 0.85 to 0.22 due to the increased 1s overlap. The β for curved structures then increases to 0.64 and 0.63 for $n = 3$ and 4, compare this to the 0.85 and 0.99 of the linear. Remarkably, at $n = 5$ the diradical character of the curved drops again until $n = 6$ with a nearly closed-shell system of $\beta = 0.25$. Here, the carbon chain has lengthened enough to promote significant overlap between the two 1s orbitals. In addition to the diradical character, CASPT2 excited states for the curved systems were calculated to provide a means to experimentally distinguish the "curved" and "linear" species (see ref [29] and APPENDIX B: Supporting Material for Chapter 3 for details).

3.2.5 Conclusions

Here, we studied the electronic structure of the SEP $(NH_3)_3BeCH_3$. The Be–CH_3 bond results in Be with an in-situ $2s^1$ configuration which the coordination of three NH_3 ligands displaces to the periphery to form an $1s^1$ SEP configuration analogous to the hydrogenic atom. We compare this to the isoelectronic $Li(NH_3)_4$ and $Be(NH_3)_4^+$ to show the Be in $(NH_3)_3BeCH_3$ bears charge intermediate to +1 and +2.

We then show how two $(NH_3)_3BeCH_3$ moieties may be linked through an alkylchain to produce a linked-SEP $(NH_3)_3Be(CH_2)_nBe(NH_3)_3$ with a single electron on each beryllium-

ammonia terminus. It is shown that the alkyl bridge has a negligible effect on the stability of the Be-NH_3 bonds. The terminal SEPs may couple to produce orbitals of σ_s, σ_s*, $\pi_{x,y}$, $\pi_{x,y}^*$, σ_z^1, and σ_z* character. We find that the carbon chain length may grow in either a staggered or gauche configuration, the former leads to greater separation between the two Be terminals and weaker coupling between their outer electrons while the latter allows the Be terminals to rotate towards each other to promote bonding interactions between the SEPs. The two isomers found are shown to be energetically competitive at CAM-B3LYP and CASPT2. It is expected that for sufficiently long carbon chains, the curved structure will win out as the steric strain introduced by rotation decreases.

3.3 Diamine Linked-SEPs: Lithium

3.3.1 Introduction

In the previous sections, it was shown how aliphatic chains may be used to bind two SEPs together. In both cases, the linkage occurs through a very strong M-CH_3 bond with a D_e of 92.96 and 57.8 kcal/mol at MP2 for B-CH_3 and Be-CH_3, respectively. As a disadvantage, this has the effect of each bond depleting the resulting SEP of an electron which limits the number of possible linkages. An alternative comes in the use of diamine ligands. We've already shown how NH_3 ligands may be substituted with carbon chains to produce SEPs using methyl and ethylamine (see Section 2.5). Previous work has shown lithium-ethylamine SEPs to have stability comparable to $Li(NH_3)_4$.[47] In addition, expanded metals composed of methylamine lithium complexes, mixed $Li(NH_3)_x(NH_2CH_3)_{4-x}$ species, have been experimentally synthesized and structurally characterized, while their electronic structure has been examined theoretically.[22,39–46]

From this, we would expect the diamines composed of terminals linked by a carbon chain will allow the production of linked-SEPs which are stable but do not consume any metal valence electrons in their formation. To this end, we investigated the system of $(NH_3)_3LiNH_2(CH_2)_nH_2NLi(NH_3)_3$ for n = 1–10.

For brevity's sake, we introduce a naming scheme for linked-SEPs. The system of $(NH_3)_3LiNH_2(CH_2)_nH_2NLi(NH_3)_3$ will be denoted as *LiAm-LSEP(n)* where *Li* denotes the metal identity, *Am* an amine linkage with carbon length of *n*, and *LSEP* denotes it as a linked-SEP. The previous system of $(NH_3)_3Be(CH_2)_nBe(NH_3)_3$ would be denoted as *BeMe-LSEP(n)* with *Me* denoting the aliphatic Be–CH_2 linkage.

3.3.2 Computational Details

The geometry optimizations for *LiAm-LSEP(n)* n = 1−10 used density functional theory (DFT) and the CAM-B3LYP[7] functional combined with the aug-cc-pVDZ[63–66] basis set for all atoms. CAM-B3LYP has been shown to provide geometries equivalent to MP2[67–69] and CCSD(T)[70,71] geometries for SEPs.[28] These geometries are used for the subsequent gas-phase calculations. The triplet state (S=1) was used for the optimization as it is single reference and described by DFT better than the multi-reference singlet state (see below). The electronic structure analysis for the ground and low-lying excited states was done with multi-reference methods using MOLPRO.[72,73] The active space for the reference complete active space self-consistent field (CASSCF) calculations included the two diffuse electrons in eight orbitals representing the 1s, $1p_x$, $1p_y$, $1p_z$ peripheral orbitals of each SEP unit (see Figure 3-8). The dynamic correlation was obtained at the CASPT2 level promoting all valence electrons to the virtual space. To remove possible divergences caused by intruder states, a

level shift value of 0.2 a.u. and an IPEA (shift parameter for orbital energies) value of 0.25 a.u. were applied.[2,3] The cc-pVDZ basis set was used for Li, N, and C, and the d-aug-cc-pVDZ for all H centers.[63–66] For the DFT calculations on the lowest singlet and triplet states with the B3LYP[74–77] and PBE[4] functionals, we used Gaussian16[78] and the cc-pVTZ (Li, N, C) aug-cc-pVTZ(H) sets.[63–66]

3.3.3 Bonding in H_2 and diradical character

The frontier peripheral orbitals of $(NH_3)_3LiNH_2(CH_2)_nH_2NLi(NH_3)_3$, *LiAm-LSEP(n)* are shown in Figure 3-8 and mirror the structure seen for $(NH_3)_3Be(CH_2)_nBe(NH_3)_3$, *BMe-LSEP(n)*, and $(NH_3)_3B(CH_2)_nB(NH_3)_3$, *BeMe-LSEP(n)*. For both *BeMe-LSEPs* and *LiAm-LSEPs*, each SEP unit bears one diffuse electron in a pseudospherical s-type orbital surrounding the metal-ammonia center and is analogous to a hydrogenic atom.

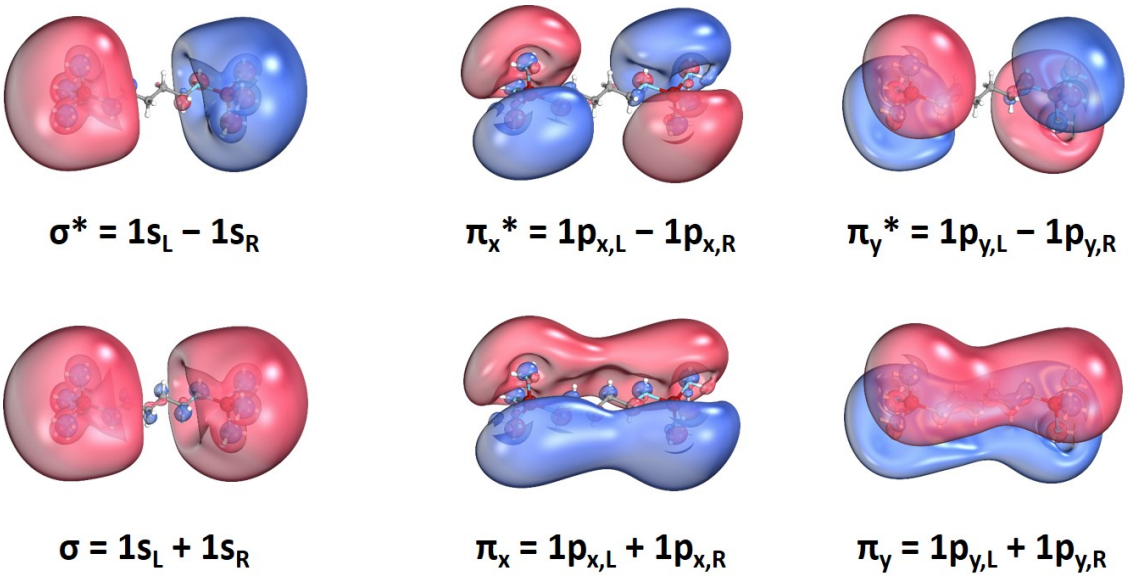

Figure 3-8. Orbitals of LiAm-LSEP for n=4.

As such, we can describe the interaction of these electrons within the framework of bonding in H_2. The electrons of two hydrogen atoms may couple into a singlet (S=0) or triplet (S=1). The wavefunctions of these two spin-states may be expressed as:

$$\left|\Psi_{S=0;M_S=0}\right\rangle = \frac{1}{\sqrt{2}}\left(\left|1s_R\,\overline{1s_L}\right\rangle - \left|\overline{1s_R}\,1s_L\right\rangle\right) \qquad 3\text{-}2$$

$$\left|\Psi_{S=1;M_S=1}\right\rangle = \left|1s_R\,1s_L\right\rangle \qquad 3\text{-}3$$

where R and L denote the right and left H atoms or SEP units, and kets denote Slater determinants. The $1s_R$ and $\overline{1s_R}$ notation denotes α and β spins, respectively. Due to the symmetry of the Hamiltonian, the $1s_R$ and $1s_L$ localized orbitals are mixed into the "bonding" and "anti-bonding" orbitals $\sigma = 1s_R + 1s_L$ and $\sigma^* = 1s_R - 1s_L$, respectively. In the σ/σ* basis, the same two wavefunctions are written equivalently as:

$$\left|\Psi_{S=0;M_S=0}\right\rangle = \frac{1}{\sqrt{2}}(|\sigma\,\overline{\sigma}\rangle - |\sigma^*\,\overline{\sigma^*}\rangle) \qquad 3\text{-}4$$

$$\left|\Psi_{S=1;M_S=1}\right\rangle = |\sigma\,\sigma^*\rangle \qquad 3\text{-}5$$

Equally, the singlet wavefunction may be expressed in the form of:

$$\left|\Psi_{S=0;M_S=0}\right\rangle = c_1|\sigma\,\overline{\sigma}\rangle - c_2|\sigma^*\,\overline{\sigma^*}\rangle \qquad 3\text{-}6$$

Here we may introduce the term diradical character β which characterizes the extent to which the two electrons are coupled and expressed as:

$$\beta = \frac{2c_2^2}{c_1^2 + c_2^2} \qquad 3\text{-}7$$

The CASSCF potential energy curve for H_2 is given in Figure 3-9. At infinite separation, the singlet and triplet states are degenerate. Here, the coefficients c_1 and c_2 of the singlet wavefunction are equivalent to give $\beta = 1.0$, indicating 100% diradical character and the two electrons are completely independent. As the two H atoms approach, the c_1 coefficient gradually increases until at the equilibrium geometry it wholly dominates to give the H−H an effectively single-reference σ^2 state. In the span between full separation and the equilibrium geometry we see a range of values for c_1 and c_2.

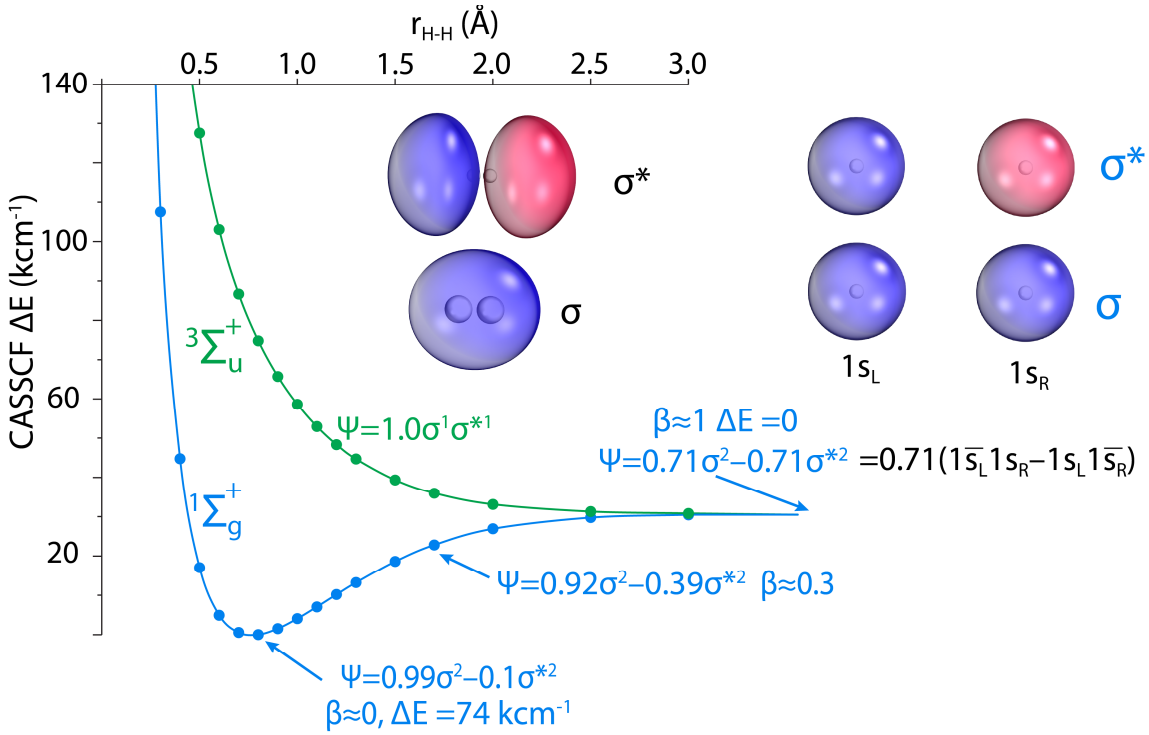

Figure 3-9. CASSCF Potential energy curve for H_2.

3.3.4 Diradical character in linked-SEPs

The *BeMe-LSEPs* and *LiAm-LSEPs* may be interpreted in much the same way to H_2 with the carbon chain length effectively fixing the H equivalent "atoms" at specific distances. Given in Table 3-2 are the CASSCF normalization coefficients (from Equation *3-6*), and the singlet-triplet splitting (ΔE, cm^{-1}). Values for BeMe-LSEP come from ref [29] (see Section 3.2). The splitting and diradical character for the *LiAm-LSEPs* are plotted in Figure 3-10.

Table 3-2. Diradical character of Linked-SEPs.

	LiAm-LSEP(n)				*BeMe-LSEP(n)*[c]	
n [d]	c_1[a]	c_2[a]	β_r	ΔE[b]	β	ΔE[b]
−1	—	—	—	—	0.165	3052.4
0	—	—	—	—	0.852	164.5
1	0.8800	0.2915	0.198	783.9	0.855	86.7
2	0.8327	0.4897	0.514	126.9	0.994	-0.2
3	0.7774	0.6089	0.760	45.2	0.988	0.6
4	0.7395	0.6657	0.895	8.5	1.000	0.03
5	0.7237	0.6863	0.947	2.8		
6	0.7142	0.6979	0.977	0.4		
7	0.7106	0.7024	0.988	0.1		
8	0.7084	0.7051	0.995	−0.01		
9	0.7077	0.7061	0.998	−0.01		
10	0.7072	0.7067	0.999	−0.01		

[a] Normalization coefficients of σ_s^2 and σ_s^{*2}, [b] singlet-triplet splitting (cm^{-1}),
[c] Values from ref [29]
[d] Number for BeMe-LSEPs are with respect to the $(NH_3)_3BeCH_2-$ moiety, as such $n = 0$ refers to $(NH_3)_3BeCH_2-CH_2Be(NH_3)_3$ and $n = -1$ is $(NH_3)_3BeCH_2-Be(NH_3)_3$

The plot of Figure 3-10 shows a clear decrease in diradical character from *LiAm-LSEP(10)* to *LiAm-LSEP(1)*, ranging from β = 0.999 or 99.9% to β = 0.198 or 19.8%. The singlet-triplet splitting inversely correlates with chain length, with the largest for $n = 1$ at 783.9 cm^{-1} dropping to <1 cm^{-1} for $n \geq 6$. The replacement of the SEP unit from $(NH_3)_3LiNH_2-$ to $(NH_3)_3BeCH_2-$ dramatically changes the electronic structure. For $n = 1$, the diradical character for the latter is already 85.5% with a splitting of 86.7 cm^{-1} (see Table 3-2). For $n \geq 2$, the two electrons are effectively coupled into an open-shell singlet (β ~ 1, ΔE ~ 0). This is a result of the diffuse electron of each $(NH_3)_3BeCH_2-$ terminus being polarized away from the chain to avoid the $-(CH_2)_n-$ side.

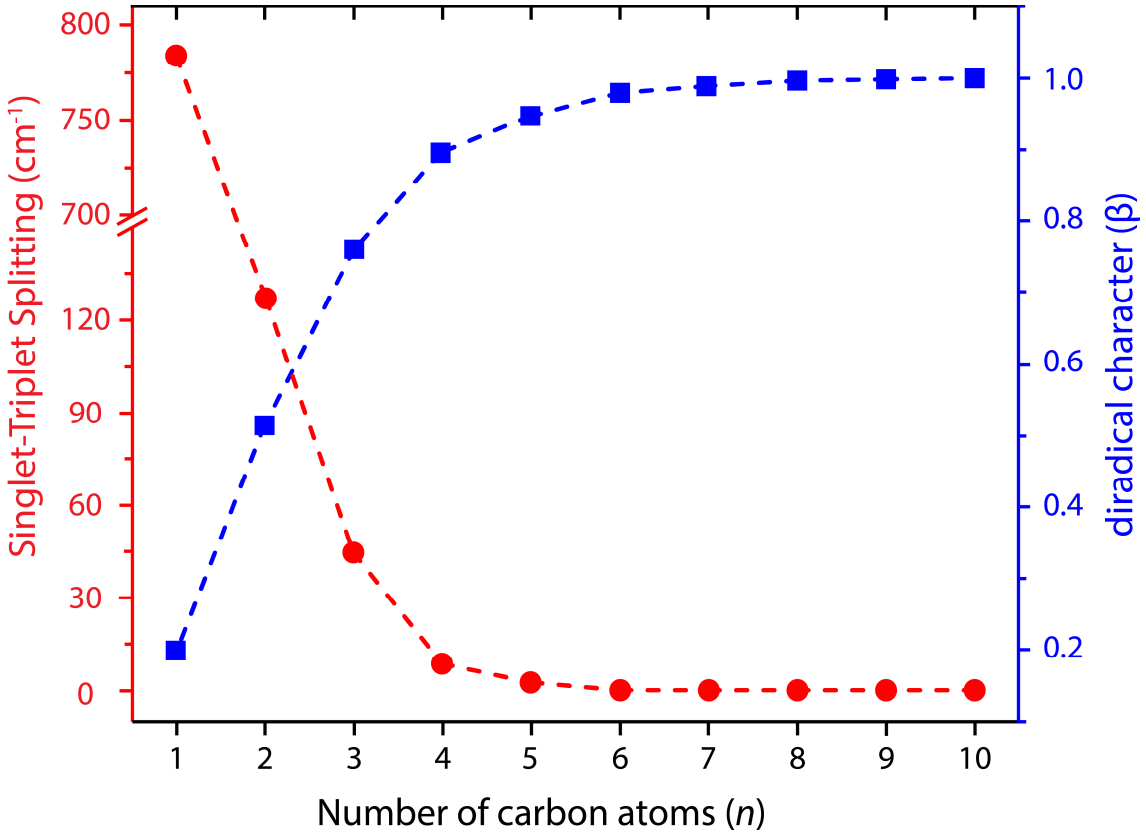

Figure 3-10. Diradical character for LiAm-LSEPs.

This minimizes the overlap of the $1s_R$ and $1s_L$ orbitals. On the other hand, the $(NH_3)_3LiNH_2$– complex distributes the density of the diffuse electron nearly evenly which facilitates the mixing of the $1s_R$ and $1s_L$ orbitals. This favors the σ^2 configuration, decreasing the diradical character and increasing the singlet-triplet splitting. If we remove one CH_2 unit from *BeMe-LSEP(1)* to make $(NH_3)_3BeCH_2–CH_2Be(NH_3)_3$ ($n = 0$ in Table 1), the diradical character is practically unchanged (85.2%) but ΔE doubles (164.5 cm^{-1}). Removing an additional CH_2 to give $(NH_3)_3Be–CH_2–Be(NH_3)$ ($n = -1$ in Table 1), gives a β that is nearly equal to that of *LiAm-LSEP(1)* at 16.5% and ΔE soars to 3052.4 cm^{-1}. Conclusively, N–H bonds along the linking molecule promote electronic conduction, whereas C–H bonds isolate the two diffuse electrons, increasing diradical character and decreasing ΔE. Based on these results, we can conclude that molecular linked-SEPs which are bridged through covalent methylene bonds

will have a significantly decreased degree of correlation between SEP electrons compared to diamine bridges.

3.3.5 LiAm-LSEP Excited States

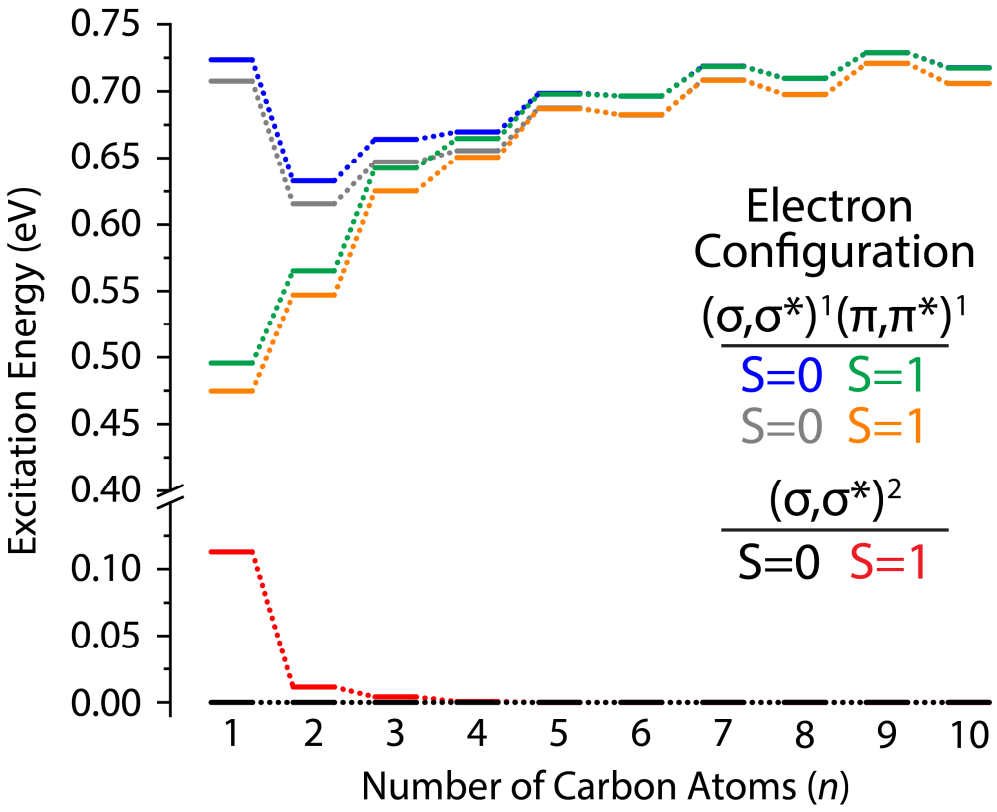

Figure 3-11. Excited states of LiAm-LSEPs.

Additionally, we examined the next four excited states of the *LiAm-LSEPs*. Consistent with our previous work on *BeMe-LSEPs*[29] and *BMe-LSEPs* [62] (see above), these electronic states involve a promotion of one electron to the π and π* orbitals of Figure 3-8. These are the constructive (+) and destructive (−) combinations of the $1p_x$ and $1p_y$ orbitals of the SEP termini. Computed excitation energies are plotted in Figure 3-11 and depict the $(\sigma, \sigma^*)^2$ states as well separated from those bearing occupation of π and π* orbitals. For n = 1, excitation to the state $\sigma^1\pi^1$ occurs at ~0.48 eV (3871.5 cm^{-1}) and increases to ~0.71 eV

(5726.5 cm^{-1}) for n = 10. The CASSCF/CASPT2 results for *LiAm-LSEPs* show ground state $(\sigma, \sigma^*)^2$ orbitals are produced from mixtures of SEP 1s orbitals and negligible hybridization of higher orbitals e.g., 1p, and states involving occupation of these higher orbitals (π and π^*) are well separated from the ground state for $n > 2$.

3.3.6 Conclusions

Here, we studied the electronic structure of $(NH_3)_3LiNH_2(CH_2)_nH_2NLi(NH_3)_3$ for n = 1−10, denoted as *LiAm-LSEP(n)*. It is shown how each $(NH_3)_3LiNH_2CH_2-$ moiety behaves as an analog to the hydrogenic atom. As such, the bonding scheme and electronic wavefunction of H_2 along its potential energy curve is used as an entry point to understand the bonding in *LiAm-LSEPs* where the alkyl chain effectively fixes the two hydrogenic atoms at specific distances along a congruent potential energy curve. A detailed analysis of the diradical character β is provided and compared to previous work on *BeMe-LSEPs* (ref [29] and Section 3.2). The diamine connection is shown to promote electron interaction at longer distances between the two SEP centers with increasing carbon chain length resulting in a much slower increase to β as compared to the *BeMe-LSEPs*. The electronic structure and SEP bonding orbitals of *LiAm-LSEPs* are shown to have strong agreement with that of *BeMe-LSEPs* and *BMe-LSEPs*. The ground state for all n is a combination of σ^2 and σ^{*2} configurations and low-lying excited states involve population of π and π^* orbitals. For $n >$ 2, these states are well separated from the ground state (>0.62 eV) and increasing with chain length.

CHAPTER 4. Lithium Diamine Materials

4.1 Introduction

In the previous chapter, we examined the structure of *LiAm-LSEPs* and showed how the use of a single diamine ligand may allow two SEPs to be stably linked together. The diamine ligands have weaker ligand bonds compared to the linked-SEPs bridged with covalent aliphatic linkages, however they offer the advantage of not depleting the metal of a valence electron when coordinating and the amine promotes electron coupling between the SEPs.

This naturally leads one to wonder: *"If we can bridge two $Li(NH_3)_4$ SEP centers when an ammonia ligand is replaced with a diamine, can we do the same for all four of the ligands? If so, can we create a material composed of a grid of many linked lithium-diamine centers?*

With the knowledge that $Li(NH_3)_4$ is tetrahedral, we have designed a novel material based on the crystal structure of diamond (also tetrahedral) where each C atom is replaced with a $Li(NH_2{-})_4$ and in place of the diamond C−C bonds are diamine chains which link each $Li(NH_2{-})_4$ center. For brevity's sake, these systems are denoted as *LiAmCn* where *Li* denotes the metal identity, *Am* the amine linker, and *C* the aliphatic chain of length *n*. For example, the repeating motif of $(NH_2(CH_2)_nNH_2)_3Li(NH_2(CH_2)_nNH_2)Li$ would be *LiAmC3*. The n = 1−10 systems are studied. A crystal structure of *LiAmC10* is shown in Figure 4-1.

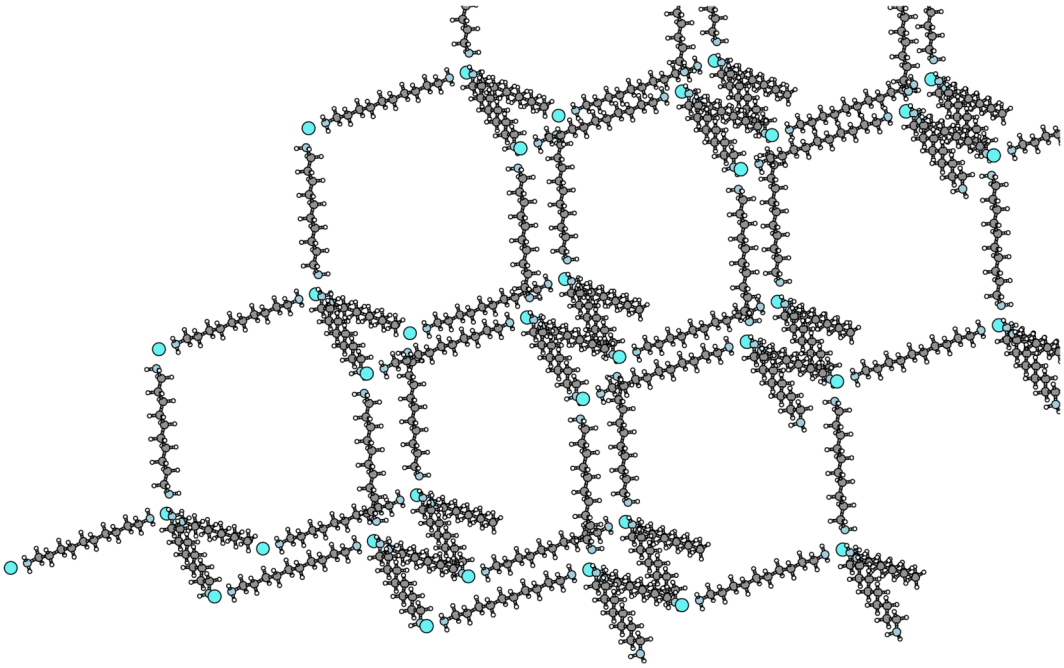

Figure 4-1. Crystal structure of LiAmC10.

As will be shown, the proposed crystalline material offers several intriguing characteristics and applications. One possible application for such materials is reduction-oxidation (redox) catalysis. The loosely bound electrons can reduce various molecular species, such as organic molecules (e.g., the Birch reduction with solvated electrons).[56,79] An important potential application is in carbon capture and sequestration methods through CO_2 conversion to industrial platform chemicals, such as methanol or lactones. Previously, we demonstrated the ability of $Li(NH_3)_4$ to readily reduce CO_2 and for the remaining $Li(NH_3)_4^+$ center to stabilize the otherwise unstable CO_2^- anion, catalyzing the CO_2 conversion with reagents like H_2 or dienes and returning the electron to $Li(NH_3)_4$ to complete the cycle (see ref [55] and Section 2.5: Application of SEPs in Catalysis). With linked-SEP materials, the adjustment of the pore size (hydrocarbon chain length) and addition of functional or steric groups to the hydrocarbon backbone can render these materials highly selective.

This work is a first exploration of a model system composed of Li^+ centers connected with diamines and surrounded by diffuse electrons (one for each Li^+ center). The electronic band structure and magnetic properties will be analyzed. An important question is: *Will results for molecular linked-SEPs allow the prediction of electronic properties of the corresponding crystalline form?* To address this, the DFT and CASTP2 results of gas-phase *LiAm-LSEPs* (Section 3.3: Diamine Linked-SEPs: Lithium) will be compared alongside DFT calculations with the PBE[4] functional and applying periodic boundary conditions for systems of well separated *LiAm-LSEP* molecules.

4.2 Computational Details

4.2.1 Molecular Linked-SEPs

See Section 3.3: Diamine Linked-SEPs: Lithium for computational details on the for DFT and CASPT2 results for gas-phase *LiAm-LSEP.*

DFT calculations under periodic boundary conditions were applied for *LiAm-LSEP(n)*, (n =1−5), in which the species were centered within cubes sufficiently sized to ensure isolation from adjacent cells, ranging from 34 Å in length for n = 1 to 41.5 Å for n = 5. These calculations were done using Quantum Espresso (QE)[80] with a uniformly spaced 2x2x2 k-space grid, an 80 Ry cut-off energy, gaussian smearing with a smearing temperature of 0.05 eV, spin polarization, and the PBE functional. Different spin states were obtained by setting initial magnetization of Li centers.

4.2.2 Crystalline Linked-SEPs

Initial geometries for the crystalline structure of Figure 4-1 were constructed based on a "diamond" crystalline structure owing to the tetrahedral structure of $Li(NH_3)_4$. The initial geometry of the linking diamine chains was obtained from the gas-phase calculations. Both the cell parameters and atomic positions were optimized with the subsequent DFT calculations using periodic boundary conditions in QE; see below for more details. The primitive unit cell was employed for the optimization; it contains two Li atoms and four linker diamine molecules (see Figure 4-2). All optimized crystal structures were of P1 symmetry. For cell parameters and geometry see the github repository provided at: https://github.com/JacksonChem/LiAmCn-Files-2023

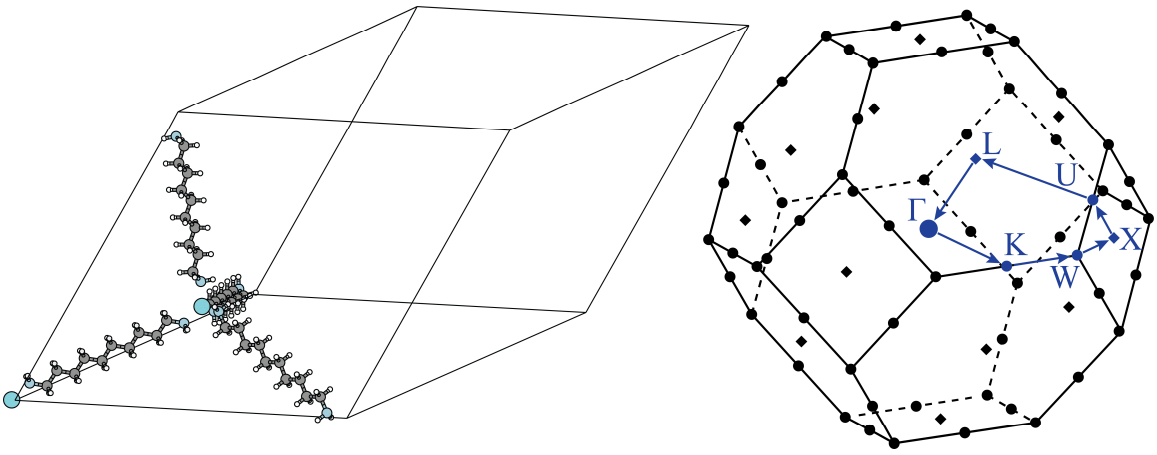

Figure 4-2. Primitive unit cell and 1st Brillouin Zone of LiAmC10.

The periodic DFT calculations were carried out with the PBE functional with two different approaches: (1) the plane waves/pseudopotentials (PW/PS) approach and the Projected Augmented Wave (PAW) formalism under periodic boundary conditions[81] as implemented in the QE computational package, and (2) the numerically tabulated atom-centered basis sets as implemented in the Fritz Haber Institute "ab initio molecular simulations" (FHI-aims) computational package.[82] In addition, for FHI-aims the PBE0[5,6] and

B3LYP[74–77] functionals were also tested. For brevity's sake we will refer to the different methodologies as Program/Functional, e.g., FHI-aims/PBE and QE/PBE. The various methods (QE/PBE, FHI-aims/PBE, FHI-aims/PBE0, and FHI-aims/B3LYP) were used to determine whether a consistent description could be obtained across methodological variation, especially because systems with diffuse electrons are known to be sensitive to such changes;[83–85] which computational package was used for which data will be highlighted throughout this work when pertinent. For QE calculations, an 86 Ry cut-off energy (ecut=86, erho=860), gaussian smearing with a smearing temperature of 0.05 eV, and spin polarization was used. The k-points mesh varied by chain length with higher mesh densities used for shorter chain-lengths (see Table C-1 of APPENDIX C: Supporting Material for Chapter 4). When using FHI-aims, the tight settings/tier2 basis set was used with a uniform 4x4x4 k-points mesh. The Pulay mixer[86] with a charge mixing parameter of 0.01 was employed to aid convergence.

Three distinct electronic systems were identified, the spin-unpolarized and spin-polarized which is either ferromagnetic or antiferromagnetic. The choice of magnetic state was made by setting in initial magnetization of −1 on one Li atom and +1 on the other for the antiferromagnetic state or +1 on both for the ferromagnetic. Magnetization on the NH_2 hydrogens was also tested and produced identical ferromagnetic/antiferromagnetic solutions. For *LiAmC1* and *LiAmC2*, only the spin-unpolarized configurations were observed regardless of applied magnetization. For *LiAmC4* and *LiAmC5*, all three spin states were obtained and their optimized crystal structures were compared using a measure of similarity between powder diffraction spectra[87] as implemented in Critic2[88]. In all examined cases, this test revealed negligible differences between each crystal structure. Therefore, only the

unpolarized states of *LiAmC6 – LiAmC10* were optimized, and these geometries were used for all subsequent calculations due to the high computational cost. K-paths used in electronic band structure calculations were generated using Xcrysden[89]. Figures include images generated from the VMD[90] and Iboview[91] software.

4.3 Molecular Linked-SEPs

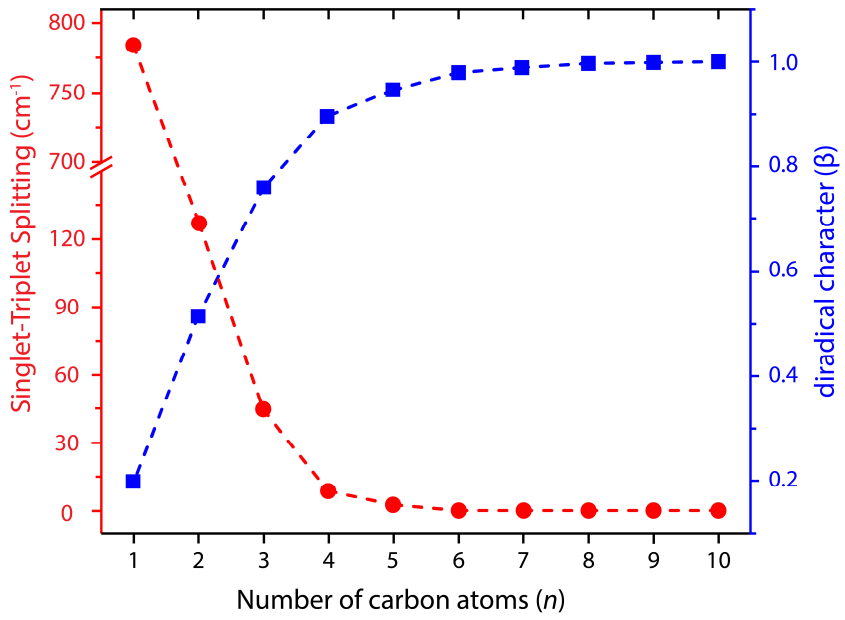

Figure 4-3. Diradical character for LiAm-LSEPs.

In Section 3.3: Diamine Linked-SEPs: Lithium, CASPT2 gas-phase calculations of the *LiAm-LSEPs* were discussed. The relation between carbon chain length and diradical character, (defined in Equation *3-7*) which defines the degree of coupling between the two terminal SEP electrons is shown again in Figure 4-3. When the diradical character is β=0 the electronic state can be readily expressed as a single reference $|\sigma^2\rangle$. When β=1, the weights of the $|\sigma^2\rangle$ and $|\sigma^{*2}\rangle$ configurations are equivalent, and the system may readily be expressed

as a combination of $|1s_R\,\overline{1s_L}\rangle$ and $|1s_L\,\overline{1s_R}\rangle$. The intermediate distances and resulting intermediate values of β produce states that have significant multireference character.

To explore the accuracy of applying density functional theory (DFT) to the study of *LiAm-LSEPs* two different functionals were applied: B3LYP, a functional often used for gas-phase calculations, and PBE, which is standard in condensed-phase calculations. We also performed DFT calculations with the PBE functional under periodic boundary conditions for a system of well separated *LiAm-LSEP(n)* molecules.

The primary issue with the use of DFT lies in describing the electronic structure of the singlet spin state, which we demonstrate above to be multireference in character, a mixture of closed-shell and open-shell (diradical) states. DFT methods assume a single Slater determinant is a sufficient representation of an electronic state; this is insufficient to reproduce multireference character like that seen above for *LiAm-LSEPs*. Therefore, we considered both restricted-DFT (S=0R) and unrestricted-DFT (S=0U) singlets, or equivalently, the unpolarized (S=0R) and polarized-antiferromagnetic (S=0U) periodic calculations, respectively.

Table 4-1 lists energy differences between the two "types" of singlet states and of the triplet state. For n = 1, the CASPT2 wavefunction was found primarily closed shell (β = 19.8%), and this reflects to the DFT/PBE calculations. For both gas and condensed phase PBE calculations, the S=0U calculation converges to the S=0R solution, i.e., the α and β orbitals are identical to $1s_R + 1s_L$. On the other hand, B3LYP predicts the S=0R higher than the S=0U by 77.9 cm^{-1}.

Table 4-1. Singlet and triplet relative energies for LiAm-LSEPs. Relative energy (cm^{-1}) for the singlet (S=0R and S=0U) and triplet (S=1) states of LiAm-LSEP(n) for (n = 1−10) with various methods.

	CASPT2	DFT/B3LYP			DFT/PBE			DFT/PBE (periodic) [a]		
n	S=1	S=0U[b]	S=0R[c]	S=1	S=0U[b]	S=0R[c]	S=1	S=0U[d]	S=0R[e]	S=1[f]
1	783.9	0.0	77.9	972.9	—	0.0	1451.9	—	0.0	—
2	126.9	0.0	1043.6	117.2	0.0	318.0	116.6	0.0	313.0	49.4
3	45.2	0.0	1435.1	42.6	0.0	524.7	28.1	0.0	425.3	-21.5
4	8.5	0.0	1772.3	10.3	0.0	720.7	0.2	0.0	530.7	-24.8
5	2.8	0.0	1939.9	3.7	0.0	780.4	0.1	0.0	561.8	-15.1

[a] Applying periodic boundary conditions and using QE. [b] Unrestricted open-shell singlet.
[c] Restricted closed-shell singlet. [d] Polarized antiferromagnetic. [e] Unpolarized.
[f] Polarized ferromagnetic.

For $n > 1$, the S=0U is always lower in energy than S=0R. This energy difference increases for larger n which agrees with the fact that the S=0R part diminishes for larger n in the CASPT2 wavefunction. The S=0U is also lower than the S=1 state and becomes degenerate (within 10 cm^{-1}) for $n \geq 5$ for both B3LYP and PBE, which agrees with the CASPT2 results. Compared to CASPT2, PBE produces the same trend for singlet-triplet splitting but predicts lower ΔE. Interestingly, when periodic boundary conditions are employed QE/PBE erroneously predicts a ferromagnetic (S=1) ground state configuration, but otherwise follows the trend of approaching degeneracy for longer chains. Overall, the agreements here suggest DFT (and the PBE functional) to be a safe choice for *LiAm-LSEP(n)* when $n = 1$ and $n \geq 4$, where the wavefunction is clearly of S=0R ($n = 1$) or S=0U ($n \geq 4$). Extending this to *LiAmCn*, we can predict a similar conclusion to hold with carbon chains that are very short with highly coupled SEPs and long chains with well-separated SEP centers will be adequately described using DFT and the PBE functional. But we would expect DFT to be less accurate for the intermediate chain lengths ($n = 2-4$).

An important observation pertains to the composition and energy of the *LiAm-LSEP(n)* frontier orbitals for the S=0U and S=1 states obtained with DFT. The wavefunction of S=1 can be equivalently described as $|1s_R 1s_L\rangle$ or $|\sigma\ \sigma^*\rangle$. The σ, σ* orbitals are orthogonal, and their energy difference is zero at infinite separations and increasingly large at short distances. Due to the imposed orthogonality within the α-orbitals, our calculations converge to the $|\sigma\ \sigma^*\rangle$ Slater determinant. As far as the open-shell singlet state is concerned, the α and β electrons allows the "symmetry-broken" $|1s_R\ \overline{1s_L}\rangle$ solution, and the S=0U state converges to a $|1s_R\ \overline{1s_L}\rangle$ Slater determinant failing to provide the correct spin-adapted form of $|\Psi_{S=0;M_S=0}\rangle = \frac{1}{\sqrt{2}}(|1s_R\ \overline{1s_L}\rangle - |\overline{1s_R}\ 1s_L\rangle)$. It appears that the $1s_R$ and $1s_L$ orbitals are effectively equivalent and have the exact same energies. The orbital energies for S=1 and S=0U for DFT/PBE are listed in Table 4-2. In the next section we will see how these observations are reflected in the electronic band structure of the crystalline *LiAmC1 – LiAmC10* species.

Table 4-2. Relative energies of UB3LYP LiAm-LSEP orbitals. UB3LYP/cc pVDZ(Li,N,C), d-aug-cc-pVTZ(H) orbital energies (a.u.) of the α and β electrons occupying the outer diffuse orbitals for the LiAm-LSEP(n) species, n = 1−6.

	S=0U			S=1		
n	α	β	ΔE [a]	α	α	ΔE [b]
1	-0.07492	-0.07492	0.000	-0.08431	-0.07498	0.254
2	-0.07855	-0.07855	0.000	-0.08019	-0.07681	0.092
3	-0.07781	-0.07781	0.000	-0.07868	-0.07680	0.051
4	-0.07715	-0.07715	0.000	-0.07752	-0.07670	0.022
5	-0.07658	-0.07658	0.000	-0.07685	-0.07627	0.016
6	-0.07613	-0.07613	0.000	-0.07625	-0.07600	0.007

[a] Energy difference (eV) between the α and β orbitals.
[b] Energy difference (eV) between the two orthogonal α orbitals.

The smaller singlet-triplet gaps in DFT can be attributed to the different delocalization error in the two states induced by the different occupied orbitals (σ/σ* vs. $1s_R/1s_L$).[92] The

delocalization error (absent for CASPT2) can cause inaccurate energy and density descriptions of a system. Hybrid functionals (such as B3LYP or PBE0) can mitigate some of the effects of delocalization error,[93] but they are computationally more demanding than PBE (a GGA functional). Consistency between the PBE and PBE0 functional would be a strong indicator of reliable calculations. To address this for *LiAmCn*, we provide not only DFT/PBE results from two different solid state computational chemistry packages with different methodologies for orbital description, but also we compare different functionals using FHI-aims with PBE, PBE0, and B3LYP. Recent advances in both computing resources, and the efficiency of the FHI-aims code make these solid-state hybrid functional calculations practical, where they were not previously.

4.4 Crystalline Linked-SEPs

The various systems of *LiAmCn* may be divided into three categories: the long-chains (n = 10−6), the intermediate chains (n = 5−3), and the short-chains (n = 1−2). We begin with the discussion of the long chains.

4.4.1 Long-chain LiAmCn

In Figure 4-2, the optimized cell and geometry of *LiAmC10* is shown. Three distinct electronic states are obtainable for this system: the spin-polarized ferromagnetic or antiferromagnetic states and the spin-unpolarized, non-magnetic state; the electronic spin density of each is shown in Figure 4-4. The spin-polarized states depict a unit cell containing two isolated SEPs with an electronic structure analogous to a lone $Li(NH_3)_4$ or $(NH_3)_3Li(NH_2)^-$ it possesses one solvated electron occupying a diffuse s-type orbital surrounding the periphery of the $Li(NH_2^-)_4$ center; the effect of the diamine ligands cause

the diffuse SEP electron to be polarized away from the chains into the direction of the voids within the lattice. However, the diffuse electron remains localized to the space immediately around the lithium-amine center.

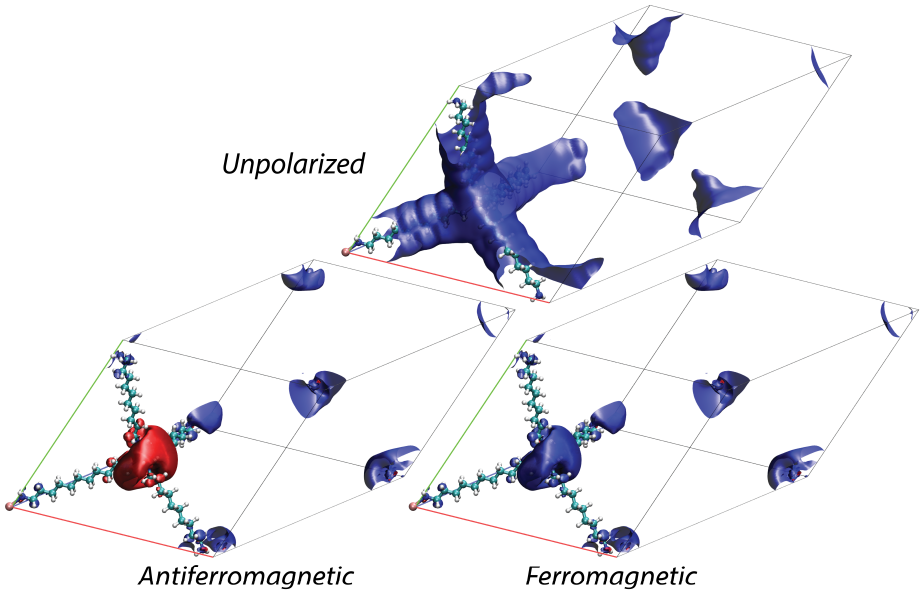

Figure 4-4. Electronic spin density of LiAmC10 of FHI-aims/PBE. For the spin polarized, red denotes the β and blue the α density.

The two electrons at each SEP center may couple with the same spin to give the ferromagnetic or opposite spins to give the antiferromagnetic: analogous to the triplet (S=1) and open shell singlet (S=0U) in *LiAm-LSEP(n)*, respectively. At this separation, the association between the two electrons is minimal and the two states are nearly degenerate (see Table 4-3). The spin-unpolarized solution requires adjacent centers to couple in σ-type bonding. However, the large separation of the adjacent centers significantly destabilizes this state, it is less stable by 885.7 cm^{-1} and 3735.7 cm^{-1} as calculated using FHI-aims with the PBE and PBE0 functional (Table 4-3). This holds true for all chain length $n \geq 4$, the unpolarized state is significantly higher in energy relative to the spin-polarized states.

Table 4-3. Relative energies of LiAmCn states. Relative energies (cm^{-1}) for the singlet (S=0R and S=0U) and triplet (S=1) states (cm^{-1}) of LiAmCn (n = 1−10) with various methods, denoted as Program/Functional. For n = 1−2, Quantum Espresso (QE) and FHI-aims only produces an unpolarized, closed shell (S=0R) state.

	QE/PBE			**FHIaims/PBE**		
n	S=0U[a]	S=1[b]	S=0R[c]	S=0U[a]	S=1[b]	S=0R[c]
1			0.0			0.0
2			0.0			0.0
3	0	N/A[d]	27.8	0.0	275.2	188.8
4	0.0	33.3	507.4	0.0	16.9	1017.4
5	0.0	91.4	181.6	0.0	41.1	663.2
6	0.0	-42.0	436.9	0.0	3.5	876.8
7	0.0	-38.5	331.3	0.0	2.7	754.8
8	0.0	-16.6	179.4	0.0	0.0	481.9
9	0.0	-7.7	403.3	0.0	0.0	759.5
10	0.0	-1.3	537.5	0.0	0.0	885.7

	FHIaims/PBE0			**FHIaims/B3LYP**	
n	S=0U[a]	S=1[b]	S=0R[c]	S=0U[a]	S=1[b]
1			0.0	0	0
2			0.0	0	0
3	0.0	201.7	1537.4	0.0	258.5
4	0.0	25.4	N/A[d]	0.0	47.1
5	0.0	8.6	2731.2	0.0	32.4
6	0.0	1.0	3119.5	0.0	3.8
7	0.0	-4.1	3186.5	0.0	1.3
8	0.0	-0.4	3084.6	0.0	0.6
9	0.0	0.1	3446.8	0.0	0.1
10	0.0	4.4	3735.7	0.0	-0.8

[a] Spin-polarized antiferromagnetic. [b] Spin-polarized ferromagnetic. [c] Unpolarized.

The calculated band structure of Figure 4-5 shows the bands of the ferromagnetic and antiferromagnetic states. The valence band of these systems corresponds to the orbital occupied by the diffuse electron centered about the lithium-amines, depicted by the local density of states in Figure 4-5. Examining the band structure of both states, it's clear the alpha and beta bands of each are identical. Further, these bands are nearly flat, and the two states are effectively degenerate (Table 4-3). Further, the morphology of the band structure

and plotted electron density illustrate the valence band is produced from isolated SEP 1s orbitals which see no meaningful hybridization with higher energy 1p orbitals. This agrees with orbital structure seen for *LiAm-LSEPs* in the previous section (see Figure 3-11). Altogether, we can view the two electrons at this distance (r_{Li-Li}=15.997 Å) occupying orbitals equivalent to isolated SEPs which negligibly interact with the other.

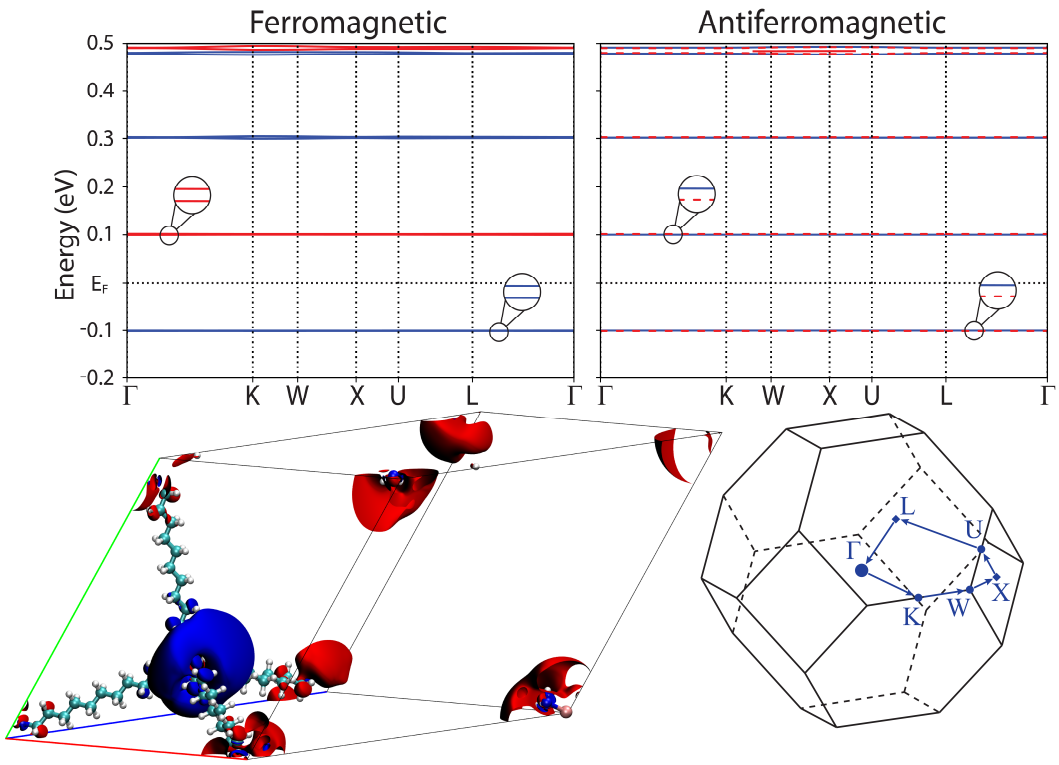

Figure 4-5. Band structure of LiAmC10. Red denotes the β and blue the α spin channels. The structure of the Brillouin zone and the k-path used for band calculations is given. The bottom left figure depicts the integrated local density of states for antiferromagnetic LiAmC10 in the energy range of (−0.2−EF) calculated at QE/PBE. Note that figure insets for the band structure are added to emphasize that two degenerate bands coincide at -0.1 and 0.1 eV.

As the carbon chain becomes shorter, we see that the degeneracy or near degeneracy of the valence and conduction bands of Figure 4-5 is lifted only in the ferromagnetic case (see Figure 4-6). The same is observed for the corresponding triplet spin *LiAm-LSEP(n)* gas-

phase species and is a result of the orthogonality of the occupied orbitals (σ, σ*); see Table 4-2. In the anti-ferromagnetic or the corresponding singlet spin of the *LiAm-LSEPs*, the two occupied orbitals are not orthogonal and are localized separately on the two SEP centers (unrestricted or polarized calculations). Their identical nature imposes the observed degeneracy of the α and β valence bands across the k-space.

Throughout the n = 6−10 range, the spin-polarized states are effectively degenerate with the singlet-triplet splitting as ~0 cm^{-1} (n = 8−10), 2.7 cm^{-1} (n = 7), and 3.5 cm^{-1} (n = 6) at FHI-aims/PBE (Table 4-3). Application of hybrid functionals PBE0 and B3LYP and the use of QE/PBE all effectively give the same result with relative energies ranging between 0−4 cm^{-1} for n = 10−6 (see Table 4-3).

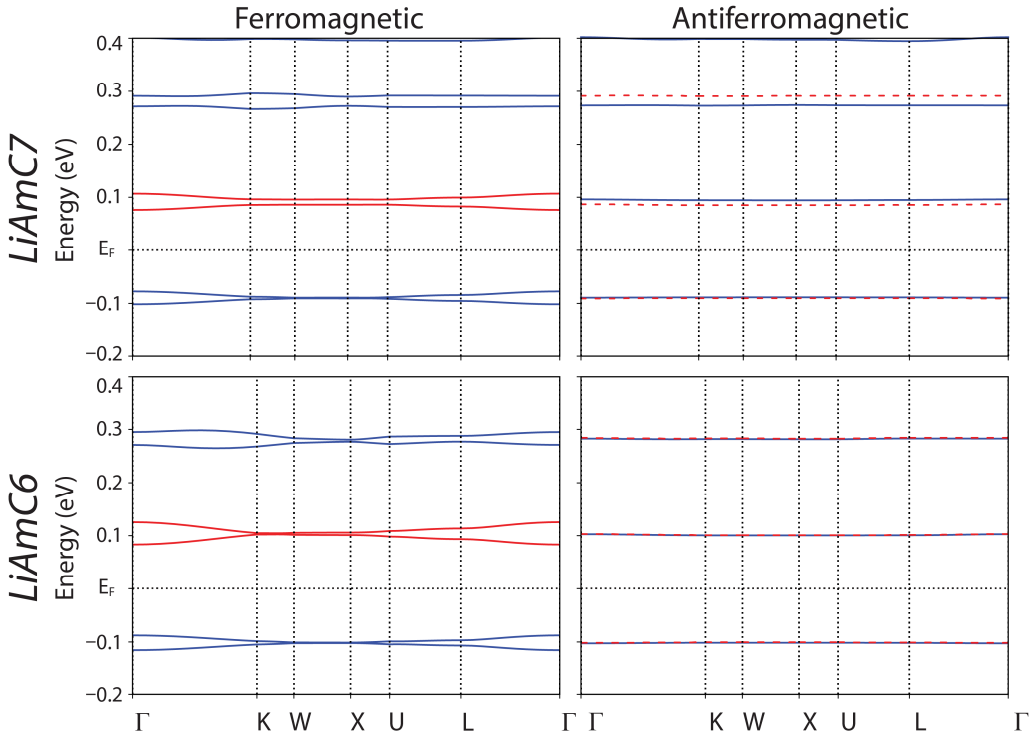

Figure 4-6. Band structure of LiAmC6 and LiAmC7. Computed using FHI-aims/PBE. Red denotes the β and blue the α spin channels. For the Brillouin zone refer to Figure 4-5.

Comparing the electronic band structures produced from the various methods tested, we see that FHI-aims/PBE, FHI-aims/PBE0, and FHI-aims/B3LYP, all show a remarkable agreement in the morphology of the antiferromagnetic and ferromagnetic band structures (see Figure C-1 to Figure C-8 of APPENDIX C: Supporting Material for Chapter 4). Moving from PBE to the hybrid functionals PBE0 and B3LYP, the band gap E_G for all $n = 6-10$ increases significantly. For example, the E_G of *LiAmC10* increases from 0.20 to 1.03 and 0.82 eV for FHI-Aims/PBE, FHI-Aims/PBE0, and FHI-Aims/B3LYP, respectively (see Table 4-4). This behavior is to be expected; it's well understood that the 'band gap problem' causes the PBE functional to significantly underestimate E_G and use of hybrid functionals tends to reduce this.[93] Comparing the band structure calculated with FHI-aims/PBE and QE/PBE, QE predicts a stronger interaction between SEP centers, as illustrated by the relatively "flat" bands of FHI-aims and the "curvy" bands of QE; this difference is minimal for $n = 10-8$ and increases markedly for $n < 7$ (see Figure 4-6 and Figure C-1 to Figure C-8 of APPENDIX C: Supporting Material for Chapter 4). Altogether, we see that all methods strongly agree for the long-chains ($n > 5$). Here, the spin-centers are well separated, and interaction is relatively weak. Returning to the *LSEPs*, we showed there exists strong agreement between DFT and CASPT2 when the linked SEP centers are well separated. This result and the consistency between various methodologies for long-chained *LiAmCn* provides validation that DFT can adequately describe the electronic structure of these systems. An interesting note is QE, despite the strong agreement in E_g and band structure morphology, identifies the ferromagnetic S = 1 as the ground state for $n > 5$. This agrees with the finding of QE/PBE for the *LiAm-LSEPs* which erroneously predicted a ferromagnetic (S = 1) ground state under periodic boundary conditions. Based on this and the agreement of

FHI-aims for PBE, PBE0, and B3LYP we can conclude the overstabilization of the ferromagnetic state by QE/PBE to be erroneous.

Table 4-4. Band gap of LiAmCn. Electronic band gap E_G (eV) for the anti-ferromagnetic LiAmCn calculated using various methodologies.

n	QE/PBE	FHI-aims/PBE	FHI-aims/PBE0	FHI-aims/B3LYP
1	–	–	–	–
2	–	–	–	–
3	0.07	0.13	0.92	0.74
4	0.11	0.20	1.07	0.86
5	0.12	0.16	1.03	0.81
6	0.21	0.20	1.05	0.84
7	0.19	0.17	1.03	0.81
8	0.16	0.12	0.97	0.77
9	0.20	0.17	1.03	0.82
10	0.23	0.20	1.07	0.84

4.4.2 LiAmCn Chains of Intermediate Length

Moving to our intermediate length chains (n = 3−5), the two spin-polarized states are no longer degenerate with the antiferromagnetic lower in energy by 41.1 cm^{-1} and 16.9 cm^{-1} for n = 5 and n = 4, respectively (FHI-aims/PBE, see Table 4-3). It's for this group that we see the greatest discrepancy between the results of QE/PBE and FHI-aims/PBE. Comparing the band structure of the two methods for *LiAmC5* we still see the pattern of increasing divergence of α and β bands along K → Γ and L → Γ. However, the divergence markedly increases for the ferromagnetic QE/PBE leading to a crossing of the valence α and conduction β bands below the Fermi energy and a prediction of material with no band gap while FHI-aims/PBE predicts an E_G of 0.10 eV (see Figure 4-7). For the antiferromagnetic, QE/PBE still predicts a band gap (E_G = 0.12 eV) and FHI-aims/PBE band structure remains effectively flat for the valence and conduction bands, describing only weak interaction between adjacent

cells. The different functionals of FHI-aims agree in morphology for both ferromagnetic and antiferromagnetic- only increasing the antiferromagnetic band gap from 0.16 eV with PBE to 1.03 and 0.81 eV for PBE0 and B3LYP, respectively (see Figure C-6). The same observations hold true for *LiAmC4* (see Figure 4-8 and Figure C-7). Notably, the QE/PBE band structure for the ferromagnetic *LiAmC4* state is the only system wherein the conduction band is shown to mix with a higher energy band (the blue band of Figure 4-8), counter to the CASPT2 results of the *LiAm-LSEPs* and all FHI-aims band structures.

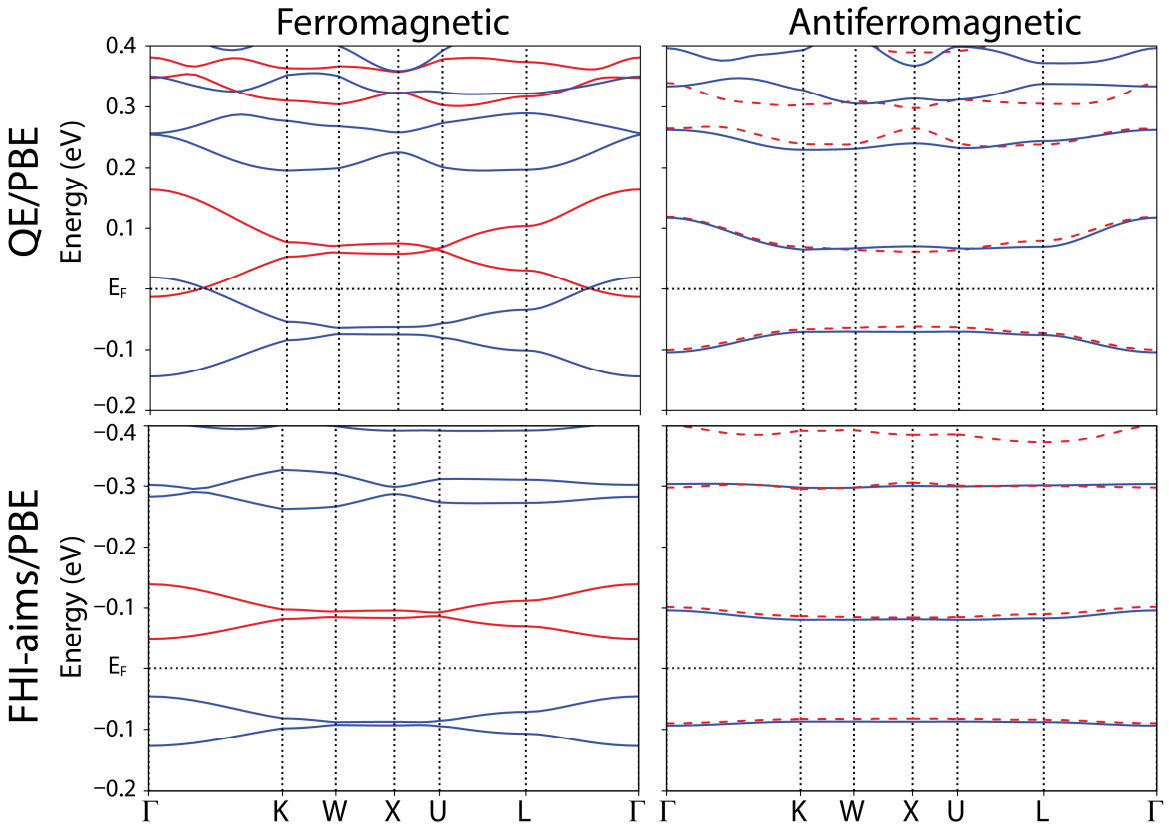

Figure 4-7. Band structure of LiAmC5. Computed using FHI-aims/PBE and QE/PBE. Red denotes the β and blue the α spin channels. For the Brillouin zone refer to Figure 4-5.

For *LiAmC3*, we see stronger agreement between FHI-aims and QE. The band morphology of QE/PBE and FHI-aims/PBE are near identical for both unpolarized and antiferromagnetic states (see Figure C-8). E_G agrees at 0.07 and 0.13 eV for the antiferromagnetic at QE/PBE and FHI-aims/PBE, respectively. However, QE/PBE predicts a small absolute magnetization of 0.72 μ_B compared to 1.34 μ_B for FHI-aims (see Table 4-5). While QE can readily converge to an antiferromagnetic state, we were unable to locate a true ferromagnetic state with all attempts converging to an unpolarized solution. QE favors the antiferromagnetic (S=0U) state by 27.8 cm^{-1} over the unpolarized. FHI-aims favors the antiferromagnetic ground state with the unpolarized (S=0R) higher by 188.8 cm^{-1} and increasing to 1537.4 cm^{-1} at PBE and PBE0, respectively (Table 4-3).

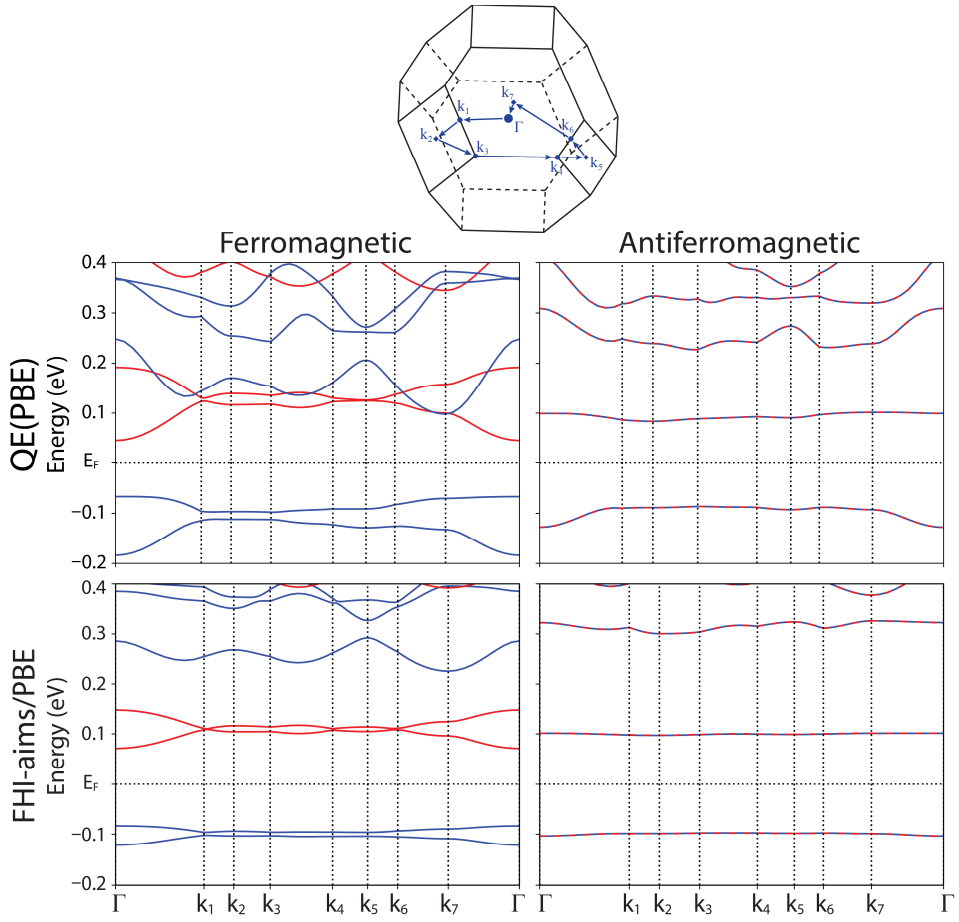

Figure 4-8. Band structure of LiAmC4. Computed using FHI-aims/PBE and QE/PBE. Red denotes the β and blue the α spin channels.

In total, these discrepancies are illustrative of the complex electronic structure of the intermediate chain lengths (n = 3−5) which, due to the aforementioned delocalization error[93] and use of single-determinant representations, density functional theory and the functionals employed struggle to adequately describe. This mirrors the results observed for the gas-phase linked-SEPs where intermediate chains lengths n = 2−4 posed a challenge for description by DFT due the significant multi-reference character (to nearly the exact same chain length).

Table 4-5. Magnetic Moments of LiAmCn. Calculated magnetic moments for LiAmCn with FHI-Aims and Quantum Espresso (QE) using the PBE functional. B_0 and $|B_0|$ denote total

and absolute magnetization, respectively in units of μ_B. Magnetization calculated from the integrated α and β spin density.

	QE/PBE				FHI-aims/PBE			
	Antiferromagnetic		Ferromagnetic		Antiferromagnetic		Ferromagnetic	
n	B_0	$\lvert B_0 \rvert$	B_0	$\lvert B_0 \rvert$	B_0	$\lvert B_0 \rvert$	B_0	$\lvert B_0 \rvert$
1	–	–	–	–	–	–	–	–
2	–	–	–	–	–	–	–	–
3	0.02	0.72	–	–	0.01	1.34	0.78	0.79
4	0.00	1.78	1.98	2.02	0.00	1.97	1.99	2.04
5	0.01	1.61	1.55	1.58	0.01	1.92	1.94	2.00
6	0.00	1.97	2.00	2.04	0.00	2.03	1.99	2.05
7	0.00	1.99	1.99	2.04	0.00	2.02	1.98	2.03
8	0.00	1.97	1.96	2.01	0.00	1.87	1.82	1.88
9	0.00	2.03	1.99	2.04	-0.01	2.03	1.98	2.04
10	0.00	2.04	2.00	2.05	0.00	2.05	1.99	2.05

4.4.3 LiAmCn Short Chains

Where the long-chains were characterized as clearly spin-polarized and the intermediate-chains a mixture of competing spin-polarized and spin-unpolarized states, the shortest chains (n = 1–2) suggest a total transition to the spin-unpolarized. For both FHI-aims/PBE and QE/PBE, only the unpolarized state was observed. The band structure of the two closely agree in morphology and predict a metallic character (see Figure 4-9). For *LiAmC1*, FHI-aims/PBE and QE/PBE disagree only in the Fermi energy; QE shifts the maximum of the conduction band by ~0.2 eV relative to FHI-aims.

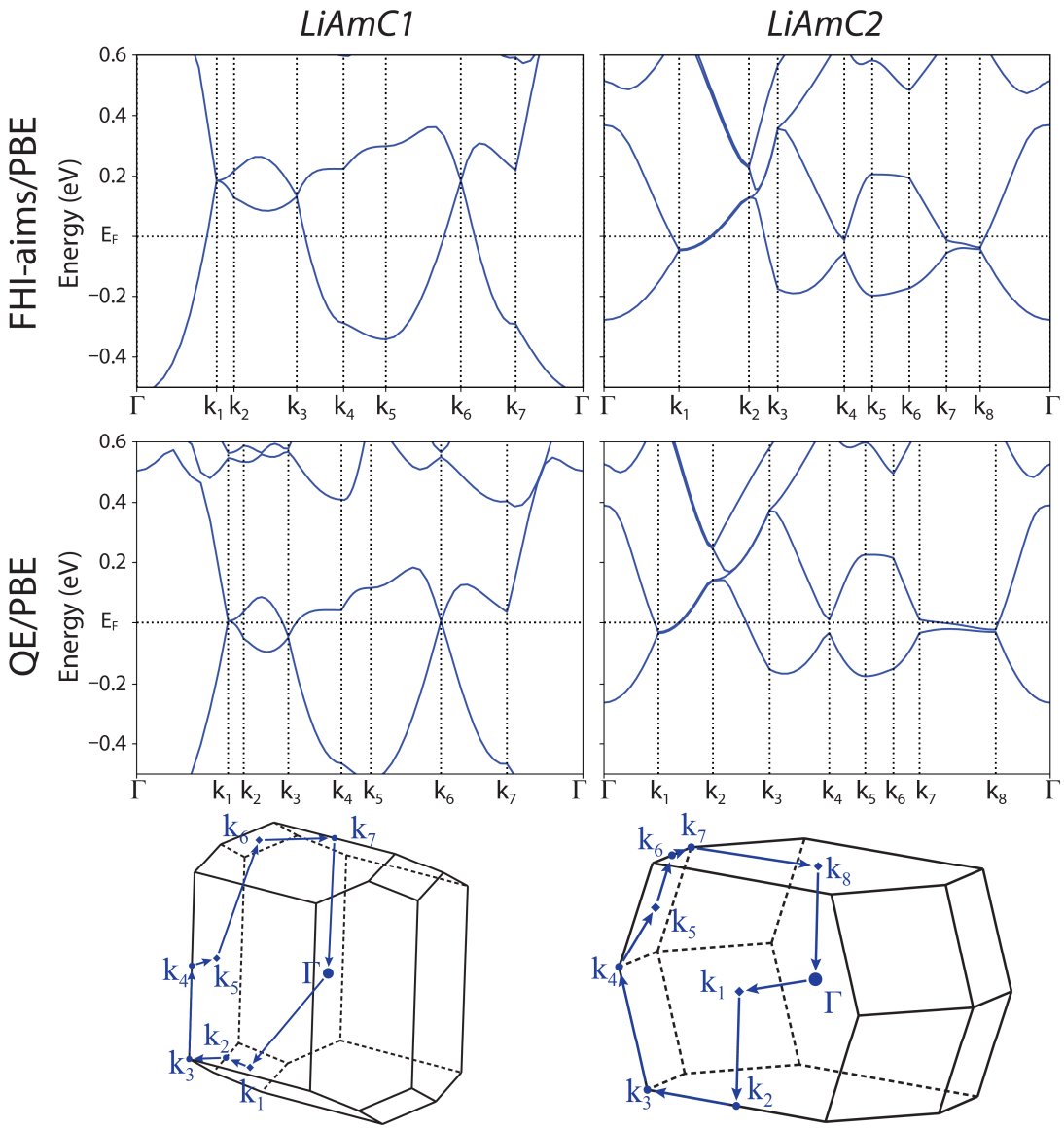

Figure 4-9. Band structure of LiAmC2 and LiAmC1.

4.4.4 Projected Density of States

Figure 4-10 depicts the band structure for *LiAmC4* with a wider energy range accompanied by atomic-projected density of states plots for α and β spins. It is shown that N, C, and H contribute to the bands below the 4 eV, which clearly correspond to the C−H, N−H, and C−N bonds. Li can be fairly represented as Li^+ as its contribution is minimal across the whole energy range. The valence and conduction bands near the Fermi level are

dominated by H contributions, as expected since the diffuse electrons are in the periphery of the H centers. In the gas-phase calculations this contribution is provided by the augmented series of basis sets in contrast with the plane waves in the periodic DFT calculations.

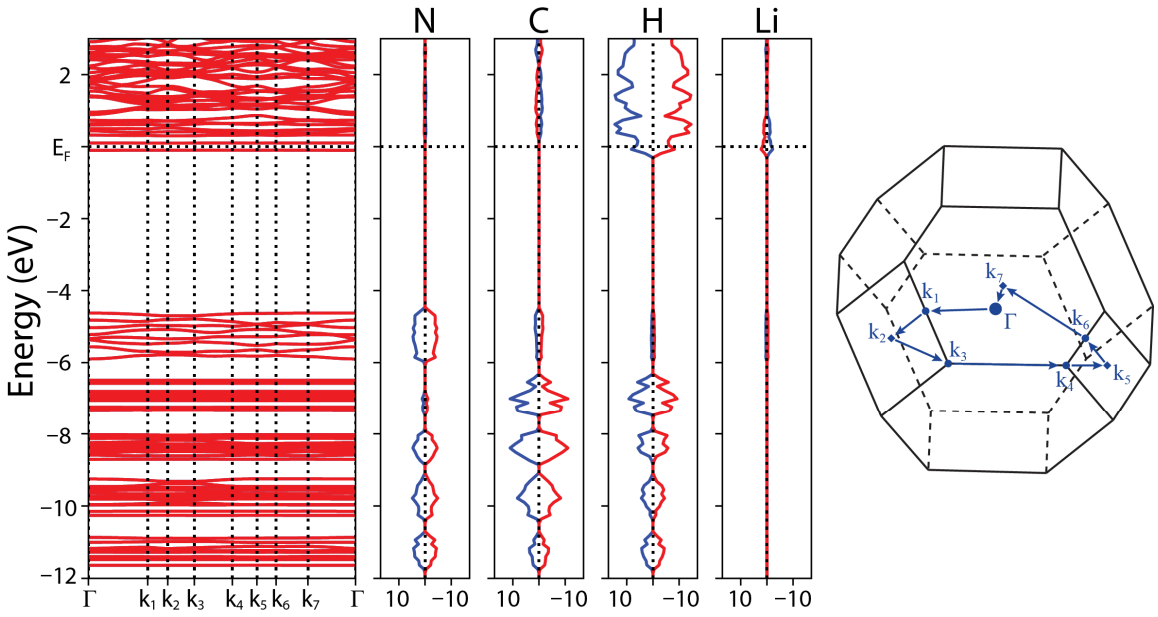

Figure 4-10. Atomic-projected density of states for LiAmC4. Left: Electronic band structure of ferromagnetic LiAmC4. Middle: atomic-projected density of states for N, C, H, and Li. The alpha and beta spin components are plotted in blue and red, respectively. Right: Brillouin zone and k-path. The x-axis of the projected density of states is in units of $(eV \cdot Å)^{-1}$.

4.4.5 Isolating Spin States in LiAmCn Supercells

A final note remains pertaining to the discussion of magnetic coupling in *LiAmCn*. Supercells (2x2x2) were constructed for n = 5−7 by repeating the optimized primitive cell twice in the x, y, and z direction to give a cell containing 16 total SEP centers. FHI-aims/PBE and the tight/tier2 basis set with a uniform 2x2x2 k-point mesh was used for the following results. Shown in Figure 4-11 are spin density plots of the three spin states- an

antiferromagnetic, a ferromagnetic, and one corresponding to a ferromagnetic state in which the spin of one SEP center has flipped.

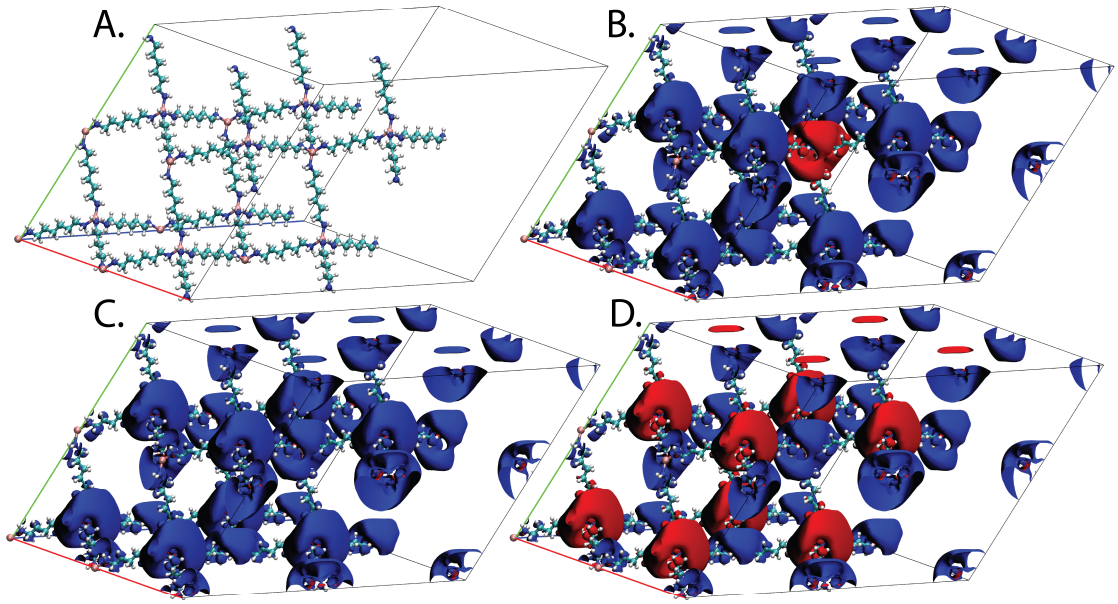

Figure 4-11. LiAmC6 Supercells. A.) The structure of LiAmC6 2x2x2 supercell containing 8 LiAmC6 primitive cells. The spin density of: B.) the ferromagnetic with one spin flipped center, C.) the ferromagnetic, and D.) the antiferromagnetic is depicted as well. Red denotes the β and blue the α spin density.

Comparison of the ferromagnetic and antiferromagnetic states provides a measurement of the J-coupling between the SEP centers. J-coupling was calculated according to refs. [94,95]. For *LiAmC6,* this value is 0.17 K and the energy to spin-flip one center is 0.67 K (see Table C-2). The ability to computationally isolate specific spin states within bulk *LiAmCn* is an exciting find which offers future avenues of exploration for potential applications of *LiAmCn* in quantum computing and digital storage.

4.4.6 Conclusions

In this work, we introduce a new kind of material in which positively charged metal centers linked by diamines are surrounded by diffuse electrons. We specifically employed the Li^+ centers and diamines with hydrocarbon chains of one through ten carbon atoms. We initially considered dimers where two Li^+ centers are connected with a single diamine molecule and coordinated to three ammonia molecules each. Then, we expanded our work to a three-dimensional, diamond-like, crystalline structure composed of Li^+ linked with diamines. Our goal was to investigate in detail the electronic structure of the molecular systems and examine the transferability of the findings to the crystalline form.

Our work on the molecular dimeric species demonstrated that single determinant methods, specifically density functional theory, sufficiently describes the species with short and long hydrocarbon chains, but present methodological issues for intermediate lengths. Referring to *LiAm-LSEP(n)*, at CASPT2 the one-carbon chain stabilizes the closed-shell singlets as it favors the coupling of the two electrons in the same orbital. For long chains ($n > 4$), the diradical singlets and triplet states dominate and are nearly degenerate. For chains with $n = 2-4$, the singlet state reveals strong multi-reference character mixing the closed-shell and diradical electronic configurations. However, DFT does not allow this mixing, as a result the singlet state changes abruptly from closed shell to diradical character at the two-carbon chain length and a smaller energy splitting is observed for DFT. At long chain length, for which diradical configurations dominate, DFT better describes the system. For all species the singlet state is always lower in energy with the splitting decreasing smoothly as the hydrocarbon chain becomes longer. These results on gas-phase molecular linked-SEPs are used as an entry point to understand the electronic structure of condensed-phase *LiAmCn*.

To validate the accuracy of DFT calculations of the crystalline linked-SEPs, *LiAmCn*, methodological effects are examined through the comparison of results from two different quantum chemical packages, QE and FHI-aims, and results from different functionals, PBE, PBE0, and B3LYP. Findings therein follow that of *LiAm-LSEP(n)*, demonstrating that gas-phase calculations on the *LiAm-LSEP(n)* species provide useful qualitative insights for the *LiAmCn* crystal. Results show that short chains (n = 1–2) stabilize the unpolarized solution while the antiferromagnetic is favored for n > 2. For short chains, electrons of nearby SEP centers are highly correlated. At long chain lengths, antiferromagnetic and ferromagnetic (singlet and triplet) states become nearly degenerate and electronic bands flatten indicating minimal electron correlation between nearby SEP centers. Intermediate chain length (n = 3–5) represents a transition between unpolarized and spin-polarized descriptions which poses a significant challenge to description by DFT.

Comparing methodology, the overall trend of increasing interaction strength between SEP centers with decreasing chain length is agreed by all methods tested though this effect is stronger for QE than FHI-aims. The trend of approaching degeneracy of ferromagnetic and antiferromagnetic states with increasing chain length is observed for all FHI-aims results. Agreement is strongest for the long-chains (n > 5) and the short chains (n < 3). These observations agree with predictions made based on gas-phase linked-SEPs which indicates that gas-phase calculations may be used to inform future designs and predictions for SEP-based materials. This offers a benefit in that gas-phase calculations may be cheaper computationally and permit use of more accurate quantum chemical methods.

Much work remains to be done in the investigation of *LiAmCn* and SEP-based materials. The present chapter is intended to provide the first insight into the electronic

structure of these materials with the aim to spark interest and identify future avenues for development of quantum technologies and redox catalysts.

REFERENCES

1 I. R. Ariyarathna, S. N. Khan, F. Pawłowski, J. V. Ortiz and E. Miliordos, *Journal of Physical Chemistry Letters*, 2018, **9**, 84–88.

2 G. Ghigo, B. O. Roos and P. Å. Malmqvist, *Chem Phys Lett*, 2004, **396**, 142–149.

3 B. O. Roos and K. Andersson, *Chem Phys Lett*, 1995, **245**, 215–223.

4 J. P. Perdew, K. Burke and M. Ernzerhof, *Phys Rev Lett*, 1996, **77**, 3865–3868.

5 M. Ernzerhof and G. E. Scuseria, *J Chem Phys*, 1999, **110**, 5029–5036.

6 C. Adamo and V. Barone, *J Chem Phys*, 1999, **110**, 6158–6170.

7 T. Yanai, D. P. Tew and N. C. Handy, *Chem Phys Lett*, 2004, **393**, 51–57.

8 S. N. Khan and E. Miliordos, *Journal of Physical Chemistry A*, 2020, **124**, 4400–4412.

9 B. A. Jackson and E. Miliordos, *J Chem Phys*, 2021, **155**, 014303.

10 I. R. Ariyarathna, F. Pawłowski, J. V. Ortiz and E. Miliordos, *Physical Chemistry Chemical Physics*, 2018, **20**, 24186–24191.

11 E. Zurek, P. P. Edwards and R. Hoffmann, *Angewandte Chemie International Edition*, 2009, **48**, 8198–8232.

12 C. A. Kraus, *J Am Chem Soc*, 1907, **29**, 1557–1571.

13 G. E. Gibson and W. L. Argo, *J Am Chem Soc*, 1918, **40**, 1327–1361.

14 E. Huster, *Ann Phys*, 1938, **425**, 477–508.

15 N. W. Taylor and G. N. Lewis, *Proceedings of the National Academy of Sciences*, 1925, **11**, 456–457.

16 S. Freed and N. Sugarman, *J Chem Phys*, 1943, **11**, 354–360.

17 U. Schindewolf and M. Werner, *Journal of Physical Chemistry*, 1980, **84**, 1123–1127.

18 J. J. Lagowski and M. J. Sienko, in *Proceedings of an International Conference on the Nature of Metal Solutions*, ed. Butterworth-Heinemann, 1970.

19 M. T. J. H. Lodge, P. Cullen, N. H. Rees, N. Spencer, K. Maeda, J. R. Harmer, M. O. Jones and P. P. Edwards, *Journal of Physical Chemistry B*, 2013, **117**, 13322–13334.

20 H. P. Cady, *Journal of Physical Chemistry*, 1897, **1**, 707–713.

21 G. N. Chuev, P. Qúmerais and J. Crain, *Journal of Chemical Physics*, , DOI:10.1063/1.2812244.

22 S. Hayama, N. T. Skipper, J. C. Wasse and H. Thompson, *Journal of Chemical Physics*, 2002, **116**, 2991–2996.

23 N. M. S. Almeida and E. Miliordos, *Physical Chemistry Chemical Physics*, 2019, **21**, 7098–7104.

24 I. R. Ariyarathna and E. Miliordos, *Physical Chemistry Chemical Physics*, 2019, **21**, 15861–15870.

25 N. M. S. Almeida, F. Pawłowski, J. V. Ortiz and E. Miliordos, *Physical Chemistry Chemical Physics*, 2019, **21**, 7090–7097.

26 I. R. Ariyarathna and E. Miliordos, *Physical Chemistry Chemical Physics*, 2020, **22**, 22426–22435.

27 I. R. Ariyarathna, N. M. S. Almeida and E. Miliordos, *Journal of Physical Chemistry A*, 2019, **123**, 6744–6750.

28 I. R. Ariyarathna, F. Pawłowski, J. V. Ortiz and E. Miliordos, *Journal of Physical Chemistry A*, 2020, **124**, 505–512.

29 B. A. Jackson and E. Miliordos, *J Chem Phys*, 2022, **156**, 194302.

30 Y.-R. Luo, *Comprehensive Handbook of Chemical Bond Energies*, CRC Press, 2007.

31 A. Kramida, Y. Ralchenko, J. Reader and N. A. Team, NIST Atomic Spectra Database (version 5.6.1), https://physics.nist.gov/asd.

32 J. V. Barnes, B. L. Yoder and R. Signorell, *Journal of Physical Chemistry A*, 2019, **123**, 2379–2386.

33 A. H. C. West, B. L. Yoder, D. Luckhaus, C. M. Saak, M. Doppelbauer and R. Signorell, *Journal of Physical Chemistry Letters*, 2015, **6**, 1487–1492.

34 S. B. Dawes, D. L. Ward, R. He. Huang and J. L. Dye, *J Am Chem Soc*, 1986, **108**, 3534–3535.

35 A. Ellaboudy, J. L. Dye and P. B. Smith, *J Am Chem Soc*, 1983, **105**, 6490–6491.

36 I. R. Ariyarathna, *Inorg Chem*, 2022, **61**, 579–585.

37 L. Mones, G. Pohl and L. Turi, *Physical Chemistry Chemical Physics*, 2018, **20**, 28741–28750.

38 J. A. Walker and D. M. Bartels, *Journal of Physical Chemistry A*, 2016, **120**, 7240–7247.

39 A. G. Seel, E. Zurek, A. J. Ramirez-Cuesta, K. R. Ryan, M. T. J. Lodge and P. P. Edwards, *Chemical Communications*, 2014, **50**, 10778–10781.

40 P. P. Edwards, A. R. Lusis and M. J. Sienko, *J Chem Phys*, 1979, **72**, 3103–3112.

41 S. Hayama, J. C. Wasse, N. T. Skipper and A. K. Soper, *Journal of Physical Chemistry B*, 2002, **106**, 11–14.

42 K. Maeda, M. T. J. Lodge, J. Harmer, J. H. Freed and P. P. Edwards, *J Am Chem Soc*, 2012, **134**, 9209–9218.

43 Y. Nakamura, M. Niibe and M. Shimoji, *Nuclear Magnetic Resonance Study of Lithium in Liquid Ammonia and Methylamine*, 1984, vol. 88.

44 A. G. Seel, H. Swan, D. T. Bowron, J. C. Wasse, T. Weller, P. P. Edwards, C. A. Howard and N. T. Skipper, *Angewandte Chemie - International Edition*, 2017, **56**, 1561–1565.

45 A. M. Stacy, D. C. Johnson and M. J. Sienko, *J Chem Phys*, 1982, **76**, 4248–4254.

46 H. Thompson, J. C. Wasse, N. T. Skipper, S. Hayama, D. T. Bowron and A. K. Soper, *J Am Chem Soc*, 2003, **125**, 2572–2581.

47 I. R. Ariyarathna and E. Miliordos, *Physical Chemistry Chemical Physics*, 2021, **23**, 20298–20306.

48 B. M. Reinhard and G. Niedner-Schatteburg, *Physical Chemistry Chemical Physics*, 2002, **4**, 1471–1477.

49 P. E. Mason, H. C. Schewe, T. Buttersack, V. Kostal, M. Vitek, R. S. McMullen, H. Ali, F. Trinter, C. Lee, D. M. Neumark, S. Thürmer, R. Seidel, B. Winter, S. E. Bradforth and P. Jungwirth, *Nature*, 2021, **595**, 673–676.

50 C. Berg, U. Achatz, M. Beyer, S. Joos, G. Albert, T. Schindler, G. Niedner-Schatteburg and V. E. Bondybey, *Int J Mass Spectrom Ion Process*, 1997, **167–168**, 723–734.

51 A. C. Harms, S. N. Khanna, B. Chen and A. W. Castleman, *J Chem Phys*, 1994, **100**, 3540–3544.

52 R. Takasu, F. Misaizu, K. Hashimoto and K. Fuke, *J Phys Chem A*, 1997, **101**, 3078–3087.

53 B. M. Reinhard and G. Niedner-Schatteburg, *J Chem Phys*, 2003, **118**, 3571–3582.

54 I. R. Ariyarathna and E. Miliordos, *Physical Chemistry Chemical Physics*, 2019, **21**, 15861–15870.

55 B. A. Jackson and E. Miliordos, *Chemical Communications*, 2022, **58**, 1310–1313.

56 H. E. Zimmerman, *Acc Chem Res*, 2012, **45**, 164–170.

57 C. Van Der Linde, A. Akhgarnusch, C. K. Siu and M. K. Beyer, *Journal of Physical Chemistry A*, 2011, **115**, 10174–10180.

58 C. Van Der Linde, R. F. Höckendorf, O. P. Balaj and M. K. Beyer, *Chemistry - A European Journal*, 2013, **19**, 3741–3750.

59 E. Barwa, T. F. Pascher, M. Ončák, C. van der Linde and M. K. Beyer, *Angewandte Chemie - International Edition*, 2020, **59**, 7467–7471.

60 T. W. Lam, C. Van Der Linde, A. Akhgarnusch, Q. Hao, M. K. Beyer and C. K. Siu, *Chempluschem*, 2013, **78**, 1040–1048.

61 G. A. Olah, G. K. S. Prakash and A. Goeppert, *J Am Chem Soc*, 2011, **133**, 12881–12898.

62 Z. Jordan, S. N. Khan, B. A. Jackson and E. Miliordos, *Electronic Structure*, 2022, **4**, 015001.

63 T. H. Dunning, *J Chem Phys*, 1989, **90**, 1007–1023.

64 R. A. Kendall, T. H. Dunning and R. J. Harrison, *J Chem Phys*, 1992, **96**, 6796–6806.

65 D. E. Woon and T. H. Dunning, *J Chem Phys*, 1995, **103**, 4572–4585.

66 B. P. Prascher, D. E. Woon, K. A. Peterson, T. H. Dunning and A. K. Wilson, *Theor Chem Acc*, 2011, **128**, 69–82.

67 M. Head-Gordon, J. A. Pople and M. J. Frisch, *Chem Phys Lett*, 1988, **153**, 503–506.

68 M. J. Frisch, M. Head-Gordon and J. A. Pople, *Chem Phys Lett*, 1990, **166**, 275–280.

69 M. J. Frisch, M. Head-Gordon and J. A. Pople, *Chem Phys Lett*, 1990, **166**, 281–289.

70 J. Čížek, *J Chem Phys*, 1966, **45**, 4256–4266.

71 G. D. Purvis and R. J. Bartlett, *J Chem Phys*, 1982, **76**, 1910–1918.

72 H.-J. Werner, P. J. Knowles, G. Knizia, F. R. Manby and M. Schütz, *Wiley Interdiscip Rev Comput Mol Sci*, 2012, **2**, 242–253.

73 H.-J. Werner, P. J. Knowles, G. Knizia, F. R. Manby, M. Schütz, others, P. Celani, W. Györffy, D. Kats, T. Korona, R. Lindh, A. Mitrushenkov, G. Rauhut, K. R. Shamasundar, T. B. Adler, R. D. Amos, S. J. Bennie, A. Bernhardsson, A. Berning, D. L. Cooper, M. J. O. Deegan, A. J. Dobbyn, F. Eckert, E. Goll, C. Hampel, A. Hesselmann, G. Hetzer, T. Hrenar, G. Jansen, C. Köppl, S. J. R. Lee, Y. Liu, A. W. Lloyd, Q. Ma, R. A. Mata, A. J. May, S. J. McNicholas, W. Meyer, T. F. Miller III, M. E. Mura, A. Nicklass, D. P. O'Neill, P. Palmieri, D. Peng, K. Pflüger, R. Pitzer, M. Reiher, T. Shiozaki, H. Stoll, A. J. Stone, R. Tarroni, T. Thorsteinsson, M. Wang and M. Welborn, 2019.

74 P. J. Stephens, F. J. Devlin, C. F. Chabalowski and M. J. Frisch, *J Phys Chem*, 1994, **98**, 11623–11627.

75 S. H. Vosko, L. Wilk and M. Nusair, *Can J Phys*, 1980, **58**, 1200–1211.

76 A. D. Becke, *J Chem Phys*, 1993, **98**, 5648–5652.

77 C. Lee, W. Yang and R. G. Parr, *Phys Rev B*, 1988, **37**, 785–789.

78 M. J. Frisch, G. W. Trucks, H. B. Schlegel, G. E. Scuseria, M. A. Robb, J. R. Cheeseman, G. Scalmani, V. Barone, G. A. Petersson, H. Nakatsuji, X. Li, M. Caricato, A. V Marenich, J. Bloino, B. G. Janesko, R. Gomperts, B. Mennucci, H. P. Hratchian, J. V Ortiz, A. F. Izmaylov, J. L. Sonnenberg, D. Williams-Young, F. Ding, F. Lipparini, F. Egidi, J. Goings, B. Peng, A. Petrone, T. Henderson, D. Ranasinghe, V. G. Zakrzewski, J. Gao, N. Rega, G. Zheng, W. Liang, M. Hada, M. Ehara, K. Toyota, R. Fukuda, J. Hasegawa, M. Ishida, T. Nakajima, Y. Honda, O. Kitao, H. Nakai, T. Vreven, K. Throssell, J. A. Montgomery Jr., J. E. Peralta, F. Ogliaro, M. J. Bearpark, J. J. Heyd, E. N. Brothers, K. N. Kudin, V. N. Staroverov, T. A. Keith, R. Kobayashi, J. Normand, K. Raghavachari, A. P. Rendell, J. C. Burant, S. S. Iyengar, J. Tomasi, M. Cossi, J. M. Millam, M. Klene, C. Adamo, R. Cammi, J. W. Ochterski, R. L. Martin, K. Morokuma, O. Farkas, J. B. Foresman and D. J. Fox, 2016.

79 J. R. Hwu, Y. S. Wein and Y.-J. Leu, *J Org Chem*, 1996, **61**, 1493–1499.

80 P. Giannozzi, S. Baroni, N. Bonini, M. Calandra, R. Car, C. Cavazzoni, D. Ceresoli, G. L. Chiarotti, M. Cococcioni, I. Dabo, A. Dal Corso, S. de Gironcoli, S. Fabris, G. Fratesi, R. Gebauer, U. Gerstmann, C. Gougoussis, A. Kokalj, M. Lazzeri, L. Martin-Samos, N. Marzari, F. Mauri, R. Mazzarello, S. Paolini, A. Pasquarello, L. Paulatto, C. Sbraccia, S. Scandolo, G. Sclauzero, A. P. Seitsonen, A. Smogunov, P. Umari and R. M. Wentzcovitch, *Journal of Physics: Condensed Matter*, 2009, **21**, 395502.

81 P. E. Blöchl, *Phys Rev B*, 1994, **50**, 17953–17979.

82 V. Blum, R. Gehrke, F. Hanke, P. Havu, V. Havu, X. Ren, K. Reuter and M. Scheffler, *Comput Phys Commun*, 2009, **180**, 2175–2196.

83 E. R. Johnson, A. Otero-de-la-Roza and S. G. Dale, *J Chem Phys*, 2013, **139**, 184116.

84 Q. Zhao and H. J. Kulik, *J Chem Theory Comput*, 2018, **14**, 670–683.

85 K. Lejaeghere, G. Bihlmayer, T. Björkman, P. Blaha, S. Blügel, V. Blum, D. Caliste, I. E. Castelli, S. J. Clark, A. Dal Corso, S. de Gironcoli, T. Deutsch, J. K. Dewhurst, I. Di Marco, C. Draxl, M. Dułak, O. Eriksson, J. A. Flores-Livas, K. F. Garrity, L. Genovese, P. Giannozzi, M. Giantomassi, S. Goedecker, X. Gonze, O. Grånäs, E. K. U. Gross, A. Gulans, F. Gygi, D. R. Hamann, P. J. Hasnip, N. A. W. Holzwarth, D. Iuşan, D. B. Jochym, F. Jollet, D. Jones, G. Kresse, K. Koepernik, E. Küçükbenli, Y. O. Kvashnin, I. L. M. Locht, S. Lubeck, M. Marsman, N. Marzari, U. Nitzsche, L. Nordström, T. Ozaki, L. Paulatto, C. J. Pickard, W. Poelmans, M. I. J. Probert, K. Refson, M. Richter, G.-M. Rignanese, S. Saha, M. Scheffler, M. Schlipf, K. Schwarz, S. Sharma, F. Tavazza, P. Thunström, A. Tkatchenko, M. Torrent, D. Vanderbilt, M. J. van Setten, V. Van Speybroeck, J. M. Wills, J. R. Yates, G.-X. Zhang and S. Cottenier, *Science (1979)*, , DOI:10.1126/science.aad3000.

86 P. Pulay, *Chem Phys Lett*, 1980, **73**, 393–398.

87 R. de Gelder, R. Wehrens and J. A. Hageman, *J Comput Chem*, 2001, **22**, 273–289.

88 A. Otero-de-la-Roza, E. R. Johnson and V. Luaña, *Comput Phys Commun*, 2014, **185**, 1007–1018.

89 A. Kokalj, *J Mol Graph Model*, 1999, **17**, 176–179.

90 W. Humphrey, A. Dalke and K. Schulten, *J Mol Graph*, 1996, **14**, 33–38.

91 G. Knizia, *J Chem Theory Comput*, 2013, **9**, 4834–4843.

92 J. Gräfenstein, E. Kraka and D. Cremer, *Phys. Chem. Chem. Phys.*, 2004, **6**, 1096–1112.

93 K. R. Bryenton, A. A. Adeleke, S. G. Dale and E. R. Johnson, *WIREs Computational Molecular Science*, , DOI:10.1002/wcms.1631.

94 I. G. Ryabinkin and V. N. Staroverov, *Phys, Chem. Chem. Phys.*, 2011, **13**, 21615.

95 T. Soda, Y. Kitagawa, T. Onishi, Y. Takano, Y. Shigeta, H. Nagao, Y. Yoshioka and K. Yamaguchi, *Chem Phys Lett*, 2000, **319**, 223–230.

APPENDIX A: Supporting Material for Chapter 2

Appendix A contains full copies of the following article. Reprints were made with permission of the publishers.

B. Jackson and E. Miliordos, *Chemical Communications* ***58****, 1310 (2022)*

ChemComm

ROYAL SOCIETY OF CHEMISTRY

COMMUNICATION

View Article Online
View Journal | View Issue

Cite this: *Chem. Commun.*, 2022, **58**, 1310

Received 26th August 2021,
Accepted 22nd December 2021

DOI: 10.1039/d1cc04748e

rsc.li/chemcomm

Simultaneous CO_2 capture and functionalization: solvated electron precursors as novel catalysts†

Benjamin A. Jackson and Evangelos Miliordos *

Metal complexes with diffuse solvated electrons (solvated electron precursors) are proposed as alternative catalysts for the simultaneous CO_2 capture and utilization. Quantum chemical calculations were used to study the reaction of CO_2 with H_2 and C_2H_4 to produce formic acid, methyldiol and δ-lactone. Mechanisms of a complete reaction pathway are found and activation barriers are reasonably low. The metal ligand complex readily reduces CO_2 and significantly stabilizes $CO_2^{\bullet-}$. Ligand identity minimally influences the reaction. Additional reactions and future strategies are proposed with the goal of inducing experimental interest.

Solvated electron precursors (SEPs) are a class of metal–ligand complexes consisting of a metal $M^{n+}(L)_x$ core surrounded by n metal electrons which are displaced to the periphery of the complex – these constitute the microscopic structure of solvated electron solutions in the dilute regime.[1] The study of SEPs poses an exciting avenue for the development of novel reduction catalysts. The diffuse nature of the outer solvated electron orbital is highly reactive while functionalization of SEP ligands suggests a potentially high degree of tunability and a wide range of applications.

Solvated electrons are powerful reducing agents capable of reducing benzene rings as evidenced in the well-known Birch reduction.[2] Previous experimental work in SEP reactivity has illustrated the ability of metal SEP hydrates to reduce O_2, CO_2, CH_3CN, and NO.[3–6] However, the mechanism of this reduction remains poorly understood. To this end, two gas-phase reaction systems involving the SEP $Li(NH_3)_4$ are mechanistically studied: the conversion of CO_2 and H_2 to formic acid/methyldiol and that of CO_2 and ethene to δ-lactone. In addition, SEP ligand effects are explored using ammonia, methylamine, ethylamine, water, and methanol.

The capture and utilization of CO_2 has been the topic of intense interest in the literature. A review of the used methods/materials is beyond the scope of this communication, but it is worth mentioning that practical applications involve two different molecular systems, one for the capture and one for the catalytic transformation of CO_2 to a platform chemical. For example, the work of Prakash and co-workers employed a polyamine system to capture CO_2 and a Ru-based catalyst for its conversion to methanol.[7–9] The present work reveals that SEPs can perform both tasks simultaneously.

The transition states (TS), reactants, intermediates, and products for the two gas-phase reaction systems were generally optimized in Gaussian 16[10] under density functional theory (DFT) using the CAM-B3LYP functional and the cc-pVTZ (Li, N, O, C) and aug-cc-pVTZ (H) basis sets.[11–14] This functional and basis set combination has been shown to provide accurate structures in SEP systems.[15,16] Augmentation of C and O basis sets is shown to minimally effect reaction energetics (see Fig. S10, ESI†). All optimal structures were of doublet spin multiplicity. Select structures were optimized at second-order Moller–Plesset perturbation theory (MP2) level and double-ζ basis sets.[17] Coupled-cluster singles, doubles, and perturbatively connected triples, CCSD(T), calculations were also obtained using Molpro 2015.5.[18,19] See the ESI† for a detailed discussion of computational methodology. The higher level CCSD(T) results were used to benchmark CAM-B3LYP energies for $Li(NH_3)_4$ and $Li(H_2O)_4$ which on average agree within ±1.5 kcal mol^{-1} (see Fig. S2 and S3 of ESI†).

The $Li(NH_3)_4$ complex consists of a $Li(NH_3)_4^+$ core which is surrounded by a pseudospherical diffuse orbital occupied by a single electron. The reaction pathway of $Li(NH_3)_4$ and CO_2 + $2H_2$ is given in Fig. 1. Electronic energies are used for all figures in this manuscript and free energy diagrams at 1 atm and 298 K are given in the ESI† and discussed below. The pathway begins with the coordination of CO_2 to the SEP with a binding energy of 1.7 kcal mol^{-1} (CO_2r). Following this is a transition state (eTS1) involving the transfer of the SEP electron to CO_2 to form the radical $CO_2^{\cdot-}$(CO_2p). The electronic energy activation

Department of Chemistry and Biochemistry, Auburn University, Auburn, AL 36849-5312, USA. E-mail: emiliord@auburn.edu

† Electronic supplementary information (ESI) available: The Electronic Supplementary Information file contains a more detailed description of the computational methodology. In addition, it provides optimal CAM-B3LYP geometries, harmonic vibrational frequencies, energetics for all intermediates and transition states, and free energy and enthalpy plots for the H_2 and C_2H_4 pathways. See DOI: 10.1039/d1cc04748e

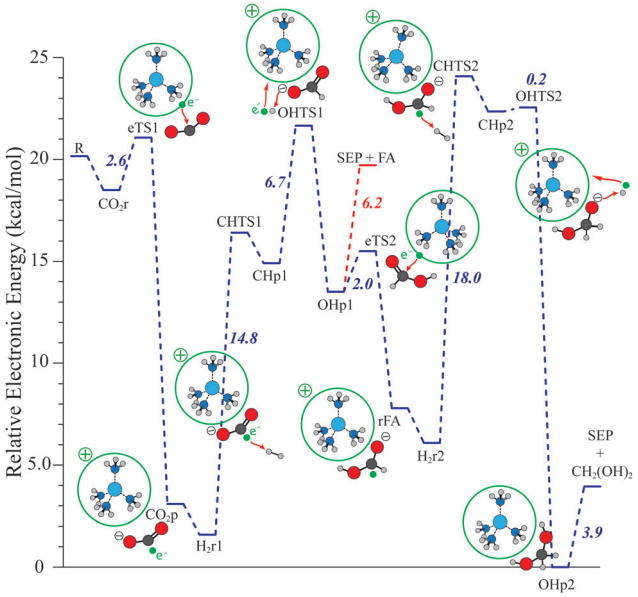

Fig. 1 Reaction pathway of $Li(NH_3)_4$ + CO_2 + 2 H_2 → $Li(NH_3)_4$ + $CH_2(OH)_2$. Graphical representations of transition states and select intermediates are given as figure insets. A green dot is used to indicate the movement of the SEP e^- throughout the pathway. Activation barriers are given in kcal mol^{-1}. Relative electronic energies are zeroed to the lowest point of the pathway. See Table S16 of ESI† for details.

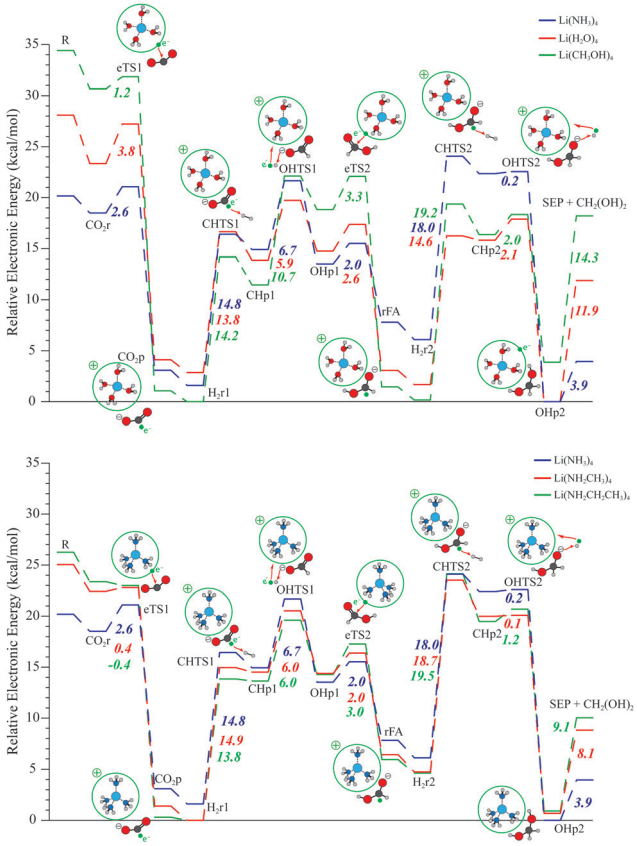

Fig. 2 Reaction pathways of $Li(X)_4$ + CO_2 + 2 H_2 → $Li(X)_4$ + $CH_2(OH)_2$, X = NH_3, NH_2CH_3, $NH_2CH_2CH_3$, H_2O, CH_3OH. Graphical representations of transition states and select intermediates are given as figure insets. A green dot is used to indicate the movement of the SEP e^- throughout the pathway. Activation barriers are given in kcal mol^{-1}. Relative electronic energies are zeroed to the lowest point of the pathway. See Table S16 of ESI† for details.

barrier (E_a) of the electron transfer is only 2.6 kcal mol^{-1}. After the transfer, an H_2 molecule binds to the complex (H_2r1). Subsequently, there is a transition state (CHTS1, E_a of 14.8 kcal mol^{-1}) involving the radical C of $CO_2^{\bullet -}$ attacking H_2 to form a C–H bond, breaking the H–H bond (CHp1). The next step is the transition state (OHTS1) involving the formation of an O-H bond and the return of an electron to the SEP (E_a of 6.7 kcal mol^{-1}) upon which formic acid (CHOOH) is formed. This may either be released, with a barrier of 6.2 kcal mol^{-1} (SEP + FA), or, with a barrier of 2 kcal mol^{-1} (eTS2), be reduced a second time to form $CHOOH^-$ (rFA). After the coordination of a second H_2 (H_2r2), a transition state involving the formation of a second C–H bond (CHTS2) with a barrier of 18 kcal mol^{-1} to form CH_2OOH^- (CHp2). This precedes the last transition state (OHTS2) of the O–H bond formation and the return of an electron to the $Li(NH_3)_4$ complex which has a barrier of 0.2 kcal mol^{-1}. This results in the formation of a methyldiol coordinated to the SEP which releases to form the separate products at a barrier of 3.9 kcal mol^{-1}.

This reaction in absence of the SEP proceeds slightly differently (see Fig. S1 of ESI†). Addition of each H_2 unit occurs in a single concerted transition state with an E_a = 13.8 kcal mol^{-1} for the first TS to give $CHOOH^-$ and E_a = 33.2 kcal mol^{-1} for the second to give $CH_2(OH)_2^-$. The first addition is lower in E_a than the combined two steps of the SEP mechanism (13.8 *vs.* 14.8 + 6.7); however, this is offset by the SEP's lower E_a barrier for the second H_2 (33.2 *vs.* 18 + 0.2). Additionally, the SEP serves an integral function in stabilizing the $CO_2^{\bullet -}$ radical. The electron affinity (EA) of CO_2 is −0.87 eV (−20.1 kcal mol^{-1}) which must first be overcome to proceed. When coordinated to $Li(NH_3)_4^+$, $CO_2^{\bullet -}$ is stabilized by 15.4 kcal mol^{-1} (CO_2p *vs.* CO_2r) over CO_2 coordinated to $Li(NH_3)_4$.

Shown in Fig. 2 is the effect of varying ligands on the reaction pathway. The ligands broken into two groups are: the hydroxy ligands (H_2O, CH_3OH) and the amine ligands (NH_3, NH_2CH_3, $NH_2CH_2CH_3$). These results indicate that the ligand choice significantly affects the pathway in only two areas: the initial electron transfer eTS and the dissociation of the products. Interchange of the ligands has no effect on the reaction mechanism and minimal effects (E_a within ± 3 kcal mol^{-1}) on the energetics of intermediate steps in the pathway (CO_2p through OHp2). Increasing the length of carbon chains in both the hydroxy and amine ligands results in an SEP electron which is more weakly bound and therefore more reductively reactive. The $Li(H_2O)_4$ complex possess the most tightly bound SEP electron with an ionization energy (IE calculated at CAM-B3LYP) of 3.67 eV to give the largest E_a for the electron transfer to CO_2 (eTS) at 3.8 kcal mol^{-1}. Addition of a methyl group (CH_3OH) lowers its IE to 3.36 eV and an E_a of eTS 1.2 kcal mol^{-1}. This trend is identical for the amine ligands NH_3: IE 3.02 eV & 2.6 kcal mol^{-1} E_a to NH_2CH_3: IE 2.76 eV & E_a

0.4 kcal mol^{-1} to $NH_2CH_2CH_3$: IE 2.59 eV. In the case of ethylamine, the SEP electron is bound so weakly that no barrier for the electron transfer exists. Finally, the hydroxy ligands more strongly coordinate the formic acid and methyldiol due to the stronger hydrogen bonds of O–H *vs.* N–H, requiring greater energy to dissociate the products.

Energetically, the H_2 pathway is electronically favorable; however, considering enthalpic and entropic effects the reaction is less so. At 298 K, the reaction is endothermic (ΔH) by 3.5 kcal mol^{-1} and endergonic (ΔG) by 12.5 kcal mol^{-1} (see Fig. S4–S7 of ESI† for details).

Transitioning to the ethene pathway, Fig. 3 depicts the reaction coordinate diagram for the conversion of CO_2 and ethene to a δ-lactone ring as catalyzed by the $Li(NH_3)_4$ and $Li(NH_2CH_3)_4$ SEPs. As in the H_2 system, the pathway begins with the reduction of CO_2 to a coordinated radical $CO_2^{\cdot-}$. Following which, an ethene coordinates to the complex (EtR) and is then attacked by the radical C of $CO_2^{\cdot-}$ (EtTS1, 9.0 and 9.1 kcal mol^{-1} E_a) to form a C–C bond, breaking the ethene π-bond and producing a terminal radical C (EtP). Following this, two things may occur: (1) The highest energy and least likely pathway involves a rearrangement (OHTS, 55.2 kcal mol^{-1} E_a) to produce a hydroxyl group and C–C double bond (OHEtP). (2) The process repeats (EtR2, EtTS2, and EtP2) to add a second ethene residue. Given that the barrier remains ∼9.0 kcal mol^{-1} for the addition of each ethene residue and that this addition is energetically downhill, either the C–C chain continues to grow as a polymerization reaction or, overcoming a barrier of 37.8/38.0 kcal mol^{-1} (LacTS), O attacks the terminal carbon to form the lactone ring and the radical electron is returned to the SEP. The subsequent step (LacP to P) involves the dissociation of lactone from the SEP - in the case of $Li(NH_2CH_3)_4$ this barrier is more than 3× that of $Li(NH_3)_4$ (5.8 *vs.* 19.1 kcal mol^{-1}).

As with the H_2 pathway, the ligand identity significantly affects only the first (eTS) and last step of the mechanism (P). The energetics and pathway of the intervening steps (SEPp through LacP) are virtually unaffected (E_a ±0.2 kcal mol^{-1}) by the ligand choice. The electronic energy activation barrier for the electron transfer to CO_2 (eTS) is smaller for methylamine due to its more weakly bound SEP electron, see above. In addition, the lactone dissociation from the methylamine complex is significantly harder due to it more strongly binding to the complex. The 38 kcal mol^{-1} barrier of LacTS will prove an initial hindrance at room temperature. This poses an avenue for future development and may be overcome through the tuning of reaction conditions, the use of ethene substituted by an electron donating functional group to promote a return of the electron to the SEP, or through the addition of further ethene residues before ring closure leading to a decrease in steric strain.

Overall, the ethene pathway offers far more promising results in terms of a viable catalytic cycle. The pathway at 298 K is exothermic by −22.3 kcal mol^{-1}. But due to the entropy penalty of converting three molecules (CO_2 + 2 C_2H_4) to one (δ-lactone) it is endergonic by 0.94 kcal mol^{-1} (for ΔG and ΔH plots see Fig. S8 and S9 of the ESI†). This naturally suggests several alternative reactants which may be used in place of ethene but should follow the same mechanism (Fig. 4). In reaction 1, the ethene pathway, three π-bonds (C═O and 2C═C) are broken to form three σ-bonds (C–O and 2C–C). In reaction 2, the use of a butadiene would decrease the entropic penalty (2 molecules → 1 molecule) but at the loss of an exothermic C–C σ-bond formation. Instead in reaction (3), the use of an octadiene would allow for the formation of the lactone ring and the three σ-bonds for an exothermic and exergonic reaction. In reaction (4), the o-xylylene and CO_2 reaction would lead to the formation of an aromatic ring-significantly increasing the free energy of the reaction at 298 K. In principle, the free energies must be calculated under the conditions that the stability of these systems is experimentally the largest, and future calculations will need input from experiment.

In summary, we provide insights into the application of SEPs as catalysts. We have used the reaction of CO_2 with H_2 and C_2H_4 as model systems for exploring this application.

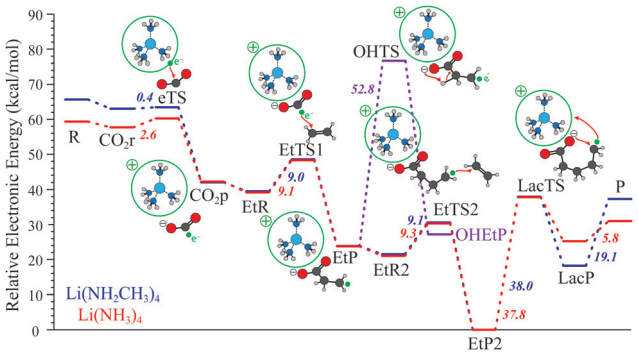

Fig. 3 Reaction pathways of $Li(NH_3/NH_2CH_3)_4$ + 2C_2H_4 + 2CO_2 → $Li(NH_3/NH_2CH_3)_4$ + $C_5H_8O_2$. Graphical representations of transition states and select intermediates are given as figure insets. A green dot is used to indicate the movement of the SEP e$^-$ throughout the pathway. Activation barriers are given in kcal mol^{-1}. Relative electronic energies are zeroed to the lowest point of the pathway. Shown in purple is a side reaction of the $Li(NH_2CH_3)_4$ system. See Table S17 of ESI† for details.

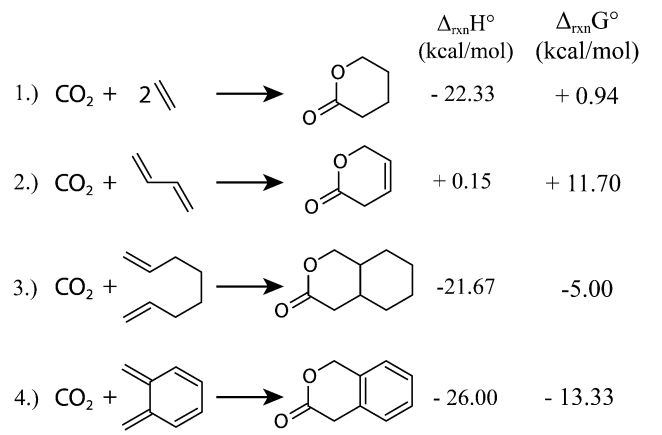

Fig. 4 Comparison of energetics for reactions analogous to the ethene pathway. Structures optimized at CAM-B3LYP. Basis sets: cc-pVTZ(C,O) aug-cc-pVTZ (H). See Tables S18 of ESI† for details.

Mechanisms for the conversion of CO_2 to formic acid/methyldiol and lactone as catalyzed by SEPs are proposed. The lithium-ligand SEP complex is shown to play an important role in stabilizing the reactant $CO_2^{\bullet -}$. Various ligands are tested, and ligand interchange is shown to have a significant effect on only two steps: the electron transfer (eTS) and the dissociation of products. The intervening steps are virtually independent of ligand identity. Increasing ligand size results in more diffuse solvated electrons and increased SEP reactivity. This degree of ligand interchange independence will allow future work to select ligands (hydroxy or amine) based on convenience. Additional insights from these results are used to propose additional reagents to produce spontaneous catalytic reactions. The CAM-B3LYP functional was benchmarked using the higher level CCSD(T) methodology and demonstrated excellent agreement in reaction energetics, validating the results herein. This work is meant to serve as a proof of concept, demonstrating the viability of SEPs in catalysis and providing insights for this application which may induce and inform future experimental work.

This material is based upon work supported by Auburn University (AU) and the National Science Foundation under Grant No. CHE-1940456. We acknowledge the support and resources provided by the Auburn University Hopper Cluster and Alabama Supercomputer Center.

Conflicts of interest

There are no conflicts to declare.

References

1 E. Zurek, P. P. Edwards and R. Hoffmann, *Angew. Chem., Int. Ed.*, 2009, **48**, 8198–8232.
2 H. E. Zimmerman, *Acc. Chem. Res.*, 2012, **45**, 164–170.
3 C. Van Der Linde, A. Akhgarnusch, C. K. Siu and M. K. Beyer, *J. Phys. Chem. A*, 2011, **115**, 10174–10180.
4 C. Van Der Linde, R. F. Höckendorf, O. P. Balaj and M. K. Beyer, *Chem. – Eur. J.*, 2013, **19**, 3741–3750.
5 T. W. Lam, C. Van Der Linde, A. Akhgarnusch, Q. Hao, M. K. Beyer and C. K. Siu, *ChemPlusChem*, 2013, **78**, 1040–1048.
6 E. Barwa, T. F. Pascher, M. Ončák, C. van der Linde and M. K. Beyer, *Angew. Chem., Int. Ed.*, 2020, **59**, 7467–7471.
7 S. Kar, A. Goeppert, V. Galvan, R. Chowdhury, J. Olah and G. K. S. Prakash, *J. Am. Chem. Soc.*, 2018, **140**, 16873–16876.
8 S. Kar, R. Sen, A. Goeppert and G. K. S. Prakash, *J. Am. Chem. Soc.*, 2018, **140**, 1580–1583.
9 G. A. Olah, G. K. S. Prakash and A. Goeppert, *J. Am. Chem. Soc.*, 2011, **133**, 12881–12898.
10 M. J. Frisch, G. W. Trucks, H. B. Schlegel, G. E. Scuseria, M. A. Robb, J. R. Cheeseman, G. Scalmani, V. Barone, G. A. Petersson, H. Nakatsuji, *et al.*, *Gaussian 16 Rev. C.01*, Wallingford, CT, 2016.
11 B. P. Prascher, D. E. Woon, K. A. Peterson, T. H. Dunning and A. K. Wilson, *Theor. Chem. Acc.*, 2011, **128**, 69–82.
12 D. E. Woon and T. H. Dunning, *J. Chem. Phys.*, 1995, **103**, 4572–4585.
13 R. A. Kendall, T. H. Dunning and R. J. Harrison, *J. Chem. Phys.*, 1992, **96**, 6796–6806.
14 T. Yanai, D. P. Tew and N. C. Handy, *Chem. Phys. Lett.*, 2004, **393**, 51–57.
15 S. N. Khan and E. Miliordos, *J. Phys. Chem. A*, 2020, **124**, 4400–4412.
16 B. A. Jackson and E. Miliordos, *J. Chem. Phys.*, 2021, **155**, 014303.
17 M. J. Frisch, M. Head-Gordon and J. A. Pople, *Chem. Phys. Lett.*, 1990, **166**, 275–280.
18 H.-J. Werner, P. J. Knowles, G. Knizia, F. R. Manby, M. Schütz, P. Celani, W. Györffy, D. Kats, T. Korona, R. Lindh, *et al.*, MOLPRO, version 2015.1, a package of *ab initio* programs, 2015.
19 J. D. Watts, J. Gauss and R. J. Bartlett, *J. Chem. Phys.*, 1993, **98**, 8718–8733.

APPENDIX B: Supporting Material for Chapter 3

Appendix B contains full copies of the following articles. Reprints were made with permission of the publishers.

B. Jackson and E. Miliordos, *Journal of Chemical Physics* **156**, 194302 (2022)

Z. Jordan, S. N. Khan, B. A. Jackson, E. Miliordos, *Electronic Structure,* **4**, 015001 (2022)

The Journal of Chemical Physics ARTICLE scitation.org/journal/jcp

The nature of supermolecular bonds: Investigating hydrocarbon linked beryllium solvated electron precursors

Cite as: J. Chem. Phys. 156, 194302 (2022); doi: 10.1063/5.0089815
Submitted: 28 February 2022 • Accepted: 26 April 2022 •
Published Online: 16 May 2022

Benjamin A. Jackson and Evangelos Miliordos[a)]

AFFILIATIONS

Department of Chemistry and Biochemistry, Auburn University, Auburn, Alabama 36849-5312, USA

Note: This paper is part of the JCP Special Topic on Nature of the Chemical Bond.
[a)]**Author to whom correspondence should be addressed:** emiliord@auburn.edu

ABSTRACT

Beryllium ammonia complexes $Be(NH_3)_4$ are known to bear two diffuse electrons in the periphery of a $Be(NH_3)_4^{2+}$ skeleton. The replacement of one ammonia with a methyl group forms $CH_3Be(NH_3)_3$ with one peripheral electron, which is shown to maintain the hydrogenic-type shell model observed for $Li(NH_3)_4$. Two $CH_3Be(NH_3)_3$ monomers are together linked by aliphatic chains to form strongly bound beryllium ammonia complexes, $(NH_3)_3Be(CH_2)_nBe(NH_3)_3$, n = 1–6, with one electron around each beryllium ammonia center. In the case of a linear carbon chain, this system can be seen as the analog of two hydrogen atoms approaching each other at specific distances (determined by n). We show that the two electrons occupy diffuse s-type orbitals and can couple exactly as in H_2 in either a triplet or singlet state. For long hydrocarbon chains, the singlet is an open-shell singlet nearly degenerate with the triplet spin state, which transforms to a closed-shell singlet for n = 1 imitating the σ-covalent bond of H_2. The biradical character of the system is analyzed, and the singlet–triplet splitting is estimated as a function of n based on multi-reference calculations. Finally, we consider the case of bent hydrocarbon chains, which allows the closer proximity of the two diffuse electrons for larger chains and the formation of a direct covalent bond between the two diffuse electrons, which happens for two $Li(NH_3)_4$ complexes converting the open-shell to closed-shell singlets. The energy cost for bending the hydrocarbon chain is nearly compensated by the formation of the weak covalent bond rendering bent and linear structures nearly isoenergetic.

I. INTRODUCTION

Metal ammonia complexes demonstrate the unique property of hosting diffuse electrons in their ground electronic states. These electrons populate hydrogenic-type orbitals in a shell model, which mimics that of the jellium or nuclear shell models.[1] For example, $Li(NH_3)_4$ holds one electron in the periphery of the $Li(NH_3)_4^+$ skeleton in an s-type orbital.[2] Even more interestingly, two such entities can bind together resembling the formation of H_2 from two H atoms.[2] Aggregates of $Li(NH_3)_4$ complexes form grids of $Li(NH_3)_4^+$ cores with free, interstitial electrons, producing a metallic material known as an expanded or liquid metal.[3,4] We have named these metal ammonia complexes solvated electron precursors (SEPs) due to their presence in metal ammonia solutions of intermediate concentrations.[5]

The first systematic work on the Aufbau principle for the diffuse electrons in SEPs was reported for $Be(NH_3)_4^{0,\pm}$ four years ago.[1] The lowest energy orbital is 1s, followed by 1p, 1d, 2s, 1f, and 2p. The adopted nomenclature was chosen to match the jellium or nuclear shell models. The same energy order has been observed for many other metals (including transition metals) clearly for the first three orbitals, but the 2s, 2p, and 1f orbitals are usually close in energy and their order may depend on the system.[1,2,6–10] In addition, two SEP molecules can bind together to form σ and π bonds similarly to traditional diatomic molecules.[2]

We recently showed that the replacement of one ammonia molecule with a methyl group enables the formation of SEPs for atoms where ammonia ligands alone are insufficient. Specifically, we demonstrated that $B(NH_3)_4$ is unstable and ammonia cannot displace all three valence electrons of boron to the periphery of the complex.[11] Instead, one methyl group can form a B–C bond and three ammonia ligands can displace the remaining two electrons, to form a stable SEP. Furthermore, we proved that bridging two $(NH_3)_3BCH_3$ entities by hydrocarbon chains forms stable

$(NH_3)_3B(CH_2)_nB(NH_3)_3$ linked-SEPs, hosting two diffuse electrons around each boron center. Currently, we examine the possibility to produce similar complexes with Be. Each beryllium center is expected to hold one diffuse electron, which leads to the questions: Do the two electrons couple into a triplet or singlet spin multiplicity? Do hydrocarbon chains bend to facilitate a chemical bond between the two electrons? What kind of orbitals are populated in the ground and excited electronic states? This work aims to answer these questions by means of density functional theory and multi-reference wavefunction methodologies. Exploration of this system will provide insight into the nature and stability of chemical bonding in supermolecular systems.

II. COMPUTATIONAL DETAILS

All structures were optimized using density functional theory (DFT) and the CAM-B3LYP functional.[12] Correlation consistent triple-ζ basis sets were used for all atoms (cc-pVTZ). For hydrogen, an additional set of diffuse functions were used (aug-cc-pVTZ).[13–15] This methodology has been shown to provide excellent agreement with second-order Møller–Plesset perturbation theory (MP2) and coupled-clusters single, double, and perturbative triples, CCSD(T), structures for similar systems.[10,16] All reported species have only real frequencies. Single-point energy calculations at the MP2 level were used to further improve binding energies. The lowest energy singlet spin states were used for the geometry optimizations (unrestricted DFT = UDFT).

Excitation energies were calculated using state-averaged complete active space self-consistent field (SA-CASSCF or simply CASSCF) followed by second-order perturbation theory (CASPT2) as implemented in RS2C in MOLPRO 2015.1.[17] A level shift value of 0.2 a.u. and an IPEA (shift parameter for orbital energies) value of 0.25 a.u. were applied.[18,19] The basis sets used for the CASSCF/CASPT2 calculations of $(NH_3)_3Be(CH_3)_nBe(NH_3)_3$ were cc-pVDZ (C, N, Be) and d-aug-cc-pVDZ (H).[13–15,20] For the linear n = 1–6 and curved n = 1–4 structures, C_{2h}, C_{2v}, or C_2 symmetry was imposed by rotation of NH_3 groups. Symmetrical structures differ from the optimal geometries by less than 1 kcal/mol. For the n = 5,6 "curved" structures, optimal C_1 geometries were used; and to ensure tractability of calculations for these two systems, the basis sets of the carbon and hydrogen atoms in the aliphatic chain included only s/p and s type functions, respectively. This approximation was proven to be very accurate for the excitation energies of the "linear" $(NH_3)_3Be(CH_2)_6Be(NH_3)_3$ molecule (see below).

The active space for the reference CASSCF calculations consists of 1 electron in 10 orbitals for $CH_3Be(NH_3)_3$, two electrons in eight orbitals for "linear" $(NH_3)_3Be(CH_2)_{1-6}Be(NH_3)_3$ species, two electrons in seven orbitals for "curved" $(NH_3)_3Be(CH_2)_{1-5}Be(NH_3)_3$ species, and two electrons in six orbitals for "curved" $(NH_3)_3Be(CH_2)_6Be(NH_3)_3$. All states reported presently are averaged together with equal weights (SA-CASSCF); see Tables S10–S21 of the supplementary material. All valence electrons are correlated at CASPT2. For the ground states, we also performed state specific CASSCF/CASPT2 calculations with two electrons in eight orbitals.

The cc-pVDZ (C, N, Be) and d-aug-cc-pVDZ (H) basis sets used for the excitation energies of "linear" and "curved" $(NH_3)_3Be(CH_2)_{1-6}Be(NH_3)_3$ species were benchmarked for the $CH_3Be(NH_3)_3$ monomer against the corresponding triple-ζ basis set combination. The two sets agree within 0.04 eV, and double-ζ is considered quite accurate.

The multi-reference configuration interaction (MRCI) calculations for $BeCH_3$ were done with the cc-pVTZ basis set for all atoms and the full valence space as active space for the reference CASSCF wavefunction. All four doublet spin states stemming from the first two Be + CH_3 channels are averaged at the CASSCF level.

III. RESULTS AND DISCUSSION

The ground state of Be (^{1}S; $1s^2 2s^2$) is of closed-shell nature but easily polarizable facilitating, for example, chemical bonds with other closed-shell systems such as NH_3 or another Be atom.[21] An alternative path is the use of its first excited state ^{3}P ($1s^2 2s^1 2p^1$), which is 21 980 cm^{-1} higher (M_J averaged value from Ref. 22) than ^{1}S. This is the case for the bond between Be and CH_3, which originates from Be (^{3}P) + CH_3 ($\tilde{X}^2A_2'$). The potential energy curves (PECs) of the Be–CH_3 approach for all doublet states stemming from the first two adiabatic channels are shown in Fig. 1. The first excited state of CH_3 is of the Rydberg character with the single electron populating the 3s orbital of carbon and lies at 46 239 cm^{-1}; thus, the first two channels are Be (^{1}S) + CH_3 ($\tilde{X}^2A_2'$) and Be (^{3}P) + CH_3 ($\tilde{X}^2A_2'$). The quartet states from the second channel are either slightly attractive or repulsive at the CASSCF level and are not considered presently.

The ground state of $BeCH_3$ is a doublet state with an unpaired electron in a primarily 2s orbital of beryllium polarized away from CH_3, avoiding the electron pair of the Be–CH_3 bond. The molecular orbitals of Fig. 2 illustrate the global minimum of $BeCH_3$ that diabatically comes from Be(^{3}P) + CH_3 ($\tilde{X}^2A_2'$). The bonding scheme in Fig. 2 shows the bonding orbital between Be and CH_3. CH_3 is initially planar[23] and as the two moieties approach each other, the unhybridized $2p_z$ of carbon gradually mixes with the other valence orbitals to become an sp^3 hybrid. The bonding orbital has a 0.61 $2p_z$

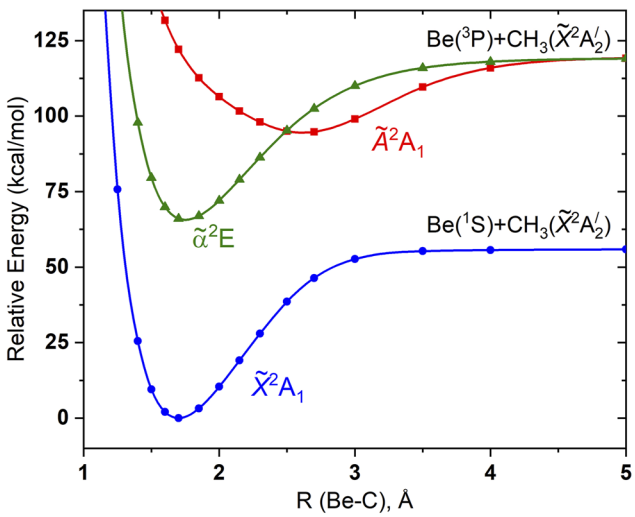

FIG. 1. MRCI potential energy curves for the Be–CH_3 approach as a function of the Be–C distance R(Be–C). All doublet spin states from the first two channels are shown, and the geometry of CH_3 is kept fixed at the equilibrium $BeCH_3$ geometry.

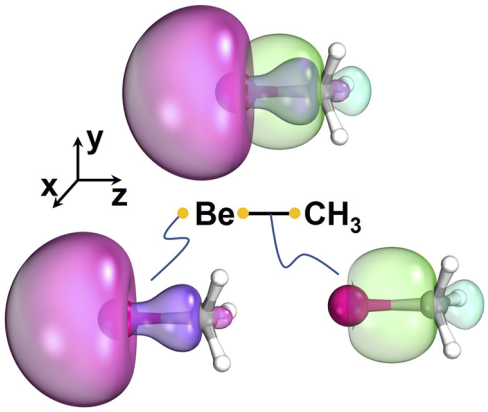

FIG. 2. Contours for the Be–C bonding and singly occupied molecular orbitals of the ground state of $BeCH_3$.

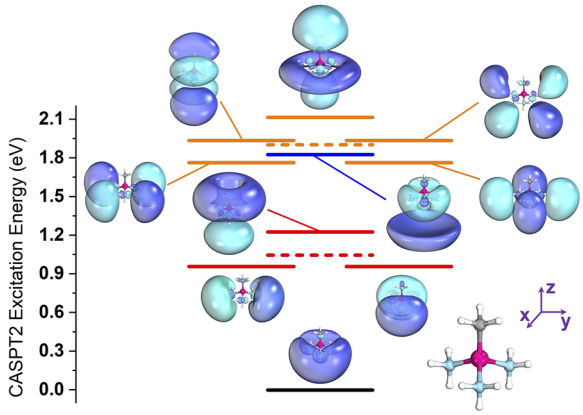

FIG. 3. Energy diagram (CASPT2 level of theory) and populated orbitals for the lowest energy electronic states of $CH_3Be(NH_3)_3$. The black line corresponds to the 1s orbital, the three solid red lines to the 1p orbitals, the blue line to the 2s orbital, and the five orange solid lines to the 1d orbitals. The red and orange dashed lines pertain to the average energies of 1p and 1d orbitals.

(C) − 0.38 2s (C) − 0.60 2s (Be) − 0.45 $2p_z$ (Be) composition and the singly occupied orbital 0.73 2s (Be) − 0.67 $2p_z$ (Be). The morphology of the PECs (see Fig. 1) is also in agreement with the proposed scheme revealing an avoided crossing between $\tilde{X}^2A_1$ and $\tilde{A}^2A_1$ in the region between 2.5 and 3 Å.

The Be–CH_3 bond is strong with a binding energy of 57.8 kcal/mol at the MP2 level of theory. The binding energy of the ammonia ligands is approximately half that: the first ammonia attaches to beryllium with 21.5 kcal/mol, the second one with 25.3 kcal/mol, and the third one with 26.3 kcal/mol. After zero-point energy corrections (at the CAM-B3LYP level), these MP2 binding energies become 18.6, 22.9, and 22.5 kcal/mol. The corresponding binding energies for $CH_3B(NH_3)_3$, which has two outer electrons, are considerably smaller at 8.6, 18.0, and 6.3 kcal/mol showing the difficulty that ammonia molecules have when displacing more than one electron.[11]

After the addition of three ammonia ligands to the metal center, the polarized 2s orbital of Be converts to a diffuse orbital at the "back" of the ammonia ligands. This orbital resembles the 1s outer orbital of $Li(NH_3)_4$ but is polarized away from CH_3 (see Fig. 3). The first excited state is degenerate and pertains to the $1p_x$ and $1p_y$ peripheral orbitals (the z-axis is along the Be–C axis). The $1p_z^1$ state is higher in energy and is polarized away from CH_3. Similarly, the reduced symmetry [compared to the isoelectronic tetrahedral $Li(NH_3)_4$ complex] splits the 1d orbitals into three groups. The $1d_{xy}$ and $1d_{x^2-y^2}$ remain degenerate and have the lowest energy among the 1d orbitals, degenerate $1d_{xz}$ and $1d_{yz}$ follow, and finally, $1d_{z^2}$ is the highest energy 1d orbital. Lying among the 1d is the 2s orbital; clearly polarized toward the end of ammonia, it has an additional radial node with respect to 1s. These orbitals and relative energetics are depicted in Fig. 3.

The vertical excitation energies at the CASSCF and CASPT2 levels combined with triple-ζ quality basis sets for the mentioned states are listed in Table I. We also report SA-CASSCF orbital energies, and for CASPT2, we provide excitation energies with double-ζ quality basis sets. More detailed information is given in Tables S1 and S2 of the supplementary material. First, we comment on different datasets of excitation energies. ΔE_{orb} are the excitation energies calculated as differences between the orbital energies at the CASSCF level. In the case of a strictly one-electron system, such as hydrogen, these will be identical to the CASSCF energies (ΔE_{CASSCF}).

A first observation is that the orbital energies apart from the 1s are all positive. Table I reveals that ΔE_{orb} falls short of ΔE_{CASSCF} by 0.14 eV for the first excited state $\tilde{A}^2E$ and the discrepancy increases to 0.54 eV for $\tilde{F}^2A_1$. Therefore, the contribution/correlation with the $CH_3Be(NH_3)_3^+$ electrons is substantial. CASPT2 increases further the vertical excitation energies by 0.24 ± 0.07 eV depending on the electronic state (here and all following ± is used to denote ranges in value). These demonstrate the need for high-level methods to accurately describe excitation energetics and CASPT2 has been shown to be equivalent to electron propagator and EOM (equation of motion)-CCSD levels of theory.[1,24] The difference in CASPT2 excitation energies between the double-ζ and triple-ζ basis sets is 0.02 ± 0.01 eV, with the double-ζ values always smaller. This small difference justifies the use of double-ζ basis sets for the larger systems examined in later in this section.

TABLE I. Electronic states, electronic configurations, CASSCF orbital energies E_{orb} (eV), relative orbital energies ΔE_{orb}, and vertical excitation energies (eV) at CASSCF (ΔE_{CASSCF}) and CASPT2 (ΔE_{CASPT2}) for $CH_3Be(NH_3)_3$.

State[a]	Config.	E_{orb}[b]	ΔE_{orb}[b]	ΔE_{CASSCF}[b]	ΔE_{CASPT2}[b]	ΔE_{CASPT2}[c]
$\tilde{X}^2A_1$	$1s^1$	−0.645	0.000	0.000	0.000	0.000
$\tilde{A}^2E$	$1p^1$	0.003	0.648	0.792	0.959	0.942
$\tilde{B}^2A_1$	$1p^1$	0.166	0.811	1.044	1.227	1.207
$\tilde{C}^2E$	$1d^1$	0.495	1.140	1.489	1.765	1.731
$\tilde{D}^2A_1$	$2s^1$	0.463	1.108	1.567	1.827	1.809
$\tilde{E}^2E$	$1d^1$	0.566	1.211	1.633	1.937	1.900
$\tilde{F}^2A_1$	$1d^1$	0.634	1.279	1.815	2.116	2.094

[a]Under C_{3v} point group.
[b]Basis set: cc-pVTZ(Be, N, C) d-aug-cc-pVTZ(H).
[c]Basis set: cc-pVDZ(Be, N, C) d-aug-cc-pVDZ(H).

Next, we compare the excitation energies of the isoelectronic "one-electron" systems $Li(NH_3)_4$, $Be(NH_3)_4^+$, and $CH_3Be(NH_3)_3$. The first system has a Li^+ center, and the second one has a Be^{2+} center. Therefore, excitation energies of $Be(NH_3)_4^+$ are expected to be greater. Comparing the two, excitations from 1s to 1p, 1d, and 2s are 0.72, 1.42, and 1.52 eV for $Li(NH_3)_4$ and 1.39, 2.37, and 3.34 eV for $Be(NH_3)_4^+$,[1,2] confirming this expectation. The corresponding excitation energies for $CH_3Be(NH_3)_3$ are 1.05 (averaged over all 1p states), 1.90 (averaged over all 1d states), and 1.81 eV. These values fall in between those for $Li(NH_3)_4$ and $Be(NH_3)_4^+$, indicating an intermediate formal charge on Be.

The use of a methyl group in the first coordination sphere of Be enables the formation of stable beryllium ammonia monomers, which are bridged by hydrocarbon chains, to give the dimeric $(NH_3)_3Be(CH_2)_nBe(NH_3)_3$. Given that the $BeCH_3(NH_3)_3$ complex behaves as an analog of a hydrogen atom, the hydrocarbon chain length permits the study of the chemical nature of supermolecular SEP bond formation comparable to the formation of H_2 from the fixed approach of two radical H atoms. A range of hydrocarbon chain lengths (1–6 carbon atoms) was employed to examine the spin coupling of the two electrons as a function of their "distance," one located about each $BeCH_2(NH_3)_3$ moiety. These can couple into a triplet and open-shell or closed-shell singlet. Long chains are expected to favor the triplet state with the open-shell singlet state being slightly above or nearly degenerate to the triplet while shorter chains are expected to prefer the closed-shell singlet and form a covalent SEP bond. These expectations are based on the mechanism of H_2 formation.

The carbon chain length can grow in two ways, either in a "linear" fashion keeping every C–C bond in a staggered conformation, or in a "curved" fashion that allows different conformations for each C–C bond, which reduces the Be–Be distance and promotes the SEP–SEP interaction. We begin with the discussion of linear systems. Figure 4 depicts the optimal geometries for the "linear" $(NH_3)_3Be(CH_2)_nBe(NH_3)_3$ species (n = 1–6). The dimers with an odd number of carbons are C_{2v} while even are C_{2h} in structure. The binding energies of the ammonia molecules to beryllium are slightly affected by the presence of the chain or the second beryllium-ammonia complex. Specifically, we calculated the binding energy of each ammonia by sequentially adding ammonia ligands (see Tables S4–S9 of the supplementary material for geometries and Table S10 for energies). The binding energies for an ammonia ligand to bind to beryllium ranging between 19.5 and 27.2 kcal/mol for all cases except four values belonging to the smallest species (n = 1–2; see Table S10 of the supplementary material). These are practically identical to the binding energies for $CH_3Be(NH_3)_3$ (21.5–26.3 kcal/mol; see above). A similar observation was made for the boron analog.[11]

The orbitals populated in the lowest electronic states and their energy are shown in Fig. 5. The in- and out-of-phase combination of the two outer 1s orbitals produces the σ_s and σ_s^* orbitals. Similarly, the $1p_x$ and $1p_y$ orbitals (the z axis considered along the Be–Be line) generate the $\pi_{x,y}$ and $\pi_{x,y}^*$ orbitals. Finally, the $1p_z$ orbitals make the σ_z and σ_z^* orbitals, which are the highest energy ones as they are highly deformed in the presence of the carbon chain. The lowest lying electronic states are investigated with CASPT2 and our complete list for all six species of Fig. 4 is given in Tables S10–S15 of the supplementary material. Table II summarizes our findings reporting excitation energies and electronic configurations.

The electronic configuration of the ground states consists of two major components σ_s^2 and σ_s^{*2}, where $\sigma_s \approx 1s_L + 1s_R$ and $\sigma_s^* \approx 1s_L - 1s_R$, with $1s_L$ and $1s_R$ being the outer 1s orbitals of the left and right terminus, respectively. The weight of the two components

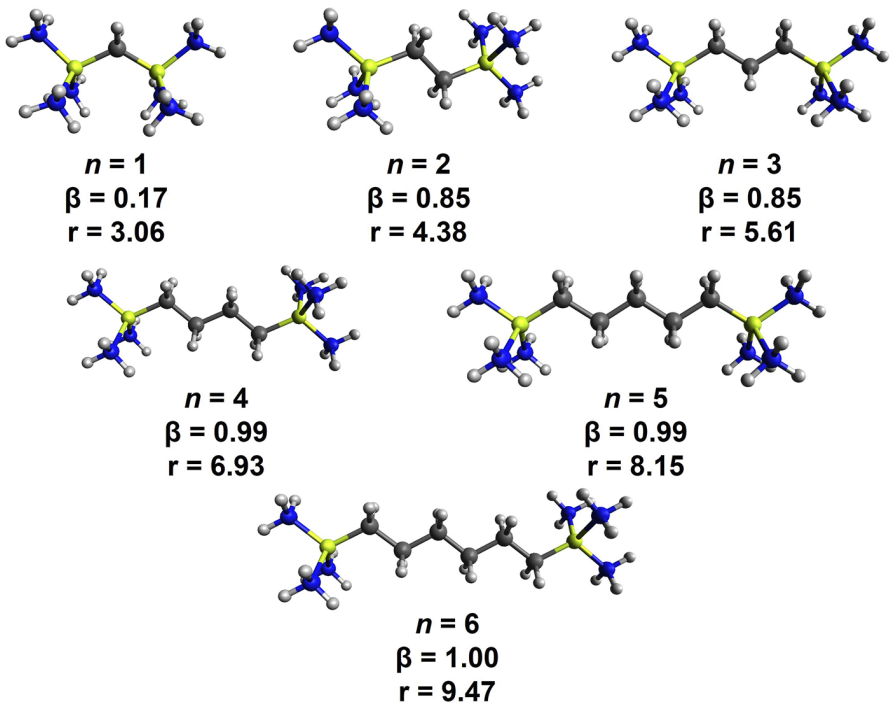

FIG. 4. Optimized geometries for the "linear" $(NH_3)_3Be(CH_2)_nBe(NH_3)_3$ species with n = 1–6. The biradical character β and the Be–Be distance r (in Å) for each species are also reported.

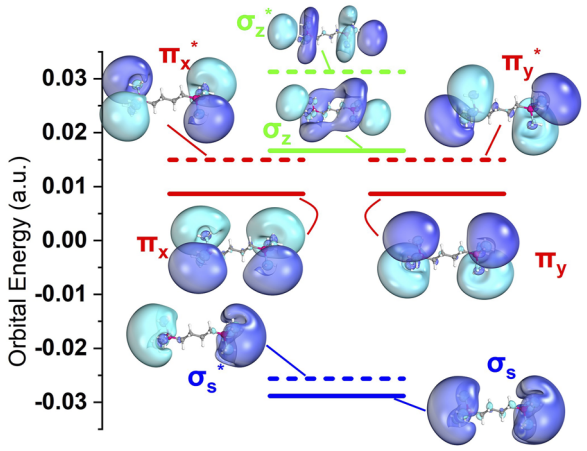

FIG. 5. Orbitals for the outer orbitals of the "linear" $(NH_3)_3Be(CH_2)_4Be(NH_3)_3$ species.

changes with the number n of carbon atoms in the hydrocarbon chain. It can be proven that when these two coefficients are equal in magnitude but have opposite signs, then the electronic configuration can be equally described as $1s_L^1\ 1s_R^1$ (open-shell singlet biradical) instead of $\sigma_s^2 - \sigma_s^{*2}$.[25] Of course when one of the two coefficients is zero, then we have a closed-shell system. For intermediate cases ($c_1\ \sigma_s^2 - c_2\ \sigma_s^{*2}$), the biradical character β can be estimated as $2c_2^2/(c_1^2 + c_2^2)$ with a value of 1.00 meaning 100% biradical.[25] It should be added that our UDFT calculations for the singlet states of the longer species converge to the broken symmetry solution $1s_L^1\ 1s_R^1$ (open-shell singlet). The spin contamination is relatively large ($\langle S^2\rangle = 1$), but the optimized geometry is not affected and is identical to the degenerate triplet state. Therefore, we consider that our UDFT calculated geometries are a good compromise avoiding computationally demanding CASPT2 geometry optimizations.

We expect that the longer the chain is, the larger the β values are, since the two terminal electrons become more and more "independent" (smaller overlap between the two outer 1s orbitals). The obtained β values are given and plotted in Fig. 6 and generally follow the expected trend. For $n = 1$, our value is 0.17 indicating a predominately closed-shell system, but for $n = 2$ and 3, we obtain two identical values 0.85 and 0.85. We believe that this is due to the fact that the C_{2v} geometry of odd n values brings four out of the six ammonia ligands to the same side facilitating a larger overlap between the two outer 1s orbitals (see inset of Fig. 6) and, thus, decreasing the biradical character. Therefore, the species with $n = 3$ has a smaller biradical character than expected. Within the odd and even n values, the β values increase smoothly to one.

The first excited state has a $\sigma_s^1\sigma_s^{*1}$ triplet spin character, which can also be described as a $1s_L^1 1s_R^1$ triplet state. The singlet-triplet energy splitting ($\Delta E_{1et\text{-}3et}$) for the n = 1–6 series drops as β and n increase as has been seen for similar systems (OXO, X = CH_2, NH, O, F^+).[25] The $\Delta E_{1et\text{-}3et}$ values are 3052.4, 116.0, 58.3, −0.3, 0.5, and 0.03 cm^{-1} for n = 1–6 (state specific CASSCF + CASPT2; see Table S30 of the supplementary material). Using the n = 1,3 species, the slope of $\Delta E_{1et\text{-}3et}$ vs β is 430.2 cm^{-1} per 10% biradical character. Practically, for $n \geq 4$, we have a pure open-shell singlet state.

Table II lists the CASPT2 excitation energies and configurations of a few more electronic states (see Tables S10–S15 of the supplementary material for more states and absolute energies). The next two states ($^3B_1$ and $^3A_1$ for n = odd; ^3B_u and ^3A_u for n = even) are triplets of primarily $\sigma_s^1\pi^1$ character. For $n = 1$, these are pure $\sigma_s^1\pi^1$ states but as n increases contributions of $\sigma_s^{*1}\pi^{*1}$ configurations

TABLE II. Electronic states, electronic configurations, and CASPT2 vertical excitation energies (eV) for "linear" $(NH_3)_3Be(CH_2)_nBe(NH_3)_3$.

State[a]	Config.	n = 1	n = 2	n = 3	n = 4	n = 5	n = 6
$^1A_1/^1A_g$[b]	σ_s^2/σ_s^{*2}	0.00	0.00	0.00	0.00	0.00	0.00
$^3B_2/^3B_u$[c]	$\sigma_s^1\ \sigma_s^{*1}$	0.33	0.03	0.02	0.00	0.00	0.00
$^3B_1/^3B_u$[d]	$\sigma_s^1\ \pi^1/\sigma_s^{*1}\ \pi^{*1}$	0.57	0.76	0.78	0.90	0.89	0.93
$^3A_1/^3A_u$[e]	$\sigma_s^1\ \pi^1/\sigma_s^{*1}\ \pi^{*1}$	0.70	0.70	0.76	0.87	0.89	0.91
$^1B_2/^1B_g$[f]	$\sigma_s^{*1}\ \pi^1/\sigma_s^1\ \pi^{*1}$		0.81	0.75	0.88	0.89	0.91
$^1A_2/^1A_g$[f]	$\sigma_s^{*1}\ \pi^1/\sigma_s^1\ \pi^{*1}$		0.85	0.86	0.90	0.89	0.93

[a]Under C_{2v}/C_{2h} point groups for odd/even n values.
[b]The CI coefficients for the σ_s^2/σ_s^{*2} configurations are 0.89/−0.28, 0.75/−0.60, 0.73/−0.60, 0.69/−0.68, 0.68/−0.68, and 0.69/−0.68 for n = 1–6.
[c]The CI coefficients are 0.96–0.97 for all n values. More accurate excitation energies are 3052.4, 116.0, 58.3, -0.3, and 0.5 cm^{-1} (state specific CASSCF/CASPT2; see Table S30 of supplementary material).
[d]The CI coefficients for $\sigma_s^1\ \pi^1$ range from 0.70 (n = 6) to 0.97 (n = 1). For $n \geq 2$, there is significant contribution from a $\sigma_s^{1*}\ \pi^{1*}$; CI coefficients range from −0.47 (n = 2) and −0.69 (n = 6).
[e]The CI coefficients for $\sigma_s^1\ \pi^1$ range from 0.71 (n = 6) to 0.97 (n = 1). For $n \geq 2$, there is significant contribution from a $\sigma_s^{1*}\ \pi^{1*}$; CI coefficients range from −0.39 (n = 2) and −0.69 (n = 6).
[f]These states are highly multi-reference, and both configurations have CI coefficients of the 0.44–0.54 range.

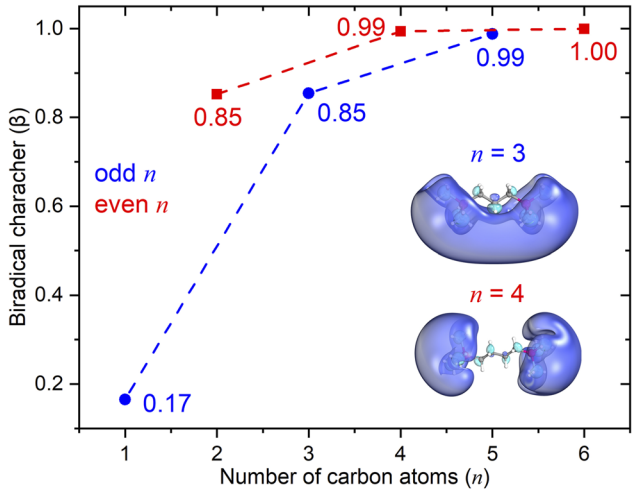

FIG. 6. Biradical character as a function of n for the "linear" $(NH_3)_3Be(CH_2)_nBe(NH_3)_3$ species with n = 1–6. The σ_s orbitals for n = 3 and 4 are depicted as insets.

also increase. This is explained as σ_s trends to degeneracy with σ_s^* for increasing n; the same occurs for π and π^* and σ_z and σ_z^* (see Fig. 4 of Ref. 11). Because of this, all states become increasingly multi-reference as n increases. These two triplets lie at 0.57 and 0.70 eV for $n = 1$, are nearly degenerate for $n = 2$, 3 at ~0.75 eV, and, finally, become degenerate for $n \geq 4$ at ~0.90 eV. The next two states ($^1B_2$ and $^1A_2$ for n = odd; ^1B_g and ^1A_g for n = even) are mixtures of different $\sigma_s^{*1}\pi^1/\sigma_s^1\pi^{*1}$ components, which contribute to coefficients in the 0.44–0.54 range. These are practically degenerate for all species at 0.8–0.9 eV. The remaining states are multi-configurational and involve excitations to σ_z and σ_z^* as well (see Tables S10–S15 of the supplementary material).

The two terminal electrons in the ground state can, in principle, induce the bending of the hydrocarbon chains, bringing the two Be centers closer to form a covalent bond as happens for two $Li(NH_3)_4$ complexes.[2] Similar binding has been reported for methylated ammonium derivatives, connected with hydrocarbon chains.[26,27] Thus, we performed geometry optimizations for "curved" $(NH_3)_3Be(CH_2)_{2-6}Be(NH_3)_3$ structures and found that such species are possible and energetically competitive compared to the "linear" isomers. For example, the rotation around the C–C bond of the $(NH_3)_3Be(CH_2)_2Be(NH_3)_3$ species brings the two beryllium ammonia units to a Gauche position (compare Figs. 4 and 7). The energy of the "curved" (Gauche) structure is 1.6 kcal/mol lower at MP2, and the biradical character decreases from 0.85 to 0.22 (see Table S17 for CI coefficients).

Similar trends are found for the larger "curved" species shown in Fig. 7. The relative stability of "linear" and "curved" species depends mainly on two factors: The strain energy that accumulates when a C–C bond rotates from the trans to the Gauche position and the binding energy for the two unpaired electrons. The latter is larger when the two beryllium-ammonia terminals are closer and the three ammonia ligands of each unit point to the three ammonia ligands of the other unit.[2] This arrangement seems to maximize the solvation energy of the formed electron pair in the middle of the two beryllium ammonia units (see Refs. 2 and 5). For instance, the binding energy for two $Li(NH_3)_4$ complexes in the optimal arrangement is 10–15 kcal/mol^2, and the trans-Gauche strain energy for each C–C bond is 0.6 kcal/mol.[28]

The structures of Fig. 7 are the lowest energy "curved" species that we were able to locate but a more systematic work may be necessary for definitive conclusions. In addition to the optimal structures, Fig. 7 reports also the energy difference at CASPT2 ΔE from the "linear" isomers, the biradical character β, and the Be–Be distance r (see Table S30 of the supplementary material). None of the $Be(NH_3)_3 \cdots (NH_3)_3Be$ interactions adopts the optimal arrangement found for two $Li(NH_3)_4$ complexes mainly due to the short hydrocarbon chain, which does not allow the better solvation of the formed electron pair. In addition, the ΔE values are always positive indicating that the "curved" species are lower in energy. Therefore, the SEP-SEP attraction is expected to be of the order of a few kcal/mol and higher than the developed strain energy of the hydrocarbon chain.

The biradical character is considerably lower for the "curved" isomers indicating partial bonding between the two unpaired electrons. For $n = 2$ goes from 0.85 to 0.22, for $n = 3$ from 0.85 to 0.64, for $n = 4$ from 0.99 to 0.63, for $n = 5$ from 0.99 to 0.39, and for $n = 6$ from 1.00 to 0.25. The most impressive difference is that for

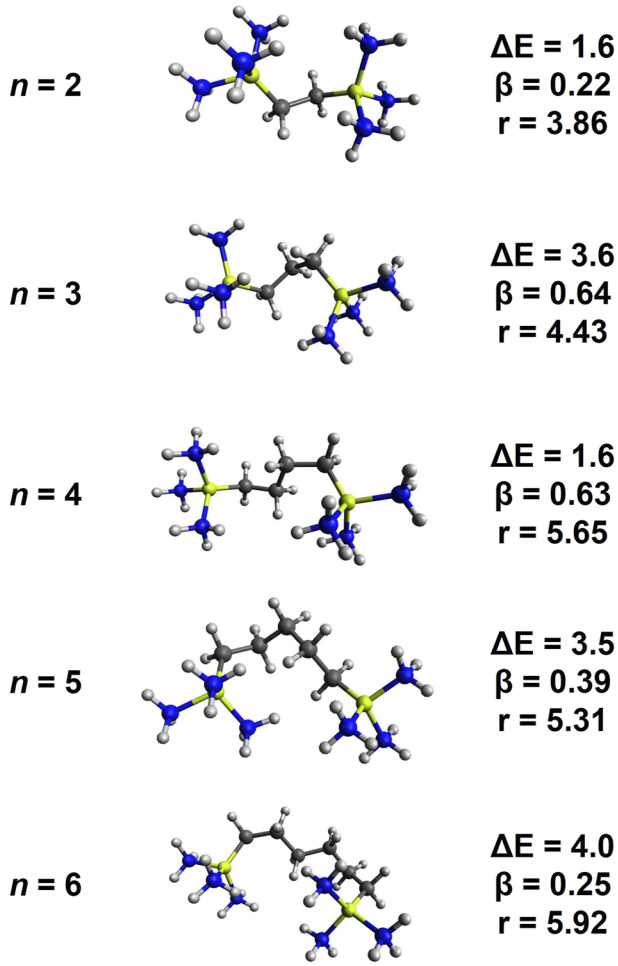

FIG. 7. CAM-B3LYP geometries for the "curved" $(NH_3)_3Be(CH_2)_nBe(NH_3)_3$ species for n = 2–6. The energy difference from the lower energy "linear" isomers ΔE (in kcal/mol; "curved" structures are always more stable than "linear") at CASPT2 (see Table S30 of the supplementary material), the biradical character β, and the Be–Be distance r (in Å) for each species are also reported.

$n = 5$, 6, where the two single electrons of the "curved" isomer form almost exclusively a two-electron bond. The structure of "curved" $(NH_3)_3Be(CH_2)_6Be(NH_3)_3$ (see Fig. 7) has four ammonia ligands and four N–H bonds solvating the electron pair localized in the middle of the molecule (see Fig. S1 of the supplementary material). Furthermore, the r value of 5.92 Å for $n = 6$ is nearly identical to the Li–Li distance of ~6 Å found for $[Li(NH_3)_4]_2$. The species with n = 3,4 have a smaller number of directional N–H bonds solvating the electron pair and, thus, a larger radical character (β = 0.63–0.64).

For "curved" systems, we also provide excitation energies for the lowest energy states listed in Tables S16–S20 of the supplementary material. These states involve σ_s, σ_s^*, π, and π^* orbitals like those in Fig. 5. Notably, the "curved" species generally have a larger number of excited states within 1.0 eV compared to the "linear." For example, the "linear" $n = 6$ species has two quasi-degenerate ground states followed by the lowest energy states at 0.91–0.97 eV

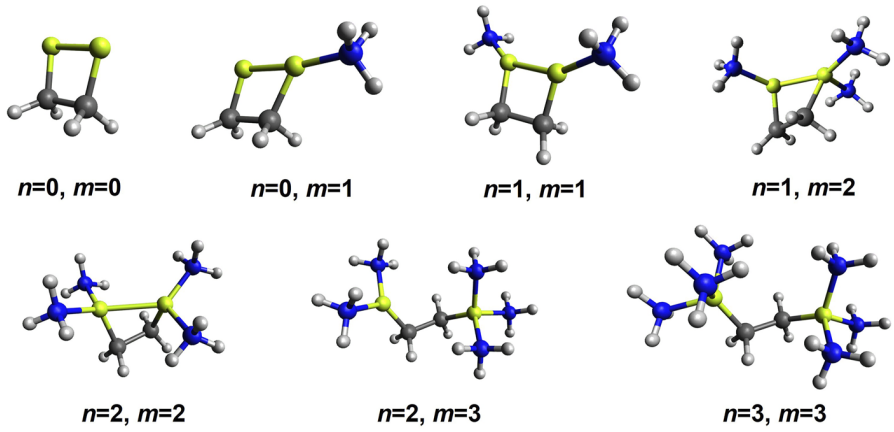

FIG. 8. CAM-B3LYP geometries for the sequential addition of ammonia ligands to $(CH_2)_2Be_2$ to form $(NH_3)_nBe(CH_2)_2Be(NH_3)_m$ and finally $(NH_3)_3Be(CH_2)_2Be(NH_3)_3$.

(see Table II and Tables S10–S15 of the supplementary material), but the "curved" isomer has five states with excitation energies spread almost evenly within 1.0 eV (0.22, 0.58, 0.74, 0.85, and 1.02 eV; see Table S21 of the supplementary material). This pattern mimics the excitation energies pattern of $[Li(NH_3)_4]_2$ (0.59, 0.66, 0.92, 1.13 eV). This trend can guide future experimental work in distinguishing and identifying the "curved" and "linear" species.

Due to the lack of symmetry in "curved" n = 5,6 structures and to enable CASTP2 calculations for these systems, we employed minimal cc-pVDZ basis sets for the C and H atoms of the hydrocarbon chain with only s function on H and s and p functions on C. The basis sets for other atoms remained the same. To validate this choice, we compare excitations energies for "linear" n = 6 species using the full cc-pVDZ(Be,N,C) d-aug-cc-pVTZ(H) basis set vs the same basis set with the minimal basis cc-pVDZ. The results listed in Table S22 of the supplementary material show that the excitation energies are affected by at most 0.01 eV justifying the use of the smaller basis set for the excitation energies of "curved" n = 5, 6 species (Tables S19–S20 of the supplementary material).

Finally, we studied the formation process of the $(NH_3)_3Be(CH_2)_{1-6}Be(NH_3)_3$ species starting from $Be(CH_2)_{1-6}Be$ depleted of ammonia ligands. These unsaturated species for n = 2 are depicted in Fig. 8. As expected, the two Be atoms bind to each other making a cyclic $(CH_2)_2Be_2$ molecule. The addition of one ammonia ligand leads to stabilization by 41 kcal/mol (at MP2) and shortening of the Be–Be bond length from 1.97 to 1.92 Å. The second ammonia elongates the Be–Be bond to 2.09 Å, and the third one shortens it to 2.02 Å. The addition of more ammonia ligands finally induces the dissociation of the Be–Be bond increasing the Be–Be distance to 2.37 (n = 4), 3.57 (n = 5), and 3.79 (n = 6) Å. The same trends are seen for larger aliphatic chains. All geometries for $(NH_3)_nBe(CH_2)_{1-6}Be(NH_3)_m$ are given in Tables S22–S26 of the supplementary material. The binding energy for the first ammonia ligand is always the largest, ranging from 25 to 41 kcal/mol. On average, the binding energy for the remaining ammonia is 15–16 kcal/mol. The cyclic structures are always lower in energy than the corresponding open ended "linear" species (no Be–Be bond occurs), and this difference increases with n. For n = 2–6, the ΔE of the "linear" and "curved" $Be(CH_2)_nBe$ is 15.0, 28.9, 40.9, 45.9, and 51.8 kcal/mol. As ammonia ligands are added and the Be–Be bond length increases, the relative difference between "linear" and "curved" decreases until saturation when the difference is 1.6–4.0 kcal/mol.

Based on these results, we can show that the character of supermolecular bonds in this system is dependent on two things: the length of SEP separation and the orientation of ammonia groups. The results of the "linear" system depict a predominantly closed-shell configuration as the two electrons couple to form a covalent SEP–SEP bond for n = 1 with a Be–Be distance of 3.1 Å and a biradical character β = 0.18. As n increases, the system becomes increasingly biradical in character. The Be–Be distance for n = 2, 3 is 4.4 and 5.6 Å while β = 0.78 and 0.81, respectively. At n = 4, the two Be atoms are separated by 6.9 Å and the two SEP electrons act as separate systems rather than bonding groups. For the "curved" systems, the covalent bonding character is much larger as the positioning of ammonia ligands improves solvation of the electron pair between the SEP centers. This is starkly seen for n = 6 where four ammonia ligands and four N–H bonds solvating the electron pair drop β from 1.00 in the "linear" to 0.25 in the "curved." In other words, converting the localized radical electrons to a nearly pure covalent bond. Within the "linear" systems, the effect of amine orientation is also seen in the case of n = 2 and 3 where, despite the longer distance of n = 3, the two have nearly equivalent β, which is explained by the C_{2v} geometries having four out of the six ammonia ligands on the same side facilitating a larger overlap between the two outer 1s orbitals. Current results appear to indicate that the SEP–SEP binding energy is not able to offset the steric strain induced by the chain curving. As chain length increases further, it is expected that the curved structure will win out due to decreased steric strain.

IV. SUMMARY AND CONCLUSIONS

In this work, we examined the electronic structure for the ground and excited states of $CH_3Be(NH_3)_3$, which is isovalent to $Li(NH_3)_4$ and $Be(NH_3)_4^+$. These species have one peripheral electron delocalized around the first coordination sphere of the metal. The methyl group captures one beryllium electron and facilitates the coordination of three ammonia ligands and the displacement of the

remaining beryllium electron to the periphery. This electron populates s-, p-, and d-type orbitals as in $Li(NH_3)_4$, but the p- and d-type orbitals are not degenerate or quasi-degenerate anymore; the orbitals along the Be–C axis are destabilized going to higher energies. Overall, the excitation energies of $CH_3Be(NH_3)_3$ fall in-between those of $Li(NH_3)_4$ and $Be(NH_3)_4^+$. The double-ζ quality basis sets are shown to give comparable excitation energies with triple-ζ and are applied for the larger systems of $(NH_3)_3Be(CH_2)_nBe(NH_3)_3$. We show that two $CH_3Be(NH_3)_3$ monomers can be linked together by aliphatic chains to form strongly bound beryllium ammonia complexes, $(NH_3)_3Be(CH_2)_nBe(NH_3)_3$, n = 1–6, with one electron around each beryllium ammonia center, the analysis of which is used to provide insight into the chemical bonding of supermolecular systems such as SEPs. The hydrocarbon chain is shown to exist either in a "linear" structure in a "curved" structure to promote interaction between the SEP centers. In the linear system, the spin coupling into a closed-shell singlet is strong for n = 1, partial for n = 2, 3, and non-existent for $n \geq 4$, where the two electrons couple clearly to an open-shell singlet. This trend reflects the biradical character β and the singlet-triplet splitting. The singlet-triplet splitting is relatively large for n = 1, small for n = 2, 3, and practically zero for $n \geq 4$. Higher energy electronic states populate π-, π^*-, σ_z-, and σ_z^*-type orbitals resembling those of traditional diatomic systems, and they are highly multi-reference states. In the curved system, the coupling is strong for the more flexible n = 6 case and for the n = 2 case, where the two electrons are in close proximity. However, the curved structures are found to be lower in energy by a few kcal/mol. We also found that the quality of the basis set of the H and C atoms of the hydrocarbon chain is small in the excitation energies and allows for the use of minimal basis sets for these atoms. In addition, we studied the formation mechanism of the dimeric species starting from the cyclic $Be_2(CH_2)_{1-6}$ molecules and adding ammonia ligands sequentially. Initially, a cyclic structure is favored with a Be–Be bond and the ammonia ligands bind rigorously to beryllium with each resulting in a weakening of the Be–Be bond until it is fully broken at ligand saturation. We believe that our calculations can reveal the existence of novel materials composed of metal centers with diffuse electrons. Such materials can be used as redox catalysts or for quantum computing purposes.

SUPPLEMENTARY MATERIAL

See the supplementary material for geometric structures, electronic configurations, excitation energies, and orbitals for the ground and several excited states of the linear and curved species.

ACKNOWLEDGMENTS

The authors are indebted to Auburn University (AU) for financial support. E.M. is especially grateful to the donors of the James E. Land endowment. This work was completed with resources provided by the Auburn University Hopper and Easley Clusters. This work was supported by the National Science Foundation under Grant No. CHE-1940456.

AUTHOR DECLARATIONS

Conflict of Interest

The authors have no conflicts to disclose.

DATA AVAILABILITY

The data that support the findings of this study are available within the article and its supplementary material.

REFERENCES

[1] I. R. Ariyarathna, S. N. Khan, F. Pawłowski, J. V. Ortiz, and E. Miliordos, J. Phys. Chem. Lett. **9**, 84–88 (2018).
[2] I. R. Ariyarathna, F. Pawłowski, J. V. Ortiz, and E. Miliordos, Phys. Chem. Chem. Phys. **20**, 24186–24191 (2018).
[3] A. M. Stacy, D. C. Johnson, and M. J. Sienko, J. Chem. Phys. **76**, 4248–4254 (1982).
[4] A. M. Stacy and M. J. Sienko, Inorg. Chem. **21**, 2294–2297 (1982).
[5] E. Zurek, P. P. Edwards, and R. Hoffmann, Angew. Chem., Int. Ed. **48**, 8198–8232 (2009).
[6] N. M. S. Almeida and E. Miliordos, Phys. Chem. Chem. Phys. **21**, 7098–7104 (2019).
[7] N. M. S. Almeida, F. Pawłowski, J. V. Ortiz, and E. Miliordos, Phys. Chem. Chem. Phys. **21**, 7090–7097 (2019).
[8] I. R. Ariyarathna, N. M. S. Almeida, and E. Miliordos, J. Phys. Chem. A **123**, 6744–6750 (2019).
[9] B. A. Jackson and E. Miliordos, J. Chem. Phys. **155**, 014303 (2021).
[10] S. N. Khan and E. Miliordos, J. Phys. Chem. A **124**, 4400–4412 (2020).
[11] Z. Jordan, S. N. Khan, B. A. Jackson, and E. Miliordos, Electron. Struct. **4**, 015001 (2022).
[12] T. Yanai, D. P. Tew, and N. C. Handy, Chem. Phys. Lett. **393**, 51–57 (2004).
[13] T. H. Dunning, J. Chem. Phys. **90**, 1007–1023 (1989).
[14] R. A. Kendall, T. H. Dunning, and R. J. Harrison, J. Chem. Phys. **96**, 6796–6806 (1992).
[15] B. P. Prascher, D. E. Woon, K. A. Peterson, T. H. Dunning, and A. K. Wilson, Theor. Chem. Acc. **128**, 69–82 (2011).
[16] I. R. Ariyarathna, F. Pawłowski, J. V. Ortiz, and E. Miliordos, J. Phys. Chem. A **124**, 505–512 (2020).
[17] P. Celani and H.-J. Werner, J. Chem. Phys. **112**, 5546–5557 (2000).
[18] G. Ghigo, B. O. Roos, and P.-Å. Malmqvist, Chem. Phys. Lett. **396**, 142–149 (2004).
[19] B. O. Roos and K. Andersson, Chem. Phys. Lett. **245**, 215–223 (1995).
[20] D. E. Woon and T. H. Dunning, J. Chem. Phys. **100**, 2975–2988 (1994).
[21] I. R. Ariyarathna and E. Miliordos, J. Phys. Chem. A **124**, 9783–9792 (2020).
[22] A. Kramida, Y. Ralchenko, J. Reader, and NIST ASD Team, NIST Atomic Spectra Database (ver. 5.7.1), National Institute of Standards and Technology, Gaithersburg, MD, 2019, available at https://physics.nist.gov/asd (11 October 2020).
[23] D. A. Dixon, D. Feller, and K. A. Peterson, J. Phys. Chem. A **101**, 9405–9409 (1997).
[24] I. R. Ariyarathna and E. Miliordos, Phys. Chem. Chem. Phys. **21**, 15861–15870 (2019).
[25] E. Miliordos, K. Ruedenberg, and S. S. Xantheas, Angew. Chem., Int. Ed. **52**, 5736–5739 (2013).
[26] M. V. Ivanov, A. I. Krylov, and S. Zilberg, J. Phys. Chem. Lett. **11**, 2284–2290 (2020).
[27] M. Díaz-Tinoco and J. V. Ortiz, J. Phys. Chem. A **123**, 10961–10967 (2019).
[28] R. M. Balabin, J. Chem. Phys. **129**, 164101 (2008).

Electronic Structure

RECEIVED
28 November 2021

REVISED
20 December 2021

ACCEPTED FOR PUBLICATION
7 January 2022

PUBLISHED
26 January 2022

PAPER

Can boron form coordination complexes with diffuse electrons? Evidence for linked solvated electron precursors

Zachary Jordan, Shahriar N Khan, Benjamin A Jackson and Evangelos Miliordos*

Department of Chemistry and Biochemistry, Auburn University, Auburn, AL 36849-5312, United States of America

* Author to whom any correspondence should be addressed.

E-mail: emiliord@auburn.edu

Keywords: solvated electron, ammonia, hydrogenic shell model, diffuse electrons, excited states

Supplementary material for this article is available online

Abstract

Density functional theory and *ab initio* multi-reference calculations are performed to examine the stability and electronic structure of boron complexes that host diffuse electrons in their periphery. Such complexes (solvated electron precursors or SEPs) have been experimentally identified and studied theoretically for several s- and d-block metals. For the first time, we demonstrate that a p-block metalloid element can form a stable SEP when appropriate ligands are chosen. We show that three ammonia and one methyl ligands can displace two of the three boron valence electrons to a peripheral 1s-type orbital. The shell model for these outer electrons is identical to previous SEP systems (1s, 1p, 1d, 2s). Further, we preformed the first examination of a molecular system consisting of two SEPs bridged by a hydrocarbon chain. The electronic structure of these dimers is very similar to that of traditional diatomic molecules forming bonding and anti-bonding σ and π orbitals. Their ground state electronic structure resembles that of two He atoms, and our results indicate that the excitation energies are nearly independent of the chain length for four carbon atoms or longer. These findings pave the way for the development of novel materials similar to expanded metals and electrides.

1. Introduction

Molecular systems containing one or more diffuse electrons have many applications in redox chemistry, catalysis, and electronics [1]. For both historic and structural reasons, such systems are divided into solutions of solvated electrons, liquid or expanded metals, and electrides (organic and inorganic) [1–26]. These electrons occupy orbitals or bands delocalized around some molecular skeleton. For example, organic electrides are traditionally composed of metal-crown-ether complexes, while expanded metals are made of metal ammonia or methylamine complexes. Experimentally, alkali and alkaline earth metals have been used to synthesize these materials.

Typically, ammonia or crown-ethers stabilize the Li^+, Na^+, K^+, Cs^+, or Ca^{2+} centers and displace the valence electron(s) to the periphery of the complex [27]. These peripheral electrons constitute the electronic bands of the material. Our research group over the past three years has focused on the electronic and geometric structure of metal ammonia complexes with diffuse electrons (dubbed solvated electron precursors (SEPs)) [28–37]. In addition to s-block metals, we have also explored transition metal (d-block) SEPs. The transition metals studied so far (Sc, V, Cr, Y, Mo) adopt formally a 2+ oxidation state with six ammonia ligands in the first coordination sphere; the metal s^2 electrons are displaced to the periphery, residing in the second coordination sphere of the complex [30, 31, 36, 37]. Y and possibly Sc can coordinate eight ammonia molecules and accommodate three peripheral electrons (formerly the metal's s^2d^1 electrons) [30, 36].

The present work targets for the first time the study of a non-metallic (metalloid) p-block element, specifically boron. Our motivation is based on the following questions: can the first coordination sphere of boron

be saturated with ammonia ligands, as in metallic SEPs? Will all three of its valence electrons ($2s^2 2p^1$) be displaced to the outer sphere of the complex? Can ammonia ligands displace a p-type orbital? To answer these questions, we performed high-level quantum chemical calculations combining density functional theory, perturbation theory, and multi-reference wavefunction theory. Our findings indicate that up to three ammonia ligands can coordinate to boron displacing two out of the three valence electrons. A fourth ammonia is not able to coordinate and move the third electron to the periphery. Instead, the addition of a methyl radical results in the formation of a B–C covalent bond and the pseudo-spherical $B(NH_3)_3(CH_3)$ complex with two outer electrons. The effect of replacing CH_3 with NH_2, F, and Cl was also probed. Finally, we connected two $B(NH_3)_3(CH_3)$ entities using a hydrocarbon chain with three to six carbon atoms making a linked-SEP dimer $(NH_3)_m BCH_2(CH_2)_{k-2}CH_2B(NH_3)_n$ [m, n = 0–3 and k = 3–6]. The stability is monitored for all possible combinations of m, n, and k; excited electronic states are examined for the fully saturated monomer and dimers. To our knowledge, this is the first work within the literature to propose or study linked-SEPs. Recent theoretical work has demonstrated SEPs to be effective catalysts in the simultaneous capture and functionalization of CO_2 [38]. The present work is the first demonstration of how SEP centers may be linked and paves the way for the development of novel, redox-active, catalytic materials.

2. Computational details

The geometries of all complexes were optimized with density functional theory. The CAM-B3LYP functional is employed. Previously, this functional has been shown to provide geometries in excellent agreement with MP2 and CCSD(T) for similar systems [35]. The correlation consistent triple-ζ basis sets were chosen for all atoms (cc-pVTZ), and a series of diffuse functions was added on chlorine, fluorine, and hydrogen (aug-cc-pVTZ). The diffuse functions on H are necessary and sufficient for the description of the outer electrons in the ground state of the systems [28]. The energetics (i.e. binding energies) were improved at the MP2 level of theory with the same basis sets. The binding energy D_e for ammonia is calculated using the electronic energies of the molecules before $[M(NH_3)_x]$ and after $[M(NH_3)_{x+1}]$ the addition of ammonia: $D_e = E[M(NH_3)_x] + E[NH_3] - E[M(NH_3)_{x+1}]$. Zero-point energy (ZPE) corrected values are obtained by adding ZPE to the previous energies. ZPE is calculated as 1/2 of the sum of all harmonic vibrational frequencies. The vibrational frequencies are all real for all species and are reported in the supplementary material (SM) (https://stacks.iop.org/EST/4/015001/mmedia).

The reported excitation energies are calculated with CASPT2 (second order perturbation theory applied on a multi-configurational wavefunction—RS2C version of MOLPRO) [39, 40]. The reference calculations are carried out with the state-averaged complete active space self-consistent field (SA-CASSCF) approach. The active space consists of two electrons in ten orbitals for the monomers, and four electrons in eight orbitals for the linked dimers. To keep the calculations manageable for the excited states of linked SEPs, we used the cc-pVDZ basis set for all atoms except for hydrogens, where a d-aug-cc-pVDZ set was used. This approximation has been shown to have little effect in the excitation energies [33, 35], and it is probed presently for the monomers. Also, for technical reasons we applied a shift and IPEA values of 0.2 and 0.25, respectively, to the CASPT2 calculations [31, 41, 42]. The Gaussian16 was invoked to perform the CAM-B3LYP and MP2 calculations [43], while SA-CASSCF and CASPT2 calculations were done with MOLPRO2015 [40]. The IboView software was used to visualize the molecular orbitals [44].

3. Results and discussion

Boron SEP monomers. The ground state of boron has a $1s^2 2s^2 2p^1$ electronic configuration. The approach of three ammonia molecules are able to displace the two 2s electrons from the valence space of boron to the periphery of the ammonia ligands, as happens for $Be(NH_3)_3$ [45]. However, the $2p^1$ electron hinders the attachment of a fourth ammonia, which prefers to populate the second solvation shell of $B(NH_3)_3$. We were actually able to locate a $B(NH_3)_4$ structure with all three valence boron electrons displaced in the periphery of the complex, but is metastable (higher in energy with respect to $B(NH_3)_3 + NH_3$) by 20 kcal mol^{-1} (18 kcal mol^{-1} after ZPE corrections). The potential energy curves for the approach of the fourth ammonia ligand is revealing and are reported in figure S1 of the SM. There is a large activation energy barrier ($\sim$40 kcal mol^{-1}) and the products of the 'reaction' are higher than the 'reactants'. The reason can be ascribed to the metalloid (and not metallic) nature of boron as demonstrated by its large third ionization energy (37.9 eV) [46] compared to that of metallic aluminum in the same group of the periodic table (28.4 eV) [46]. The occupation of the 2p orbital effectively repels the approach of a fourth ammonia while the large ionization energy prevents its displacement to the periphery.

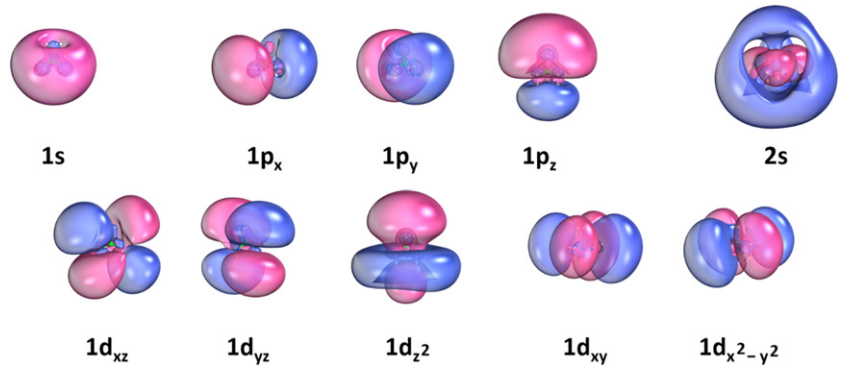

Figure 1. Molecular outer orbitals of $CH_3B(NH_3)_3$.

Table 1. MP2 plain and ZPE corrected (D_e/D_0) binding energies of CAM-B3LYP optimized, substituted boron ammonia monomers $XB(NH_3)_n$ in kcal mol^{-1}.

n	$X = F$	$X = Cl$	$X = NH_2$	$X = CH_3$
0[a]	186.3/184.3	123.2/122.0	134.0/130.1	93.0/89.7
1[b]	−10.2/−12.8	8.6/5.7	10.1/5.3	12.3/8.6
2[b]	13.4/9.4	16.9/12.4	1.8/−0.9	22.1/18.0
3[b]	6.4/4.5	−0.8/−2.0	7.8/5.2	8.0/6.3

[a]The binding energies on this line refer to the BX (ground $S = 0$ state) → B (^{2}P; $2s^2 2p^1$) + X (ground $S = 1/_2$ state) dissociation.
[b]The binding energies on these lines refer to the $XB(NH_3)_n$ (ground $S = 0$ state) → $XB(NH_3)_{n-1}$ (ground $S = 0$ state) + NH_3 ($^1A_1$) dissociation.

The saturation of the first coordination sphere of boron can be achieved by using the $2p^1$ electron to form a covalent bond or ionic bond with a ligand such as fluorine, chlorine, NH_2 or CH_3. Indeed, the potential energy curves for the approach of CH_3 are smooth leading to a stable product (compare figures S1 and S2 of SM). The proposed $XB(NH_3)_3$ (X = F, Cl, NH_2, CH_3) complexes have a pseudospherical geometry, especially for $X = CH_3$, and can accommodate two peripheral electrons. The orbitals hosting these two electrons are shown in figure 1 for $CH_3B(NH_3)_3$. These include the lowest energy 1s outer orbital, followed by three 1p, five 1d, and one 2s orbitals. The methyl group, which sits on the top side of the molecule in figure 1, creates some anisotropy to the system destabilizing orbitals with components along the z-direction, e.g. $1p_z$ and $1d_z{}^2$.

The ground state for all $XB(NH_3)_3$ species has a $1s^2$ configuration. The optimal geometries and harmonic frequencies are reported in the SM section. The binding energy of the X unit is as large as 186.3 kcal mol^{-1} for X = F (see table 1) decreasing to 134.0 kcal mol^{-1} for $X = NH_2$, 123.2 kcal mol^{-1} for X = Cl, and as small as 93.0 kcal mol^{-1} for $X = CH_3$. All are very strong as compared to the subsequent B–NH_3 bonds. The D_e value for the first ammonia is of the order of 10 kcal mol^{-1} for all systems except for X = F, where it is negative. The second ammonia binds more strongly for all species except $X = NH_2$, and the third ammonia is metastable for X = Cl. The $CH_3B(NH_3)_3$ complex is the only system with all three ammonia ligands having positive D_e and D_0 values (see table 1). The first ammonia binds with 12.3 kcal mol^{-1} energy, the second with 22.1 kcal mol^{-1}, and the third with 8.0 kcal mol^{-1}. The average D_e value of 14.1 kcal mol^{-1} is comparable to the $Be(NH_3)_3$ value of 12.8 kcal mol^{-1} [45], and that of $Li(NH_3)_4$ (13.6 kcal mol^{-1}; present MP2 calculations). $Li(NH_3)_4$ has only one outer electron and has been identified experimentally [47].

The low-lying electronic states of the $XB(NH_3)_3$ species are listed in table 2. More complete data are provided in the SM. The first excited state is a triplet with one 1s electron being promoted to one of the three 1p orbitals. The $1s^1 1p_{x,y}{}^1$ states are nearly degenerate in every case and about 0.2 eV lower in energy than $1s^1 1p_z{}^1$. Table 2 lists the energy range for all three states (0.8–1.2 eV with triple-ζ basis set). Notice that $1p_z$ is polarized toward X as opposed to 1s, which is polarized to the opposite direction. The singlet $1s^1 1p^1$ states are next (1.5–2.0 eV) following the same pattern with $1s^1 1p_{x,y}{}^1$ being lower than $1s^1 1p_z{}^1$ by a slightly larger amount (0.3–0.4 eV). The excitation energies for both singlet and triplet $1s^1 1p^1$ states is nearly independent of the X unit within 0.1–0.2 eV. The next states are a group of singlet states (1.8–2.3 eV) with $1s^1 1d^1/1p^2$ mixed character ($1s^1 \rightarrow 1d^1$ or $1s^2 \rightarrow 1p^2$ excitations) followed by the $1s^1 1d^1$ triplet states. The mingling of $1p^2$ configurations with the $1s^1 1d^1$ singlet spin states stabilize them over the $1s^1 1d^1$ triplet states, which lie at 2.0–2.5 eV. This is the opposite of what happens for the $1s^1 p^1$ states. The next electronic states are generally

Table 2. Electronic configurations (Config.), spin (S), and CASPT2 excitation energies or energy ranges for $XB(NH_3)_3$, X = F, Cl, NH_2, CH_3, and $Be(NH_3)_4$ using double-ζ (DZ)[a] or triple-ζ (TZ)[b] basis sets.

Config.	S	X = F	X = Cl	X = NH_2[c]	X = CH_3[c]	$Be(NH_3)_4$[c,d]
			Basis set = DZ			
$1s^2$	0	0.000	0.000	0.000	0.000	
$1s^1 1p^1$	1	0.826–1.161	0.853–1.112	0.740–1.087	0.776–1.072	
$1s^1 1p^1$	0	1.605–2.044	1.649–2.018	1.518–1.875	1.563–1.869	
$1s^1 1d^1/1p^2$	0	1.877–2.321	1.875–2.291	1.810–2.180	1.734–2.129	
$1s^1 1d^1$	1	2.088–2.467	2.052–2.486	1.917–2.358	1.936–2.310	
$1s^1 2s^1$	1	2.401	2.417	2.355	2.283	
$1s^1 2s^1$	0	2.551	2.514	2.464	2.427	
			Basis set = TZ			
$1s^2$	0	0.000	0.000	0.000	0.000	0.00
$1s^1 1p^1$	1	0.844–1.161	0.871–1.105	0.756–1.096	0.792–1.075	0.81
$1s^1 1p^1$	0	1.617–2.079	1.658–2.042	1.528–1.909	1.576–1.893	1.62
$1s^1 1d^1/1p^2$	0	1.908–2.343	1.903–2.338	1.838–2.202	1.762–2.146	1.65–1.82
$1s^1 1d^1$	1	2.106–2.485	2.068–2.491	1.986–2.385	1.948–2.320	1.93–2.11
$1s^1 2s^1$	1	2.432	2.453	2.391	2.300	2.24
$1s^1 2s^1$	0	2.571	2.529	2.484	2.440	2.30

[a]DZ = cc-pVDZ (B, N, C), aug-cc-pVDZ (F, Cl), and d-aug-cc-pVDZ (H).
[b]TZ = cc-pVTZ (B, N, C), aug-cc-pVTZ (F, Cl), and d-aug-cc-pVTZ (H).
[c]These molecules have additional multi-reference states between the triplet $1s^1 1d^1$ and the $1s^1 2s^1$ states. Some of them are of impure nature.
[d]Reference [28]; CASPT2/TZ.

of multi-reference character and are provided in the SM. We singled out the triplet and singlet $1s^1 2s^1$ states at ∼2.5 eV. The triplet state is lower again by 0.4–0.7 eV (see table 2).

Another comment is that the double-ζ quality excitation energies listed in table 2 are in remarkable agreement with the triple-ζ quality. This means that the double-augmentation scheme on each hydrogen center provides an adequately large number of basis functions to describe the diffuse nature of the outer electrons independently of the cardinal number of the used correlation-consistent basis set. Finally, we compare the excitation energies with those of the more symmetric (tetrahedral) $Be(NH_3)_4$ using the triple-ζ basis sets; see table 2 and reference [28]. For $Be(NH_3)_4$ the 1p orbitals are exactly degenerate, while the 1d orbitals stay within a smaller energy range due to the higher symmetry. In every case, the excitation energies of $Be(NH_3)_4$ are within the energy range of the electronic energies of $CH_3Be(NH_3)_3$.

Linked boron SEP monomers. Given the higher stability of $CH_3B(NH_3)_3$ over the other $XB(NH_3)_4$ species, we considered the linkage of two $CH_3B(NH_3)_3$ monomers via an aliphatic hydrocarbon bridge. In this section, we investigate the stability and structure of $(NH_3)_nB(CH_2)_kB(NH_3)_m$ for k = 3–6 and m, n = 1–3, and excited states of the fully coordinated $(NH_3)_3B(CH_2)_{3-6}B(NH_3)_3$ species. Smaller carbon chains led to the formation of species with B–B bonds, which are not of our interest in this study.

Figure 2 shows the structure of the species we considered for $k = 4$. Similar structures are considered for other k values. The top structure contains no ammonia ligands and the second has one ammonia ligand at one of the boron terminals. The next three rows correspond to systems with two ($m + n = 2$), three ($m + n = 3$), and four ($m + n = 4$) ammonia ligands. Each has two isomers varying how many ammonia ligands are on each terminus. For example, the two ammonia ligands can be both on one side or can attach to different boron terminals, i.e. $(m, n) = (2, 0)$ or $(0, 2)$ or $(1, 1)$. Similarly for $m + n = 3$ we have $(m, n) = (3, 0)$ or $(0, 3)$ or $(1, 2)$ or $(2, 1)$, and for $m + n = 4$ we have $(m, n) = (3, 1)$ or $(1, 3)$ or $(2, 2)$. As indicated in figure 2, the first two ammonias bind to the same boron atom, while the third and fourth prefer to bind to the other boron atom. This trend can be rationalized by looking at the binding energies for the $CH_3B(NH_3)_{1-3}$ systems of table 1. The binding energy of the third ammonia ligand to the same boron center is smaller than the binding energies for the attachment of the first two ammonia ligands. Therefore, the third and fourth ammonias prefer to bind to the second boron atom of the dimeric species. In addition, the first ammonia ligand attaches to boron always in the eclipsed position relative to the carbon chain.

Table 3 tabulates the binding energies for all ammonia ligands. The lowest energy isomer is always considered. The binding energy values are very close to those found for the monomer species (compare values below with values from table 1). Depending on the size of the carbon chain, the first ligand of each boron binds with 14.3–15.7 kcal mol^{-1} ($n + m = 1$) or 13.2–13.7 kcal mol^{-1} ($m + n = 3$). The second ligand binds with 22.2–22.5 kcal mol^{-1} ($n + m = 2$) or 21.6–22.0 kcal mol^{-1} ($n + m = 4$), and the third one by 4.6–5.1 kcal mol^{-1} ($n + m = 5$) or 4.9–5.6 kcal mol^{-1} ($n + m = 6$). Therefore, the carbon chain size minimally affects the stability of the two linked boron monomers. Table 3 also lists the energy difference for the two isomers for $m + n = 2$, 3, 4. In the first two cases, the lowest energy isomer is more stable by

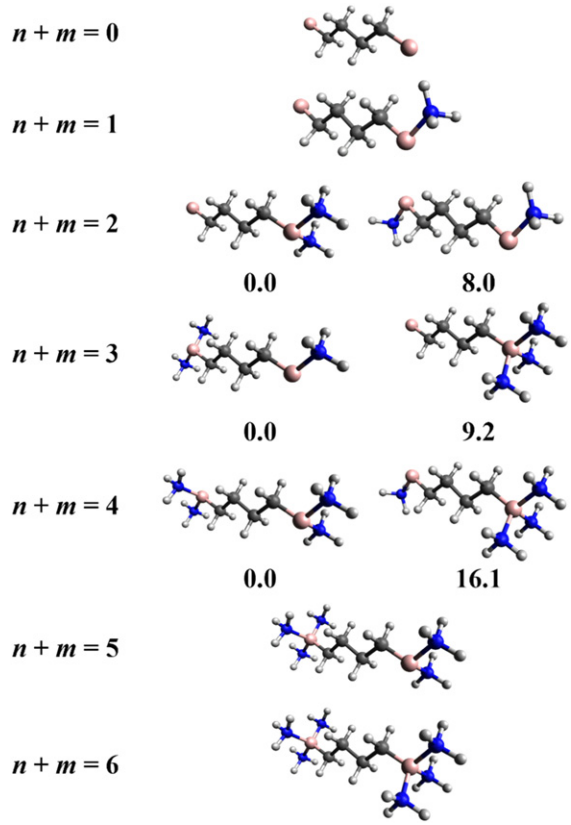

Figure 2. CAM-B3LYP global minima for $(NH_3)_nB(CH_2)_4B(NH_3)_m$. Relative energies in kcal mol^{-1} are reported for the two possible isomers with $n + m = 2$, 3, and 4.

Table 3. MP2//CAM-B3LYP binding energies (D_e) for the lowest energy isomers and energy difference between the two lowest energy isomers (ΔE) of $(NH_3)_nB(CH_2)_kB(NH_3)_m$ in kcal mol^{-1}.

$n+m$		$k=3$	$k=4$	$k=5$	$k=6$
1	D_e	15.7	14.9	14.5	14.3
2	D_e	22.5	22.2	22.4	22.2
	ΔE[a]	9.1	8.0	8.5	8.0
3	D_e	13.7	13.2	13.5	13.5
	ΔE[b]	10.2	9.2	9.2	8.9
4	D_e	22.0	21.6	21.7	21.6
	ΔE[c]	16.7	16.1	16.4	16.4
5	D_e	4.6	5.4	5.0	5.1
6	D_e	5.6	5.0	5.0	4.9

[a]The $n = 2$, $m = 0$ isomer is higher in energy.
[b]The $n = 2$, $m = 1$ isomer is higher in energy.
[c]The $n = 3$, $m = 1$ isomer is higher in energy.

9.1 $\pm$ 1.1 kcal mol^{-1}; however, for $m + n = 4$, the isomers differ by 16.4 $\pm$ 0.3 kcal mol^{-1} as the higher energy isomer involves the attachment of a third ammonia to the same boron atom.

We now turn our discussion to the fully coordinated $(NH_3)_3B(CH_2)_{3-6}B(NH_3)_3$ species. Based on the electronic structure of $(NH_3)_3BCH_3$ (*see above*), the ground state of the dimer should have two electrons in the periphery of each boron side. Due to symmetry, the two outer 1s orbitals of each side are combined with an in-phase or out-of-phase interaction to make a 'bonding' and an 'anti-bonding' combination (orbitals σ_s and σ_s^* of figure 3). Therefore, the ground state of the dimeric species has a $\sigma_s^2\sigma_s^{*2}$ electronic configuration. This electronic structure resembles that of two bonded He atoms. Under standard conditions, the He_2 is practically unstable with an equilibrium distance of 3.0 Å and an interaction energy of 11 K or 7.6 cm^{-1} [48]. In contrast, the aliphatic linkage of the boron SEPs produces a highly-stable dimeric system.

The resemblance of the studied species with traditional diatomic molecules is further demonstrated by the orbitals populated in the excited states. Specifically, the next available orbitals are of π/π^* and σ/σ^* character and made of the 1p orbitals of the two monomers (see figure 3). Identical behavior was seen for the $[Li(NH_3)_4]_2$

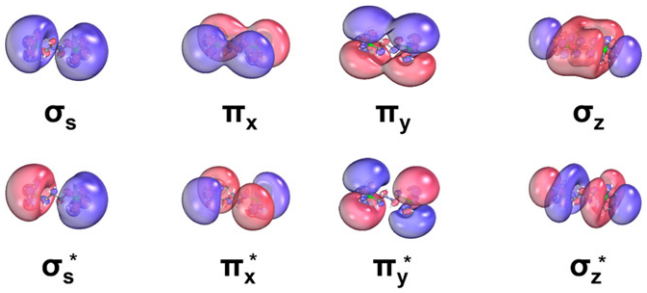

Figure 3. Molecular outer orbitals of $(NH_3)_3B(CH_2)_4B(NH_3)_3$.

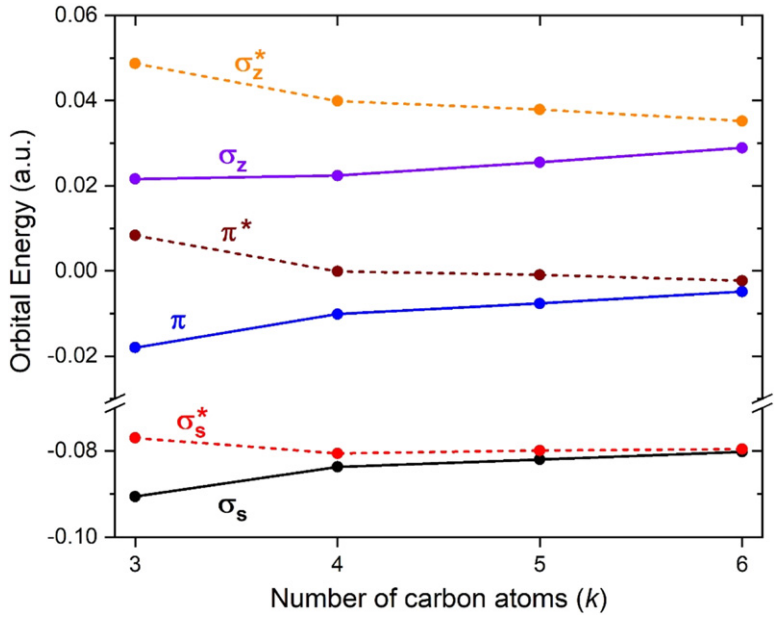

Figure 4. Energy of the $(NH_3)_3B(CH_2)_kB(NH_3)_3$, $k = 3$–6, molecular outer orbitals as a function of the carbon chain size at SA-CASSCF.

dimers [29], which are not connected via a hydrocarbon bridge but are bound via a σ-bond of the two outer 1s electrons of each $Li(NH_3)_4$ complex. As expected, σ_s is followed σ_s^* and their energy converges to degeneracy for longer carbon chains. Figure 4 shows the energy dependence of these outer orbitals (SA-CASSCF) as a function of the carbon chain length. The two π or π^* orbitals are degenerate within 0.006 a.u. for $k = 3$ and 0.0005 a.u. for $k = 6$. Unlike traditional diatomic molecules, the next orbital is not σ_z but the π followed by π^*. The reason is that the 'bonding' density of σ_z is around the carbon chain, a rather unfavorable region for the electrons (C–H bonds are not generally involved in solvating electrons). Again, π/π^* and σ_z/σ_z^* orbitals converge to the same value for longer chains as expected due to larger separation of the two monomers and thus smaller overlap between their 'atomic' outer orbitals.

The first four excited states lie within <0.1 eV from each other and around 0.75 eV from the ground state for all k values (see table 4). These triplet states are generated when one electron moves from either σ_s or σ_s^* to either a π or π^* orbital. The next two states at 1.1–1.2 eV are formed by the promotion of one σ_s or σ_s^* electron to the σ_z or σ_z^* orbitals, also of triplet spin multiplicity. The next state is a quintet state at 1.26 eV ($k = 3$) and 1.52 ± 0.03 eV for $k > 3$, when one σ_s and one σ_s^* electrons migrate to the π/π^* orbitals. Up to 1.6 eV, 11 electronic states were found of singlet, triplet, and quintuple spin multiplicity, with half of them being highly multi-configurational states. Table 4 lists the electronic configurations for the single reference states and the excitation energies for all states.

Table 4. Electronic configurations (Config.), spin (S), and CASPT2 vertical excitation energies (eV) for the low-lying electronic states of $(NH_3)_3B(CH_2)_kB(NH_3)_3$, $k = 3$–6[a].

Config.	S	$k = 3$	$k = 4$	$k = 5$	$k = 6$
$\sigma_s^2\sigma_s^{*2}$	0	0.00	0.00	0.00	0.00
$\sigma_s^2\sigma_s^{*1}\pi_x^1 - \sigma_s^1\sigma_s^{*2}\pi_y^1$	1	0.69	0.74	0.74	0.74
$\sigma_s^2\sigma_s^{*1}\pi_y^{*1} + \sigma_s^1\sigma_s^{*2}\pi_x^{*1}$	1	0.72	0.78	0.77	0.77
$\sigma_s^2\sigma_s^{*1}\pi_y^1 + \sigma_s^1\sigma_s^{*2}\pi_x^1$	1	0.75	0.74	0.74	0.74
$\sigma_s^2\sigma_s^{*1}\pi_x^{*1} - \sigma_s^1\sigma_s^{*2}\pi_y^{*1}$	1	0.76	0.76	0.76	0.76
$\sigma_s^2\sigma_s^{*1}\sigma_z^1 + \sigma_s^1\sigma_s^{*2}\sigma_z^{*1}$	1	1.14	1.17	1.17	1.17
$\sigma_s^2\sigma_s^{*1}\sigma_z^{*1} - \sigma_s^1\sigma_s^{*2}\sigma_z^1$	1	1.16	1.15	1.15	1.15
$\sigma_s^1\sigma_s^{*1}\left(\pi_x^1\pi_y^{*1} + \pi_x^{*1}\pi_y^1\right)$	2	1.26	1.54	1.49	1.51
MR[b]	1	1.35	1.52	1.49	1.50
MR[b]	0	1.37	1.53	1.50	1.51
MR[b]	0	1.43	1.51	1.51	1.51
MR[b]	1	1.47	1.50	1.51	1.50
$\sigma_s^1\sigma_s^{*1}\left(\pi_x^2 - \pi_y^2\right)$	0	1.49	1.49	1.48	1.47
$\sigma_s^1\sigma_s^{*1}\left(\pi_x^*2 - \pi_y^{*2}\right)$	0	1.50	1.55	1.55	1.54
MR[b]	1	1.52	1.50	1.49	1.48
MR[b]	1	1.54	1.56	1.55	1.54
$\sigma_s^1\sigma_s^{*1}\left(\pi_x^1\pi_x^{*1} - \pi_y^{*1}\pi_y^1\right)$	2	1.55	1.49	1.52	1.51
$\sigma_s^1\sigma_s^{*1}\pi_x^1\pi_y^1$	2	1.56	1.51	1.49	1.48
$\sigma_s^1\sigma_s^{*1}\pi_x^{*1}\pi_y^{*1}$	2	1.61	1.57	1.56	1.55

[a]DZ = cc-pVDZ (B, N, C)/d-aug-cc-pVDZ (H).
[b]Highly multi-reference states involving multiple excitations from σ_s and σ_s^* orbitals to π and π^* orbitals.

4. Summary and conclusions

High-level quantum chemical calculations are used to study the stability and electronic structure of boron-SEPs. Boron can make stable, fully coordinated (saturated) complexes with two diffuse outer electrons by attaching three ammonia ligands and one methyl radical. The outer electrons of the formed pseudo-spherical molecular system reside in a hydrogenic-type shell model, resembling the isovalent $Be(NH_3)_4$ complex. The first four orbitals follow the same 1s, 1p, 1d, 2s order observed for other s- and d-block metal SEPs. The excited states of $CH_3B(NH_3)_3$ possess the same pattern (in terms of electronic configurations and excitation energies) as $Be(NH_3)_4$ confirming that the 'behavior' of the outer electrons is practically independent of the nature of the central metal [37]. For the first time, we also showed that a hydrocarbon chain can bridge two SEPs and create an analogue of a diatomic molecule (linked SEP). The atomic-type diffuse orbitals 1s and 1p of each boron SEP monomer are combined to produce σ, σ^*, π, π^*-type orbitals. The effect of the chain length on excitation energies for states involving these orbitals is minimal for chains of four carbons and longer. Our findings are expected to guide future experimental studies toward the discovery of new materials similar to expanded metals.

Acknowledgments

The authors are indebted to Auburn University (AU) for financial support. EM is especially grateful to the donors of the James E Land endowment. This work was completed with resources provided by the Auburn University Easley Cluster. This material is based upon work supported by the National Science Foundation under Grant No. CHE-1940456. Any opinions, findings, and conclusions or recommendations expressed in this material are those of the author(s) and do not necessarily reflect the views of the National Science Foundation.

Data availability statement

All data that support the findings of this study are included within the article (and any supplementary files).

Supplementary material

The supporting information lists detailed information on the excited states, the geometries/frequencies/energies of the ground states for all species studied presently.

References

[1] Zhang X and Yang G 2020 *J. Phys. Chem. Lett.* **11** 3841–52
[2] Ellaboudy A, Dye J L and Smith P B 1983 *J. Am. Chem. Soc.* **105** 6490–1
[3] Dawes S B, Ward D L, Huang R H and Dye J L 1986 *J. Am. Chem. Soc.* **108** 3534–5
[4] Huang R H, Faber M K, Moeggenborg K J, Ward D L and Dye J L 1988 *Nature* **331** 599–601
[5] Wagner M J, Huang R H, Eglin J L and Dye J L 1994 *Nature* **368** 726–9
[6] Huang R H, Wagner M J, Gilbert D J, Reidy-Cedergren K A, Ward D L, Faber M K and Dye J L 1997 *J. Am. Chem. Soc.* **119** 3765–72
[7] Xie Q, Huang R H, Ichimura A S, Phillips R C, Pratt W P and Dye J L 2000 *J. Am. Chem. Soc.* **122** 6971–8
[8] Dye J L 2003 *Science* **301** 607
[9] Redko M Y, Jackson J E, Huang R H and Dye J L 2005 *J. Am. Chem. Soc.* **127** 12416–22
[10] Toda Y, Kubota Y, Hirano M, Hirayama H and Hosono H 2011 *ACS Nano* **5** 1907–14
[11] Lee K, Kim S W, Toda Y, Matsuishi S and Hosono H 2013 *Nature* **494** 336–40
[12] Liu C, Nikolaev S A, Ren W and Burton L A 2020 *J. Mater. Chem.* C **8** 10551–67
[13] Ammari Y and Hlil E K 2021 *Chem. Pap.* **75** 3197
[14] Yang X, Parrish K, Li Y-L, Sa B, Zhan H and Zhu Q 2021 *Phys. Rev.* B **103** 125103
[15] Edwards P P, Lusis A R and Sienko M J 1980 *J. Chem. Phys.* **72** 3103–12
[16] Hagedorn R and Sienko M J 1982 *J. Phys. Chem.* **86** 2094–7
[17] Stacy A M, Johnson D C and Sienko M J 1982 *J. Chem. Phys.* **76** 4248–54
[18] Stacy A M and Sienko M J 1982 *Inorg. Chem.* **21** 2294–7
[19] Nakamura Y, Niibe M and Shimoji M 1984 *J. Phys. Chem.* **88** 3755–60
[20] Kohanoff J, Buda F, Parrinello M and Klein M L 1994 *Phys. Rev. Lett.* **73** 3133–6
[21] Hayama S, Wasse J C, Skipper N T and Soper A K 2002 *J. Phys. Chem* B **106** 11–4
[22] Thompson H, Wasse J C, Skipper N T, Hayama S, Bowron D T and Soper A K 2003 *J. Am. Chem. Soc.* **125** 2572–81
[23] Ibberson R M, Fowkes A J, Rosseinsky M J, David W I F and Edwards P P 2009 *Angew. Chem., Int. Ed.* **48** 1435–8
[24] Maeda K, Lodge M T J, Harmer J, Freed J H and Edwards P P 2012 *J. Am. Chem. Soc.* **134** 9209–18
[25] Seel A G, Swan H, Bowron D T, Wasse J C, Weller T, Edwards P P, Howard C A and Skipper N T 2017 *Angew. Chem., Int. Ed.* **56** 1561–5
[26] Mauksch M and Tsogoeva S B 2018 *Phys. Chem. Chem. Phys.* **20** 27740–4
[27] Ariyarathna I R and Miliordos E 2021 *Phys. Chem. Chem. Phys.* **23** 20298–306
[28] Ariyarathna I R, Khan S N, Pawłowski F, Ortiz J V and Miliordos E 2018 *J. Phys. Chem. Lett.* **9** 84–8
[29] Ariyarathna I R, Pawłowski F, Ortiz J V and Miliordos E 2018 *Phys. Chem. Chem. Phys.* **20** 24186–91
[30] Almeida N M S and Miliordos E 2019 *Phys. Chem. Chem. Phys.* **21** 7098–104
[31] Almeida N M S, Pawłowski F, Ortiz J V and Miliordos E 2019 *Phys. Chem. Chem. Phys.* **21** 7090–7
[32] Ariyarathna I R, Almeida N M S and Miliordos E 2019 *J. Phys. Chem* A **123** 6744–50
[33] Ariyarathna I R and Miliordos E 2019 *Phys. Chem. Chem. Phys.* **21** 15861–70
[34] Ariyarathna I R and Miliordos E 2020 *J. Phys. Chem* A **124** 9783–92
[35] Ariyarathna I R, Pawłowski F, Ortiz J V and Miliordos E 2020 *J. Phys. Chem* A **124** 505–12
[36] Khan S N and Miliordos E 2020 *J. Phys. Chem* A **124** 4400–12
[37] Jackson B A and Miliordos E 2021 *J. Chem. Phys.* **155** 014303
[38] Jackson B A and Miliordos E Chem. *Commun.* accepted https://doi.org/10.1039/D1CC04748E
[39] Celani P and Werner H-J 2000 *J. Chem. Phys.* **112** 5546–57
[40] Werner H-J *et al* 2015 *MOLPRO version 2015.1,* a package of ab initio programs
[41] Roos B O and Andersson K 1995 *Chem. Phys. Lett.* **245** 215–23
[42] Ghigo G, Roos B O and Malmqvist P-Å 2004 *Chem. Phys. Lett.* **396** 142–9
[43] Frisch M J *et al* 2016 *Gaussian 16 Rev. C.01* (Wallingford CT: Gaussian, Inc.)
[44] Knizia G 2019 *IboView* (http://iboview.org/) (accessed 15 December 2019)
[45] Ariyarathna I R and Miliordos E 2018 *Int. J. Quantum Chem.* **118** e25673
[46] Haynes W M 2012 *CRC Handbook of Chemistry and Physics* 93rd edn (London: Taylor and Francis)
[47] Takasu R, Misaizu F, Hashimoto K and Fuke K 1997 *J. Phys. Chem* A **101** 3078–87
[48] Jeziorska M, Cencek W, Patkowski K, Jeziorski B and Szalewicz K 2007 *J. Chem. Phys.* **127** 124303

APPENDIX C: Supporting Material for Chapter 4

Appendix B contains electronic band structures and tabulated data for LiAmCn.

C.1 Tabulated Data

Table C-1. K-space grid used for *LiAmCn* calculations with Quantum Espresso (QE) and FHI-Aims.

n	QE	FHI-Aims
1	9 9 9	4 4 4
2	8 8 8	4 4 4
3	7 7 7	4 4 4
4	5 5 5	4 4 4
5	4 4 4	4 4 4
6	4 4 4	4 4 4
7	4 4 4	4 4 4
8	3 3 3	4 4 4
9	3 3 3	4 4 4
10	3 3 3	4 4 4

Table C-2. Calculated magnetic moments and total energy, energy for spin-flip of one SEP electron (ΔE^{flip}), and the J-coupling for *LiAmC6* with FHI-Aims using the PBE functional. B_0 and $|B_0|$ denote total and absolute magnetization, respectively. in units of μ_B. FM-1 Flip is the ferromagnetic state with one SEP electron flipped from alpha to beta.

State	-E (Ha)	B_0	$\|B_0\|$
Ferromagnetic	-11240.6024042	16.00	16.44
FM-1 Flip	-11240.6024222	14.00	16.40
Antiferromagnetic	-11240.6024381	0.00	16.12
Coupling J (Ha)	Coupling J (K)		
5.303E-07	0.17		
ΔE^{flip} (Ha)	ΔE^{flip} (K)		
2.121E-06	0.67		

C.2 Band Structures of *LiAmCn*

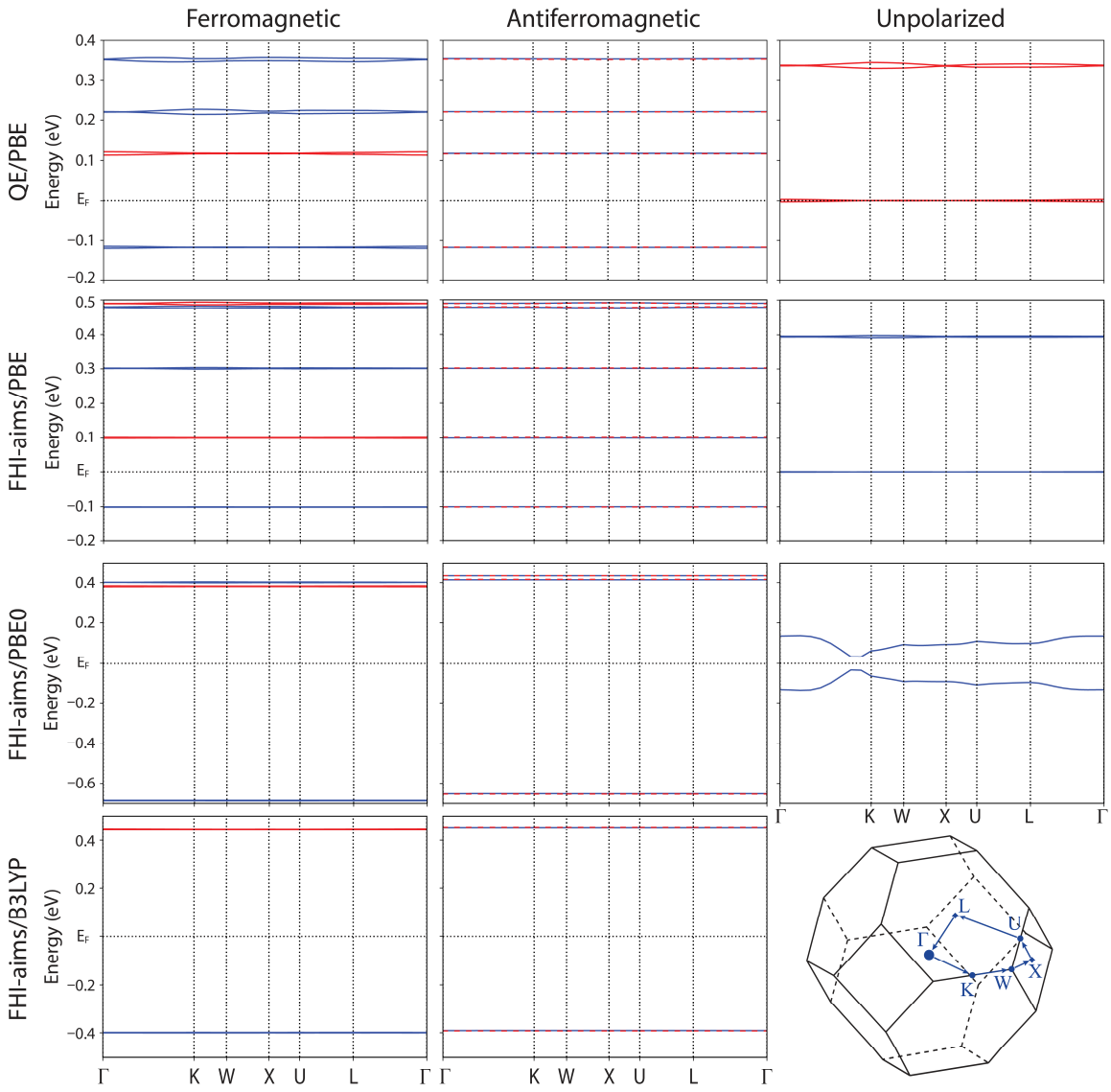

Figure C-1. Band Structure of LiAmC10. Electronic band structure of LiAmC10 computed using various methods. The structure of the Brillouin zone and the k-path used for band calculations is given.

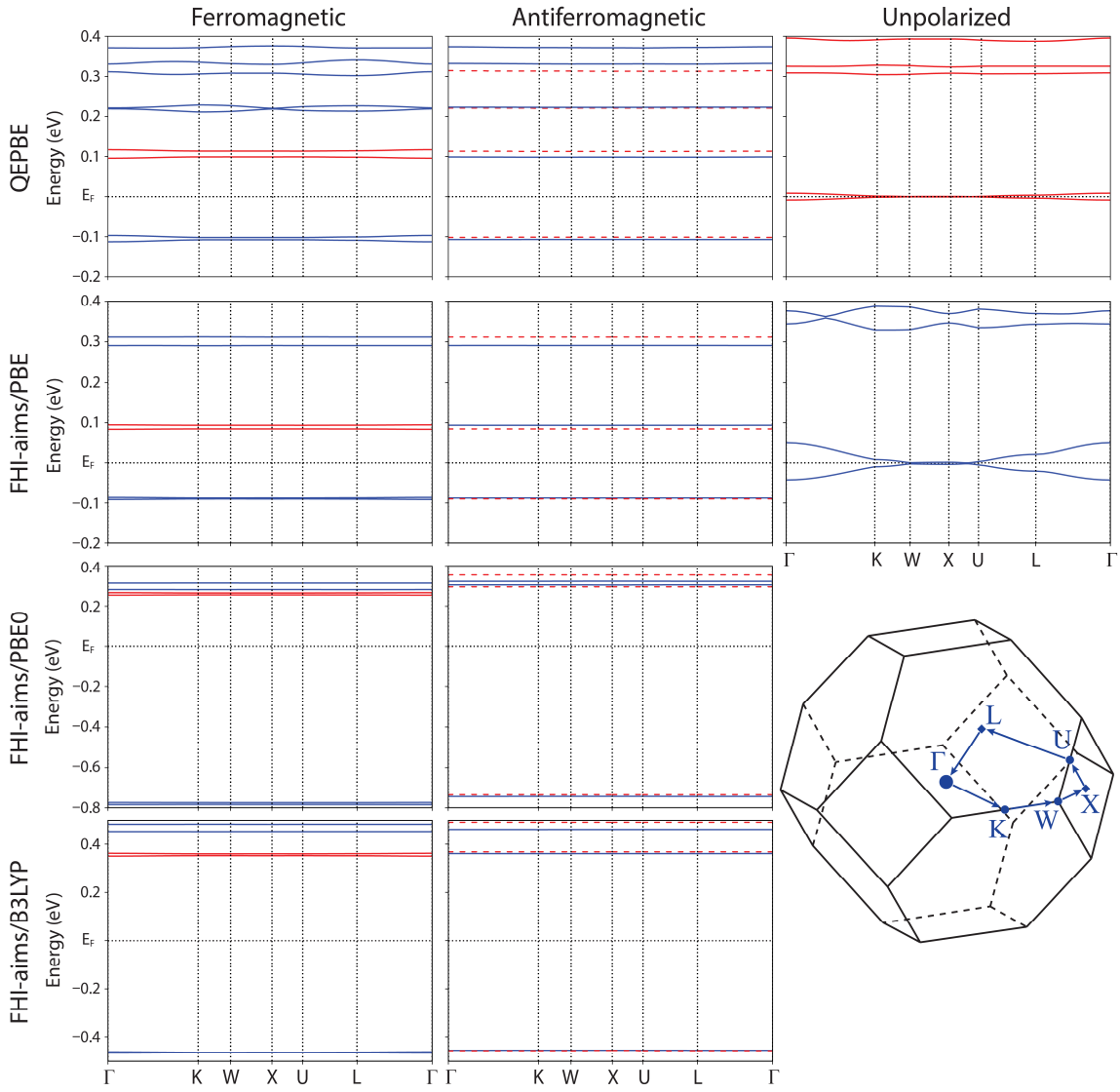

Figure C-2. Band Structure of LiAmC9. Electronic band structure of LiAmC9 computed using various methods. The structure of the Brillouin zone and the k-path used for band calculations is given.

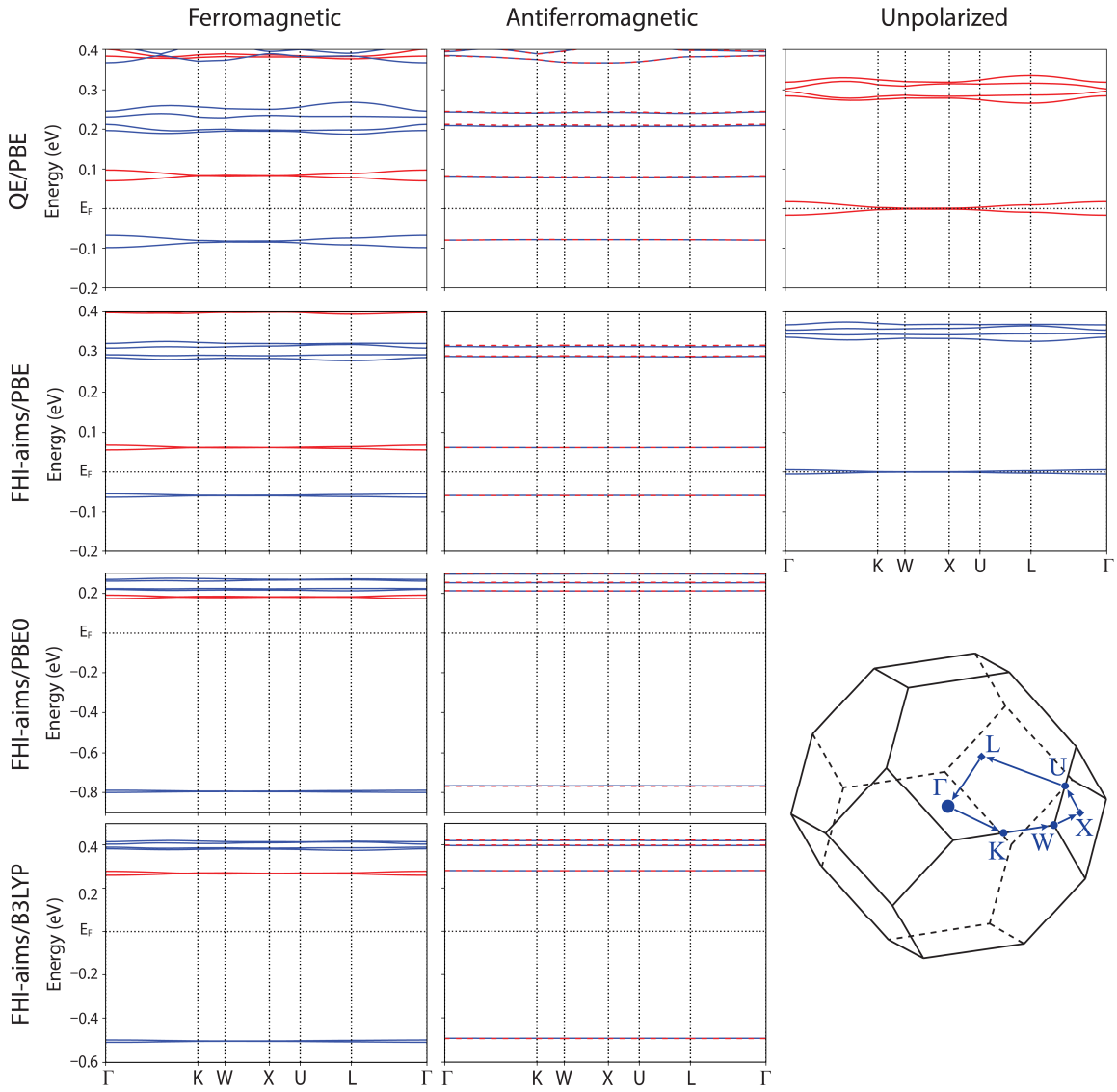

Figure C-3. Band Structure of LiAmC8. Electronic band structure of LiAmC8 computed using various methods. The structure of the Brillouin zone and the k-path used for band calculations is given.

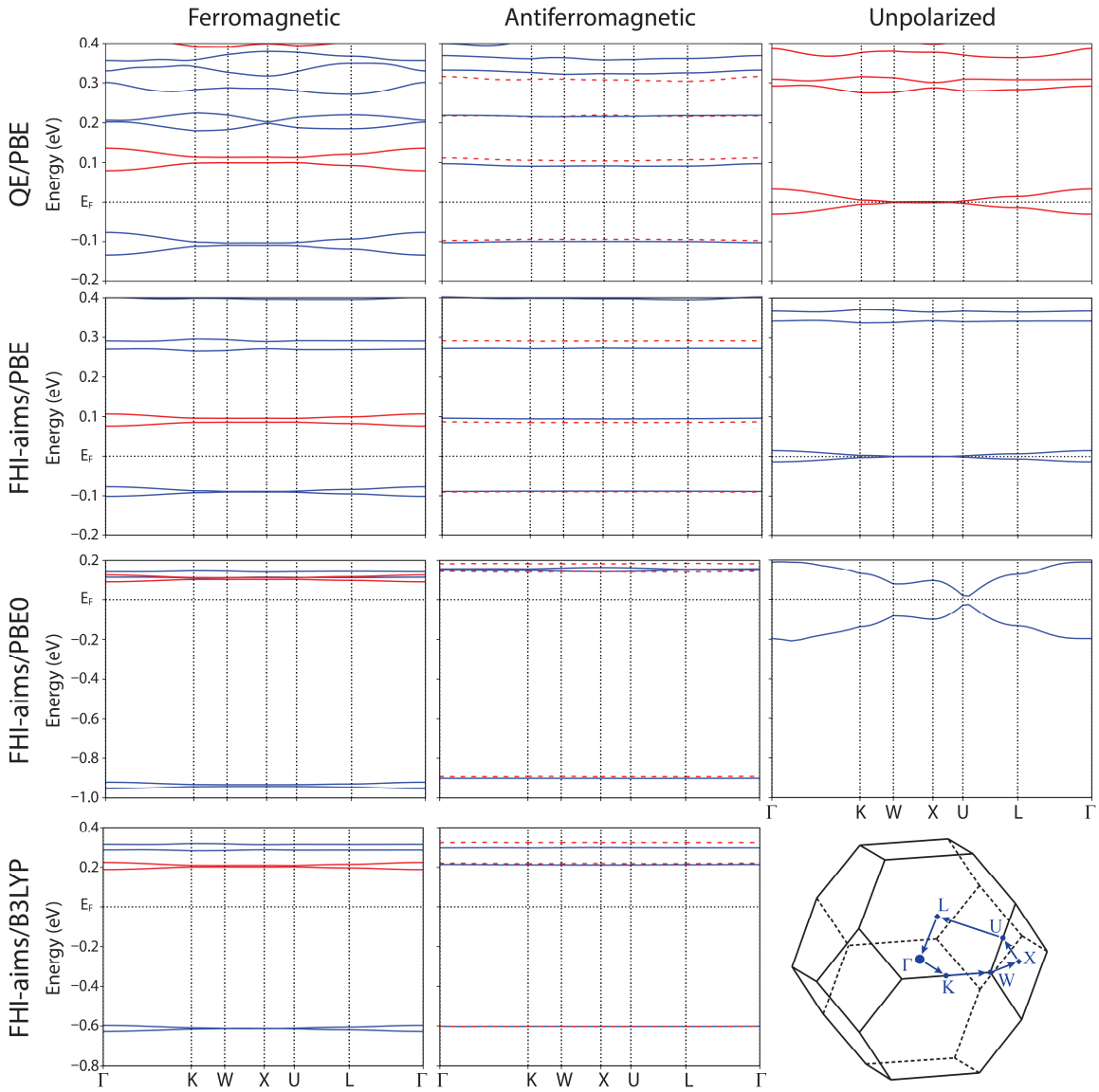

Figure C-4. Band Structure of LiAmC7. Electronic band structure of LiAmC7 computed using various methods. The structure of the Brillouin zone and the k-path used for band calculations is given.

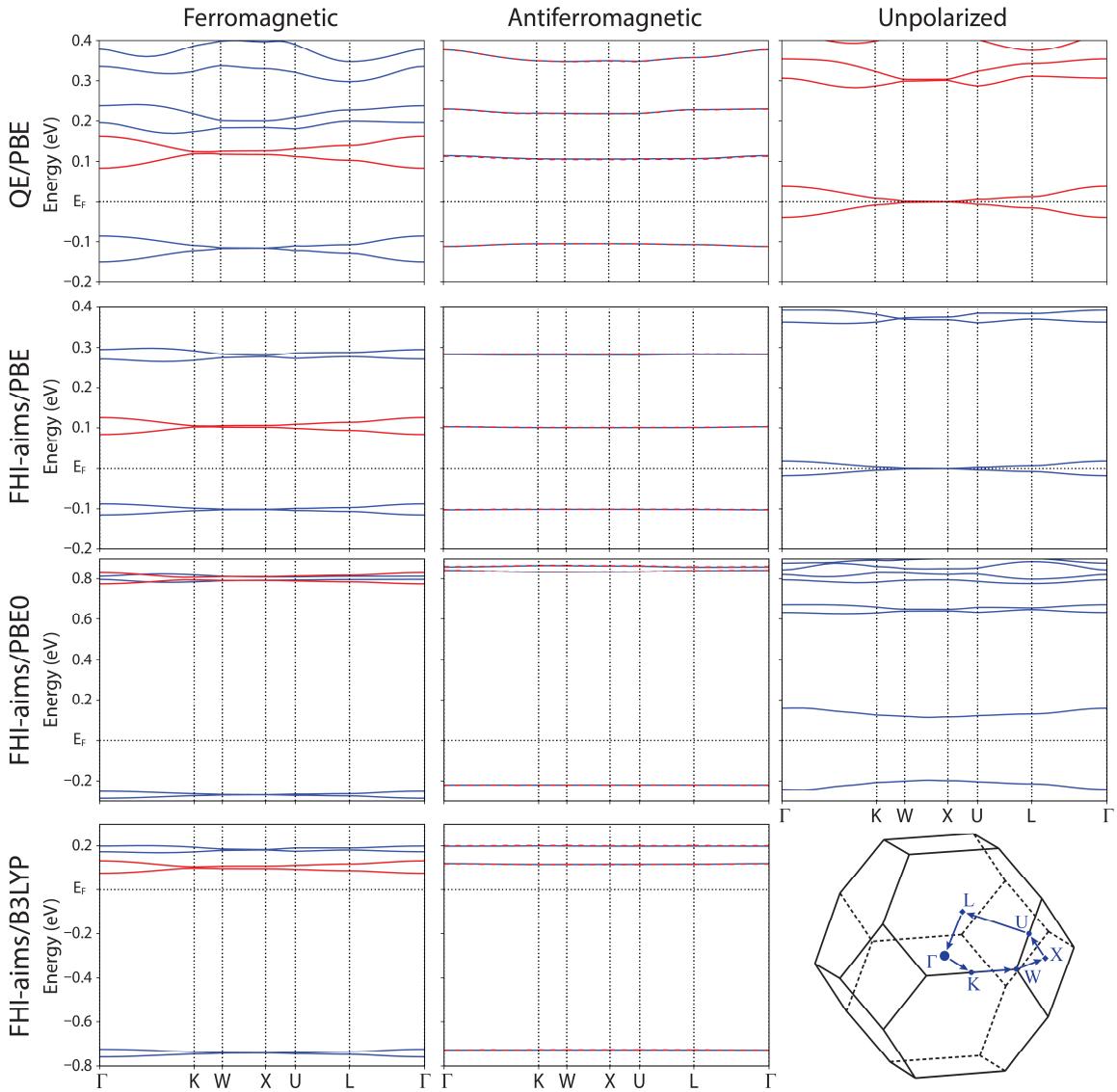

Figure C- 5. Band Structure of LiAmC6. Electronic band structure of LiAmC6 computed using various methods. The structure of the Brillouin zone and the k-path used for band calculations is given.

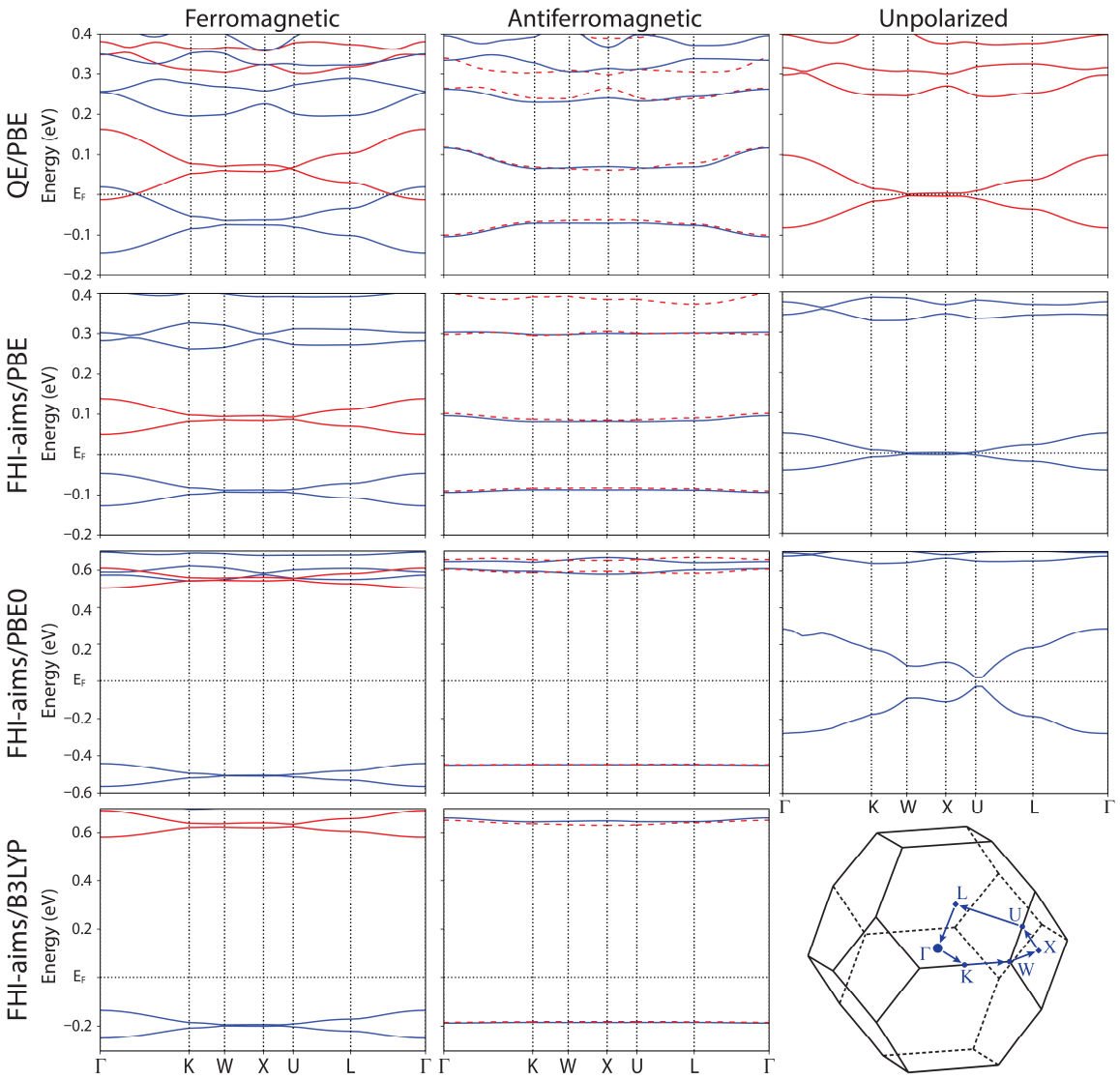

Figure C-6. Band Structure of LiAmC5. Electronic band structure of LiAmC5 computed using various methods. The structure of the Brillouin zone and the k-path used for band calculations is given.

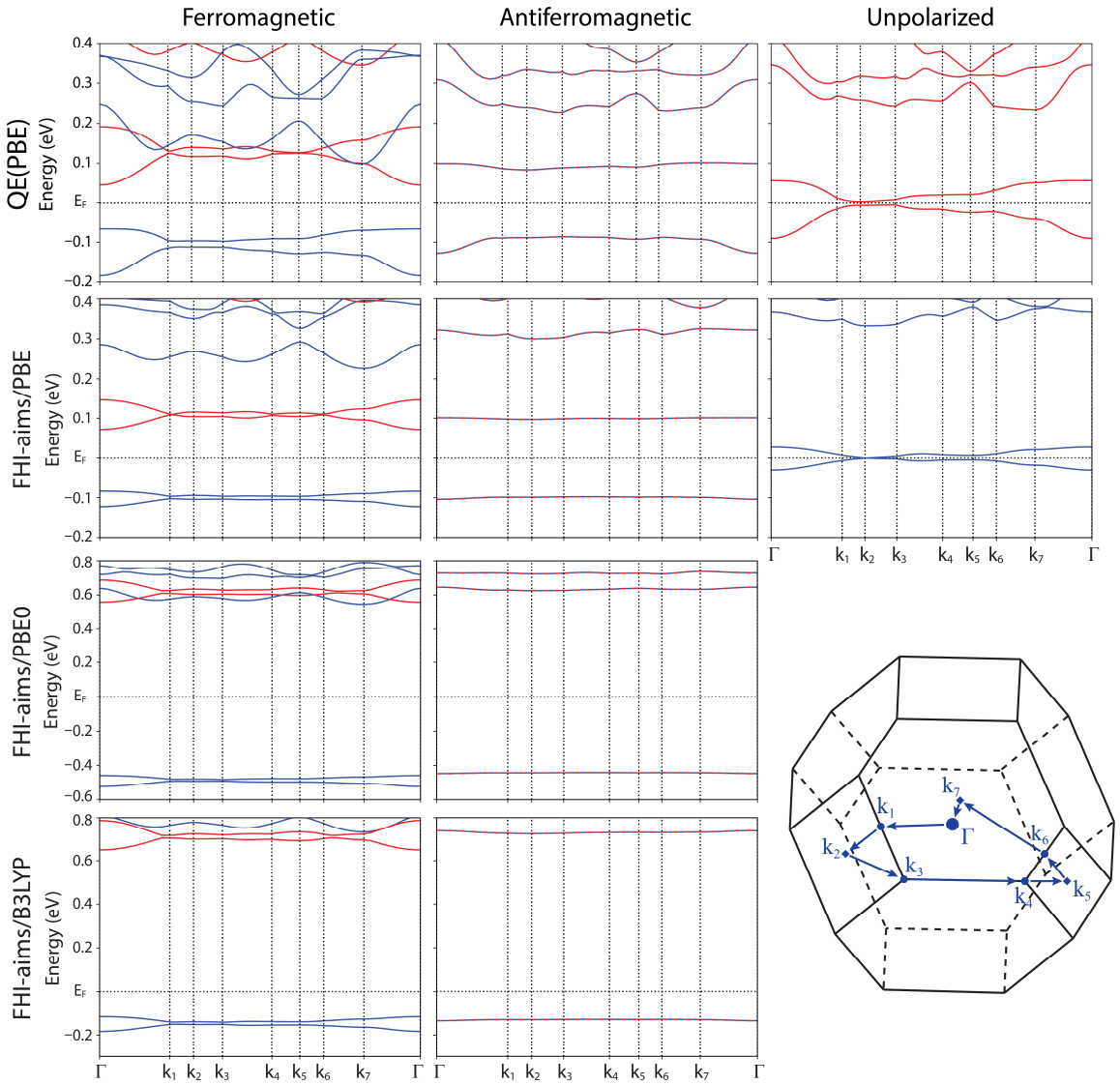

Figure C-7. Band Structure of LiAmC4. Electronic band structure of LiAmC4 computed using various methods. The structure of the Brillouin zone and the k-path used for band calculations is given.

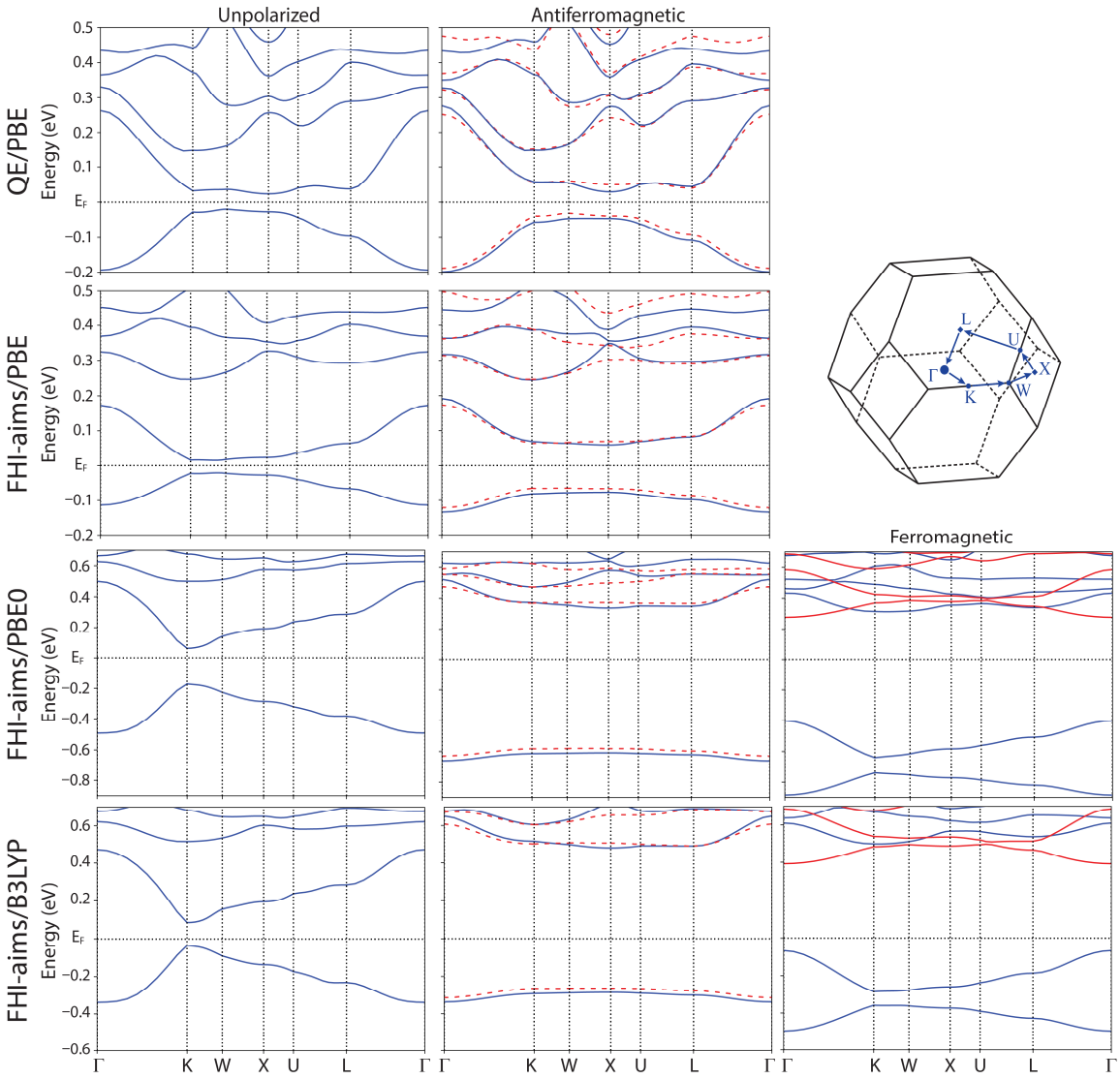

Figure C-8. Band Structure of LiAmC3. Electronic band structure of LiAmC3 computed using various methods. The structure of the Brillouin zone and the k-path used for band calculations is given.